THESIS

DEVELOPMENT OF A MARTIAN IN-SITU HYBRID ROCKET MOTOR

Submitted by

Iman Andrew Babazadeh

Department of Mechanical Engineering

In partial fulfillment of the requirements

For the Degree of Master of Science

Colorado State University

Fort Collins, Colorado

Summer 2020

Master's Committee:

Advisor: Anthony Marchese
Co-Advisor: John Mizia

Christopher Bareither

ABSTRACT

DEVELOPMENT OF A MARTIAN IN SITU HYBRID ROCKET MOTOR

One of the chief obstacles that has prevented a human mission to Mars is the excessive amount of mass that must be launched into low earth orbit to assemble the Mars-bound spacecraft. Since propellants alone account for 75% of the total mass requirements, a new concept has been proposed for both manned missions and unmanned robotic sample return missions, which relies on In-Situ Resource Utilization wherein propellants for the return trip to Earth are manufactured from raw materials available on Mars. This research focused on the development and testing of a unique propulsion system that could enable in-situ use of the Martian atmosphere as an oxidizer source and Martian soil as a fuel source for the return journey back to Earth for manned and unmanned vehicles. The propulsion system employs carbon dioxide as an oxidizer and metals as the fuel component. The need to understand and test this concept is significant as there is currently little experimental knowledge on the performance of carbon dioxide oxidizer and metallic fuels in rocket engines. Aluminum and magnesium fuels are the leading choice for burning with carbon dioxide as they can liberate the contained oxygen for rapid combustion to occur. Magnesium is favorable for its ignitability characteristics, whereas aluminum has a higher energy density but is more difficult to ignite due to the formation of its oxide layer. In the research conducted for this thesis, aluminum and magnesium particles were both considered to determine an optimal system that could be used to model an actual Mars propulsion system. The project entailed a myriad of combustion tests based on a conventional hybrid rocket motor in which the metallic fuel particles were encased in a polymer matrix binder

and oxidized through a liquid oxidizer. The hybrid rocket motor configuration is not only amenable for the Mars environment because of ease of storage, but also afforded great adaptability safety for the experimental studies described here because of the simplicity of refueling procedures and because the fuel component itself aids in keeping the combustion chamber wall cool, thereby eliminating the need for an active cooling system. Through initial testing, it was observed that adding an additional oxidizer aided in the combustion of carbon dioxide with high percentage metal fuel grains. Specifically, the results of this study suggest that using nitrous oxide as a complementary oxidizer was beneficial in attaining sustained combustion. However, it was also found that miscibility and mixing issues between the carbon dioxide and nitrous oxide oxidizers led to induced combustion instability during the hybrid test fires that had a 50% carbon dioxide and 50% nitrous oxide mixture ratio.

ACKNOWLEDGMENTS

It has been quite a ride the past few years during my time as a graduate student at Colorado State University. I have been blessed and privileged enough to be at CSU for the past ten years, and in some aspects, it will be tough to move on and to leave the friendships that I have made. I'd like to thank John Mizia for taking me in as a member of the Stoves Lab. I had so many great experiences getting to work on various projects ranging from helping build a fecal burner to building a Couette flow mixer and light array for pathogen eradication. I always enjoyed our long conversations about rockets, drones, AIs, and Elon Musk. The Stoves Lab was a great laboratory, and I really loved being a part of the team. Thank you, Max Flagge and Kyle Greer, for being kind and willing to make a joke when I was working, studying, or freaking out about an exam I had coming up. I'd like to thank Mars Rayno for always being ready with a joke about the Navy being better than the Air Force. On a more slightly serious note, I'd like to thank Mars for a comment he made when we were having a conversation about what our thesis projects were going to be: "There's no chance on earth anyone will let you work on anything rocket related." Thank you, Mars, for adding more fuel to my internal fire to research a topic that I love.

I'd like to thank Dr. Marchese for all the support and guidance he's given me the past several years. I am very thankful to have taken his class on chemical rocket propulsion as he made learning so easy and fun. I greatly appreciate all the encouragement he gave to me during my senior year on the rocket team. It meant a lot to the team and I that he was willing to be out in the 120-degree weather in the middle of the New Mexico desert to launch a rocket with us. His commitment to his students is extraordinary, and thus he is one of the best teachers I've ever had. His willingness to talk with me about my future goals has also been extremely encouraging, and

for that, I thank him. I will also always remember with fondness and laughter our homemade airbag experiments and the adventures that those experiences entailed.

To Steve Johnson: Thank you for being supportive of me during senior design and graduate school. I will always be thankful to you for providing me with the resources I needed to tackle crazy endeavors in the past few years. You have been paramount in removing so many obstacles with many projects (you are a true firefighter). Thank you for also letting me know that it's okay to take a break from working once in a while (I'm still working on this). I would also like to thank faculty members in the college of engineering for their support: Dr. Petro, Doc Schaeffer, Dr. Bareither, Dr. Wise, Dr. Azimi, Chris Garsha, Toni-Lee Viney, Ellen Aster, Steph Rosso, Sean Hershfeldt, and Jarrod Zacher.

I'd like to thank individuals at the Powerhouse as well: Dr. Windom for always being willing to talk about cool combustion experiments (I still want to test the hypergolic propellants with you at some point) and including me on the trips to talk with Robert Zubrin; Jason Golly for his continuous humor and encouragement; Matt Willman for taking the time to machine the hybrid motor nozzle carriers for me (that was a huge help!); as well as others: Kirk Evans, Mark James, Chris Van Roekel, Matt Kronwall, Liza Brown, Carter Butte, Ben Martinez, Tad Wegner, and AJ Puga. I would also like to thank the Energy Institute Sports League (EISL) for providing a great outlet to have fun with other students through sports and events.

To Edward Wranosky: Edward, the amount of kindness you have shown me has been unparalleled. I cannot thank you enough for all the materials, advice, and insight you have given me. From all the casting parties to the late nights in your kitchen talking about sounding rockets, I've enjoyed every second of it. Thank you for being a wonderful mentor and friend. Bill Colburn, thank you for answering various regression rate questions and opening up your home to

the rocket team and I to talk about old projects and share stories. I look forward to hearing about your future space shot attempt.

To the IREC teams past and present: it has been an absolute joy to be involved with this project since 2015. The first rocket team was gracious enough to answer so many questions of mine about the project and competition. Thank you to Matt Boyd and the second CSU team for having come along with you to Utah for the competition, it still means a lot to me. To my team: I think I'm still catching up on sleep from our year. I will always cherish the unique challenges we faced and how it made us bond as a team. I will never forget the days toiling away in the machine shop, listening to the Eagles and David Bowie, going to Pizza Casbah before they closed at 11:45 p.m., and heading back to the shop to work for another two to three hours, and then doing it all over again the next day. I will remember those days for a long time. Additionally, thank you to Casey, Collin, and Tanner for being willing to take out another four hours on our return trip back home from the competition to visit Roswell, where they had the museum dedicated to Robert Goddard. I know you guys were probably more interested in the UFO museum that we also visited, but I sincerely appreciate the time we had together on that trip back to Fort Collins. Thank you to the fourth team for many laughs and long, complex discussions about Isp and asteroid mining. I really appreciate the "Starman" Leatherman and DATAQ DAQ you gave me (I used that DAQ for this entire project). Thank you to the Aries V team for a year of hard work and fun. I'm so thankful for my friendships with you all. I always enjoy the jokes about me living in the glory days of my IREC team. To the current team, I'm very proud of all of you for the work that you've accomplished. I am saddened that you never had a chance to showcase that work.

To James Tillotson: thank you for the years of friendship you, Cadie, and the kids have given to me. Your kindness and willingness to help others is inspiring. I have thoroughly enjoyed our conversations about life, faith, space exploration, basement remodeling, scuba diving, and HAM radios (which we will finally do). Thank you for the rocket days with Chris and Cody at the Schoenig's house as well. I hope that it continues for years to come. I'd also like to thank friends from high school who thought it was fun to be around during a rocket test because they said: "there's a 50/50 chance it's going to fly or explode since it is made of scrap, I hope it flies for your sake, but I secretly hope it blows up". On that note, I'd also like to thank business owners in northern Colorado for not calling the police on me if they saw me raiding their garbage bins for parts and materials.

I would like to thank my church family at Vineyard for all their support and prayers that I would finally finish my thesis. It has been a joy to be in the worship band and play music with a lot of you. Finally, I would like to thank my family for their support throughout my life in anything and everything I've been a part of. Thank you to my grandma and grandpa Mama Mahin and Baba Essi for all their love and my Uncle Shaun for all the encouragement. An additional thank you to my family in California for all of their love and support. Thank you to Nadia and Lydia, especially for taking me to see the SpaceX headquarters/Falcon 9 and the space shuttle Endeavor. Thank you to my sister and brother in law Kimia and Nicki for their love and support (and trips to play basketball at the only park in town that still had hoops left due to COVID-19). A special thank you to my mom and dad; I cannot express in words how thankful I am to have you as my parents. I could not have done this project without your support and love, and I will always be thankful for that. To Brenna King (the King Queen): I will forever be thankful for all the love and continual encouragement you've given me. In addition to my

parents, I could not have accomplished this project without you. Thank you for all the times you were willing to brave the burning and frigid weather to help me with a test fire. I will always cherish those times.

TABLE OF CONTENTS

NOMENCLATURE

a: coefficient based on burning temperature

A_B: total burning surface area

A_e: nozzle exit area

A_{inj}: area of injector port

Al: aluminum

A_{port}: area of grain port

A_t: nozzle throat area

A_w: wing area

C*: characteristic velocity

C_d: coefficient of discharge

C_F: thrust coefficient

CH_4: methane

C_l: coefficient of lift

CO_2: carbon dioxide

c_p: specific heat

CuO: copper oxide

$CuCl_2$: copper chloride

D1: cylindrical port geometry

DAQ: data acquisition

d_p: fuel grain port diameter

D_p: post firing fuel grain port diameter

Dref: port diameter

F: thrust

Fe_2O_3: iron oxide

γ: ratio of specific heats

G_o: oxidizer mass flux

H_2: hydrogen

H_2O: water

H_2O_2: hydrogen peroxide

H_2SO_4: sulfuric acid

HCl: hydrochloric acid

h_{conv}: convective heat transfer coefficient

HNO_3: nitric acid

HTPB: hydroxyl terminated polybutadiene

$\Delta H_{v,eff}$: enthalpy of vaporization

IDP: Isodecyl Pelargonate

Isp: specific impulse

ISRU: in situ resource utilization

I_{tot}: total impulse

K_2SO_4: potassium sulfate

k_g: gas phase absorption coefficient

Kn: ratio of burn surface to nozzle throat area

KNO_3: potassium nitrate

L: lift

L_g: fuel grain length

m_f: final mass of launch vehicle

$m_{f\,B}$: burned fuel mass

$\dot{m}_f$: fuel mass flow rate

Mg: magnesium

MnO_2: manganese dioxide

m_o: initial mass of launch vehicle

$\dot{m}_o$: oxidizer mass flow rate

m_p: mass of the propellant

$\dot{m_{tot}}$: total mass flow rate

N_2O : nitrous oxide

n: burning (pressure) rate exponent

$NaCl$: sodium chloride

NASA: National Aeronautics and Space Administration

NH_4ClO_4: ammonium perchlorate

NH_4NO_3: ammonium nitrate

O_2: oxygen

O/F: Oxidizer to fuel ratio

ΔP: pressure differential

P1: initial pressure

P_c: combustion chamber pressure

P_e: exit pressure

P_i: combustion chamber pressure increment

Pref: reference pressure

P_t: propellant tank pressure

PTFE: polytetrafluoroethylene

PVC: polyvinyl chloride

Q_{conv}: convective heat transfer

Q_{rad}: radiative heat transfer

Q_{tot}: total heat flux

$\dot{r}_{hybrid}$: regression rate of hybrid fuel grain

$\dot{r}_{metal}$: regression rate of hybrid metal fuel grain

$\dot{r}_{solid}$: regression rate of solid propellant

ρ_{atm}: atmospheric density

ρ_f: fuel density

ρ_o: oxidizer density

σ: Stefan-Boltzmann constant

S: sulfur

SPST: single pole single throw

S_t: Stanton number

Δt: time interval

T_b: burn duration

Δv: change in velocity

V: horizontal velocity

v_e: velocity of exhaust particles

v_o: oxidizer stream velocity

W: weight

CHAPTER 1 – INTRODUCTION

Background

As the 13th century brought many improvements in the field of rocketry, the past one hundred and fifty years has shown significant advancement in utilizing rocket propulsion as a means to explore the universe. In the early 1900s, a Russian schoolteacher named Konstantin Tsiolkovsky developed one of the essential concepts that would influence man's reach beyond the Earth's atmosphere. His equation, popularly known as the "the Tsiolkovsky rocket equation," describes how to achieve a specific change in velocity by shedding mass in the form of burning propellant at a high exhaust velocity.

$$\Delta v = v_e \, ln \frac{m_o}{m_f} \tag{1-1}$$

The first considerable advancements in the manufacturing and testing of rocket motors came from Dr. Robert Goddard. During his time as an instructor at Clark University, Goddard began testing solid propellant rocket motors. These motors used the same type of compressed black powder propellant used by the Chinese in the 13th century. This consisted of potassium nitrate (saltpeter) as the oxidizer, and charcoal as the fuel. Sulfur was additionally added as a burn rate modifier to improve ignition characteristics. Later in 1926, Goddard successfully flew the first liquid propellant rocket to an estimated altitude of forty-one feet using gasoline and liquid oxygen as the propellants. This type of motor fed its propellants from their individual tanks to the combustion chamber through gas pressure. Once in the combustion chamber, a spark plug ignited the propellants, and hot exhaust gases left the nozzle. As Goddard's expertise in liquid rocket motors grew, so did the rockets. As the propellant tanks became larger, the need for

turbopumps became a necessity. Turbopumps allowed the propellant tanks to be lightweight and still provide the necessary pressure to feed the propellants into the combustion chamber. While Goddard was working on the turbopump variant of his rockets, other groups in Germany and the Soviet Union started building, static firing, and launching solid and liquid propellant rocket motors. A German group, Society for Space Travel (Verein für Raumschiffahrt), was experimenting with rockets just before the start of the second world war. Wernher Von Braun was one of the group members who stood out for having exceptional engineering leadership qualities and began taking on more responsibilities until the group dissipated as World War II began. The German military took an interest in some of the group members, primarily in Von Braun. He and his team were then given the money and resources to develop larger and more advanced propulsion systems to carry heavier payloads. This eventually turned into the V-2 rocket, a rocket capable of 60 miles in altitude and 125 miles in range [1]. At the end of World War II, Von Braun and many of the other German rocket engineers surrendered to the American Army and was taken to Fort Bliss, Texas. During this time, Sergei Korolev was working on inverse engineering captured V-2 rockets in the Soviet Union. Korolev and his team eventually were able to launch the world's first artificial satellite, Sputnik 1, into Earth orbit in October of 1957. This led to a space race between the United States and the Soviet Union led by Von Braun and Korolev, respectively. As the United States was ending the Apollo missions to the moon in the early 1970s, a new target appeared for robotic and human exploration: Mars.

Literature Review

The planet Mars has been a subject of interest and curiosity recently as satellites and rovers have been able to give significant detail on the environment and composition of the soil and atmosphere. In 1975, NASA's Viking missions found that the Martian atmosphere is 95.32%

carbon dioxide [2]. More recent missions have identified metals in the regolith, including aluminum, magnesium, titanium, iron, and potassium. Magnesium and aluminum have been found at mass percentages of five percent [2]. Reducing the payload and vehicle mass has traditionally been the primary engineering challenge of leaving the gravitational pull of Earth. Up to this point, it has not been practical to send enough fuel with a mission to mars to enable a return to Earth. This remains a significant limitation when considering complex science missions and human missions to Mars. One potential solution to this challenge is using resources from the regolith and atmosphere as chemical propellants for the return journey back to Earth [3]. The use of in situ propellants has been discussed for decades to reduce the overall mass leaving Earth [3]. Two key concepts for in-situ Martian propulsion are attaining liquid oxygen from the carbon dioxide atmosphere utilizing the Sabatier reaction, and directly using the carbon dioxide atmosphere as an oxidizer [2,3]. The Sabatier reaction employs carbon dioxide and hydrogen as reactants to retrieve water and methane products [2,3].

$$2H_2O \rightarrow O_2 + 2H_2 \tag{1-2}$$

$$CO_2 + 4H_2 \rightarrow CH_4 + 2H_2O \tag{1-3}$$

Compressors on Mars' surface would compress and cool the atmospheric carbon dioxide to a liquid where it would then be reacted with hydrogen in the presence of a catalyst [2]. The hydrogen must either be transported from Earth, or retrieved by melting ice at Mars' poles, and performing electrolysis to separate the hydrogen and oxygen [2]. Either way, the hydrogen would increase the total weight of the Earth launch vehicle as it would have to be brought from Earth in a storage tank or recovered from water with a large electrolysis plant. A methane and oxygen propellant combination provides exceptional specific impulse, high propellant density, and similar cryogenic storage temperatures. Specific impulse (Isp) is a quantification of a rocket

motor's efficiency. It is defined as the total force, or thrust, (F) generated divided by the mass flow rate of propellants delivered to the combustion chamber ($\dot{m}$) multiplied by the gravitational constant at sea level (g) and has units of time [4].

$$Isp = \frac{F}{\dot{m}\, g} \tag{1-4}$$

A high energy fuel and oxidizer combination such as hydrogen and oxygen have a specific impulse of 380 to 400 seconds at sea level [3,4]. Methane and oxygen have a lower theoretical specific impulse of 320 to 340 at sea level, which remains favorable in comparison to many other liquids and most solid propellants, that are approximately 150 to 275 seconds [3,4].

Directly utilizing the carbon dioxide atmosphere may be another viable option, trading performance for simplicity and versatility. The theoretical specific impulse of carbon dioxide as an oxidizer and a metal fuel is within the range of 185 to 220 seconds [5]. Albeit a lower performing propellant combination, the carbon dioxide only needs to be in a compressed liquid state to be viable, eliminating the need to transport liquid hydrogen, a catalyst reactor, or an electrolysis plant from Earth. The metals can either be transported from Earth, or be extracted from the soil as oxides [6]. Various metallic fuels have the potential to be oxidized by carbon dioxide in a rocket motor configuration. Lithium, beryllium, boron, magnesium, aluminum, silicon, cadmium, titanium and zirconium have been considered as possible fuel choices [7]. The most promising of these were beryllium, aluminum, and magnesium based on specific impulse and oxidizer to fuel ratio, as seen in Figure 1-1. Hydrides have been added to combustion models to aid in increasing the specific impulse [7]. It was found that beryllium, while having the highest theoretical specific impulse out of the selected group of metals, would be difficult to implement as a viable propellant with carbon dioxide due to its high toxicity [7]. Experiments with magnesium and aluminum are the most likely to result in viable solutions for an in-situ

propellant combination. Aluminum and magnesium have their respective advantages and disadvantages. Aluminum has a higher adiabatic flame temperature compared to magnesium resulting in a slightly higher theoretical specific impulse. Aluminum also has a higher ignition temperature due to the formation of its oxide layer [2]. Magnesium features a lower ignition temperature that makes it attractive to use as it requires less energy to ignite an engine on the Martian surface. The possibility exists that an alloy of magnesium and aluminum could be explored for the desired properties of low ignition temperature and high specific impulse.

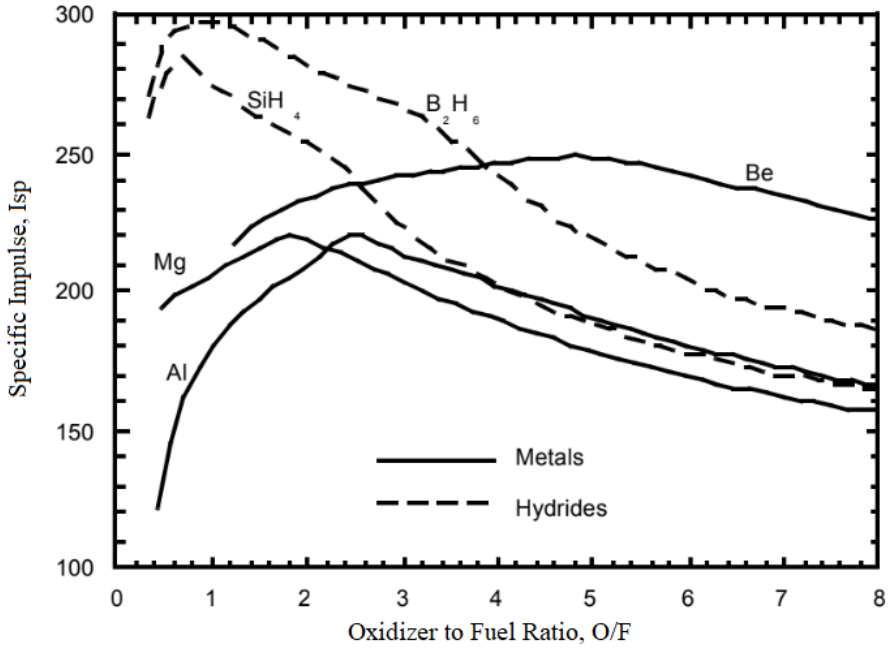

Figure 1-1. Specific impulse of various metals and hydrides burned with CO_2 at 150 psi [5].

Two Stage to Martian Orbit

If the propulsion requirements grew to accommodate more payload weight, one way of solving this could be using a traditional rocket propellant combination that utilizes nitrogen tetroxide and monomethyl hydrazine or unsymmetrical dimethyl hydrazine with the proposed in-situ metal and carbon dioxide propellant. Nitrogen tetroxide has historically been used as an oxidizer since the 1930s and continues to be used in different propulsion systems today [4]. It is

hypergolic (ignites solely through the chemical interaction between the oxidizer and fuel without the need for an external ignition source) with various fuels, including monomethyl and unsymmetrical dimethyl hydrazine. This propellant combination is simple as it does not require a separate system for the ignition and startup of the engine, and it is storable for an extended period of time (months to years). Additionally, the chemical reaction rate of hypergolic propellants is high, so that a higher mass flow rate can be implemented for transporting the propellants from the tanks to the combustion chamber. This results in a higher combustion chamber pressure, which in turn results in higher thrust. The nitrogen tetroxide and monomethyl hydrazine combination has a specific impulse of approximately 320 seconds compared to the 185 to 220 seconds of the less efficient metal and carbon dioxide combination [6]. To return a sample array from Mars back to Earth requires a Martian orbital velocity of just over three miles per second (Earth's escape velocity is seven miles per second). On Earth, escaping the pull of gravity is accomplished through staging where multiple rocket engines and their tanks are stacked on top of one another. These stages are deployed when their respective propellant tanks are emptied, thus shedding unusable mass, making the entire vehicle lighter. This typically results in a three stage to orbit vehicle to escape Earth's seven miles per second orbital velocity. Shafirovich, Gükalp, and Baker have proposed a two stage to orbit vehicle for Mars sample return missions where the Martian orbital velocity and the vehicle mass are both significantly lower and thus more favorable [6]. This two stage vehicle would use carbon dioxide and metallic powders for the first stage and nitrogen tetroxide and monomethyl hydrazine for the second stage [6]. The first stage would propel the vehicle out of the thickest portion of the Martian atmosphere to allow the second, more efficient stage to attain the required velocity to make the return journey back to Earth [6].

Rocket Propulsion versus Air Breathing Propulsion

Ramjets and turbojet engines using the carbon dioxide Martian atmosphere as an oxidizer have been proposed to carry large experiments or crews to other locations of interest as an alternative to rocket propulsion [7]. Air-breathing propulsion is attractive for surveying Mars as aerodynamic surfaces providing lift enables the propulsion system does not require a thrust to weight ratio greater than one wherein a rocket propulsion system does have that requirement. Therefore, the question arises; why use a rocket propulsion system over a winged air-breathing propulsion vehicle system?

Figure 1-2. Concepts of an air-breathing propulsion system and a helicopter lift system [8, 9].

The main topic of concern with carbon dioxide and metal combustion is the formation of oxide exhaust products [7]. Aluminum and magnesium oxide exhaust particles would be an engineering challenge to overcome as they could quickly erode delicate turbomachinery such as turbine blades in a turbojet engine. This problem is more easily dealt with in a rocket motor, as the exhaust particles are only exiting a nozzle and not a set of rotating turbine blades. Additionally, the pressure of the Martian atmosphere is 0.6% of Earth's atmospheric pressure, and thus the decrease in density makes it much more difficult for a winged vehicle to fly [7]. The equation below displays how much lift (L) (equivalent to the weight (W) of the total vehicle) is

produced by a vehicle based on its coefficient of lift (C_l), atmospheric density (ρ_{atm}), horizontal velocity (V), and wing area (A_w) [10].

$$\text{L} = \text{W} = C_l(\tfrac{1}{2}\,\rho_{atm}\,V^2)A_w \tag{1-5}$$

As an example, suppose a future mission to Mars required a winged vehicle the size of a MQ-1 Predator drone [11]. The coefficient of lift (C_l) is 0.75 for a 2.5° angle of attack, the atmospheric density (ρ_{atm}) is 3.853 x 10^-5 $\frac{Slugs}{ft^3}$, the wing area (A_w) is 123 ft^2, and the desired velocity (V) is approximately 150 $\frac{ft}{s}$. When the values for the known terms are implemented, a maximum lift and weight of 40 pounds is calculated. Therefore, a drone that weighs 2,200 pounds on Earth could weigh no more than 40 pounds on Mars to achieve the same horizontal velocity of 150 $\frac{ft}{s}$. This is mainly attributed to the low Martian atmospheric density.

Figure 1-3. MQ-1 Predator Unmanned Aerial Combat Vehicle [11].

Figure 1-4 shows the required horizontal velocity needed to lift a specific weight through the low-density Martian atmosphere.

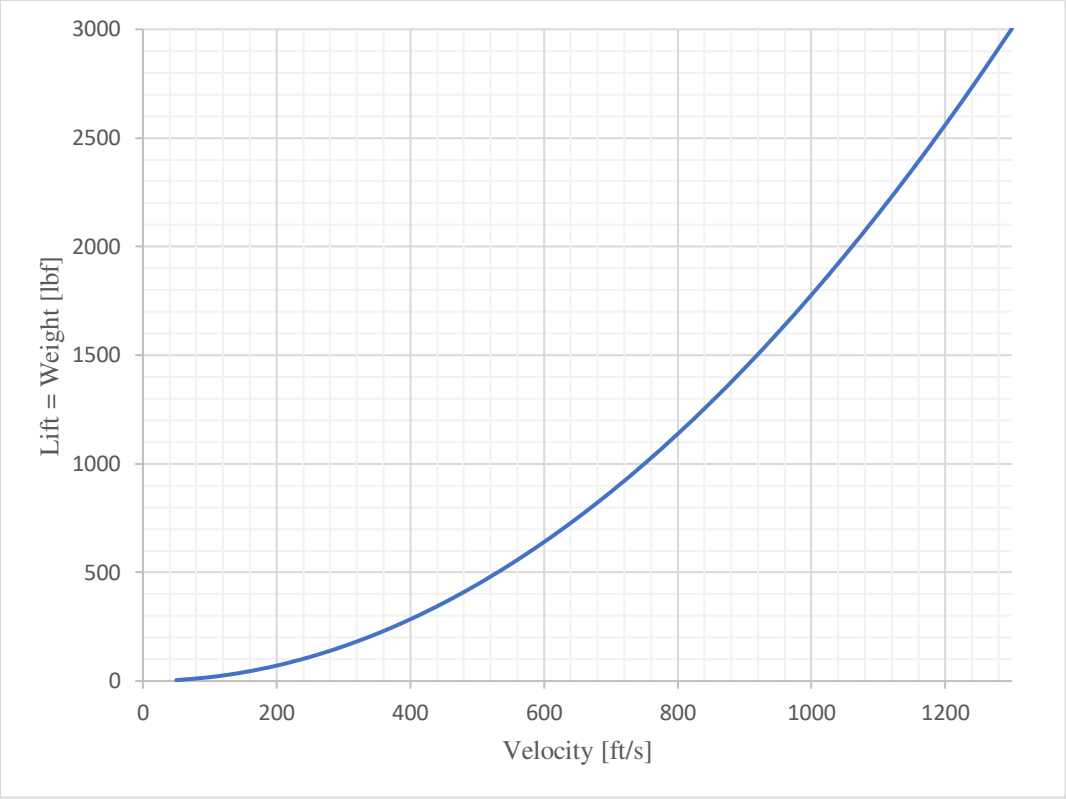

Figure 1-4. Lift and weight versus velocity for the MQ-1 Predator on Mars.

The analysis above suggests that new aircraft designs suited for the low density Martian atmosphere would need to be developed. Additionally, while winged and rotor vehicles certainly have their place in Martian exploration, rocket propulsion could offer distinct thrust to weight advantages, primarily in sample return missions and crewed missions requiring traversing the landscape.

CHAPTER 2 – DESIGN PLAN

Modes of Combustion

Many modes of combustion have been considered for successfully combusting aluminum and magnesium with carbon dioxide as an oxidizer. Figure 2-1 displays these methods of combustion. The first mode (Figure 2-1a) is a combination of a hybrid motor and a solid motor. Carbon dioxide is contained in a separate tank, while a fuel rich solid rocket motor resides beneath it [5].

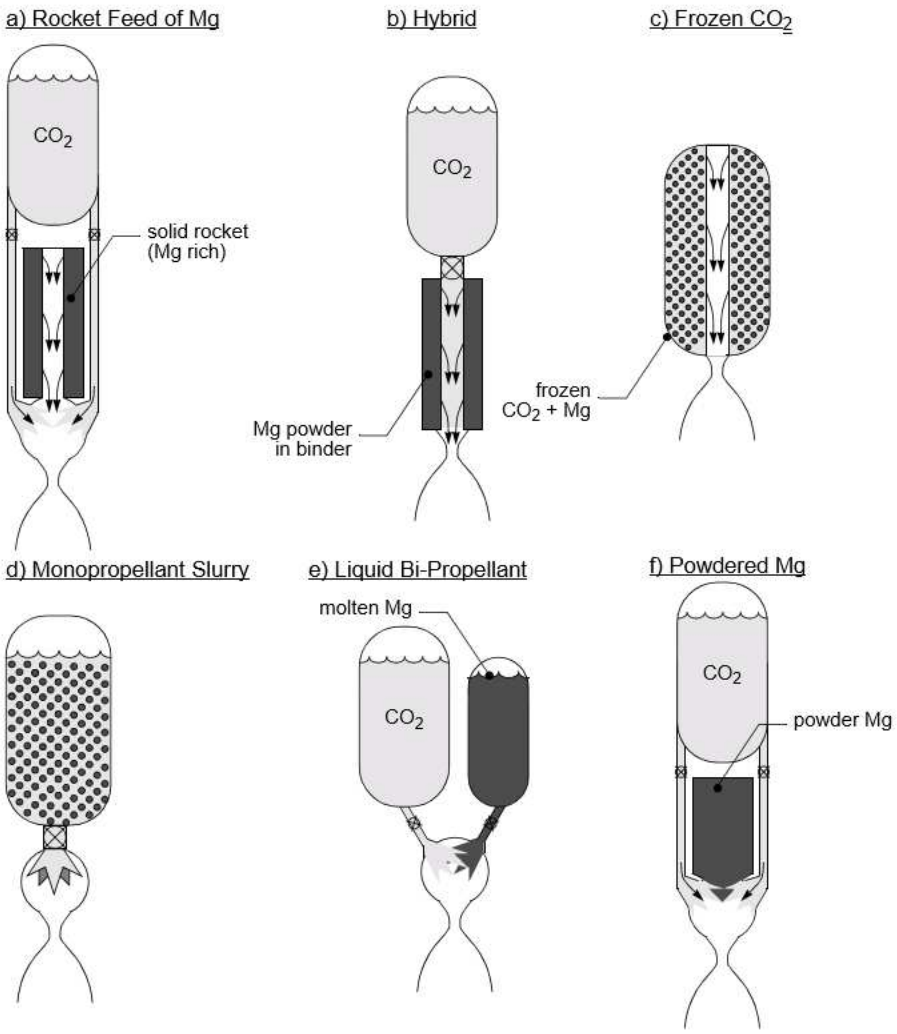

Figure 2-1. Modes of carbon dioxide and magnesium combustion [5].

Enough solid oxidizer is present in the grain so that combustion is self-sustaining without any external oxidizing sources. The carbon dioxide is routed around the solid propellant casing and is mixed in a combustion chamber below it before the exhaust products finally exit through a nozzle. The second configuration is a conventional hybrid mode in which the metallic fuel is encased in a matrix binder (Figure 2-1b). This mode could afford great versatility as refueling procedures would be akin to changing out cartridges for the fuel grain and compressing liquified carbon dioxide for the oxidizer. Additionally, the fuel component itself would keep the combustion chamber wall cool, eliminating an active cooling system. The disadvantage would be the need to bring a binder for the metal particles.

Other proposed modes include magnesium and aluminum suspended in frozen carbon dioxide (Figure 2-1c); monopropellant slurry in which the solid magnesium and aluminum particles are suspended in liquid carbon (Figure 2-1d); and liquid carbon dioxide and molten magnesium and aluminum (Figure 2-1e) [12]. Suspending magnesium and aluminum in frozen carbon dioxide is simplisticly attractive, as it would resemble a solid rocket motor lacking the complexity of moving parts, simplifying storage, ignition, and operation. The disadvantage is in producing a homogenous mixture for stable combustion to occur. A significant drawback, which is one that currently plagues all solid rocket motors, is that the thrust cannot be throttled. The monopropellant slurry possesses similar advantages to the solid propellant, as the only moving part would be a single moving valve to allow the propellant to flow into the combustion chamber, thus making it throttleable by varying the propellant flow rate. The drawback of this design is the settling of metallic fuel within the liquid oxidizer, which changes the oxidizer to fuel ratio. The liquid carbon dioxide and the molten magnesium and aluminum would act most similar to a traditional liquid propellant motor but would require extensive energy to keep the

metallic fuel liquid [13]. The last method encompasses burning floated powder in the combustion chamber (Figure 2-1f). The main advantage of this mode is the increased surface area of the metallic powder, which reduces the required energy for ignition. Missions on Mars that require hopping to various geographic locations would benefit from this method. The added plumbing and the need for an active cooling system could potentially increase the complexity of the system. An important variable to consider is that the oxidizer to fuel ratio (O/F) for the conventional hybrid motors (Figure 2-1a, 2-1b) will change over time. In contrast, the solid motor and liquid motor configurations (Figure 2-1c, 2-1d, 2-1e, 2-1f) are able to maintain a constant mass flow rate (and thus a constant oxidizer to fuel ratio) of both oxidizer and fuel. Due to time, cost, and complexity, the conventional hybrid motor design (Figure 2-1b) and the powdered metal design (Figure 2-1f) were chosen as the main modes of combustion for investigation to determine which would be eventually used for hot fire testing.

Powdered Metal Design

The powdered metal design has been the traditional mode of combustion for as long as in situ propellants have been proposed on Mars. It could be the most versatile form of In-Situ Resource Utilization (ISRU) as the metal fuel could be brought from Earth, taken from spent aluminum and magnesium stages of the descent vehicle, or processed from the Martian soil. Missions that would require hopping on the surface could take off from its starting point, land in the area of interest, replenishment its carbon dioxide, and take off again either to a new destination or back to the original base, as seen in Figure 2-2 [14].

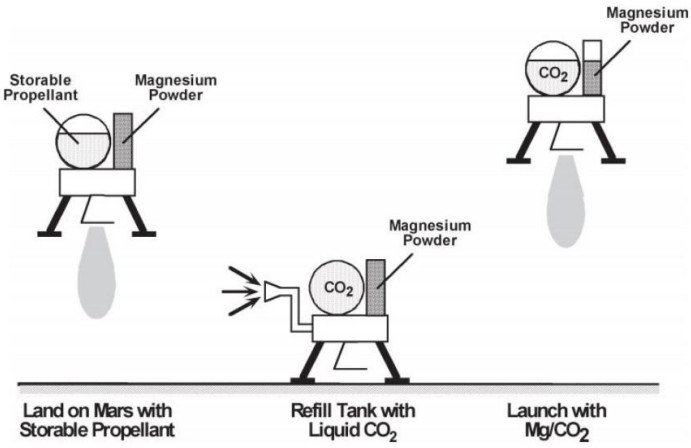

Figure 2-2. Hopper refueling configuration [14].

One of the main problems with the powdered metal design is the powder feed system. Clogging within a feed system could cause changes in fuel mass flow rate affecting combustion. Lead screws, carrier gases, venturi nozzles, and various other designs exist for the transport of powders. A preliminary design utilizing a venturi nozzle was adopted with the carbon dioxide oxidizer, additionally acting as a carrier gas to help transport the metal powder into the combustion chamber (Figure 2-3). A speaker assembly was added to the top of the head of the metal powder tank to agitate the powder to aid in preventing orthokinetic coagulation from occurring [15].

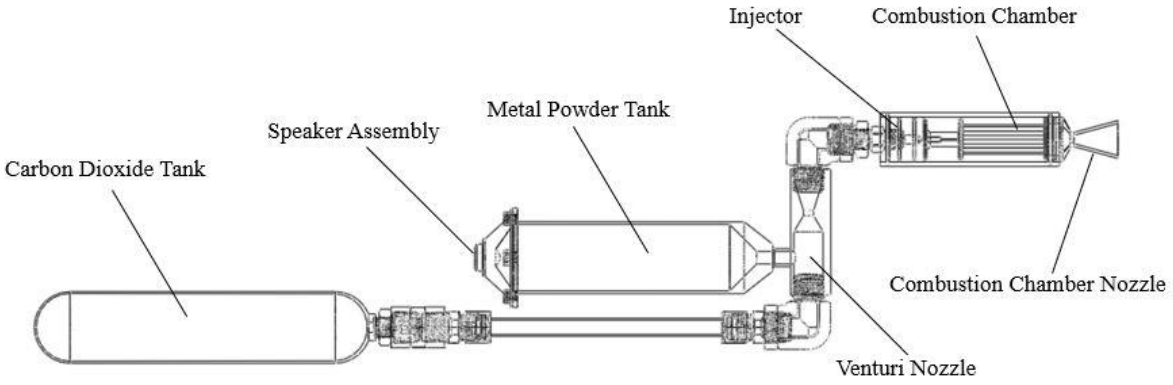

Figure 2-3. Powdered metal speaker design.

Wickman Spacecraft and Propulsion Company developed a small rocket motor that used magnesium powder and gaseous carbon dioxide that could fire for approximately five seconds [16]. The motor suffered from powder clogging, which negatively affected the combustion [16]. As many designs exist for powder transport, a passive system appears to be the simplest solution to implement. Two different designs were modeled to observe the pressure and velocity of a venturi and annulus approach for powder transport utilizing the carbon dioxide oxidizer as a transport carrier (Figure 2-4 a, and b).

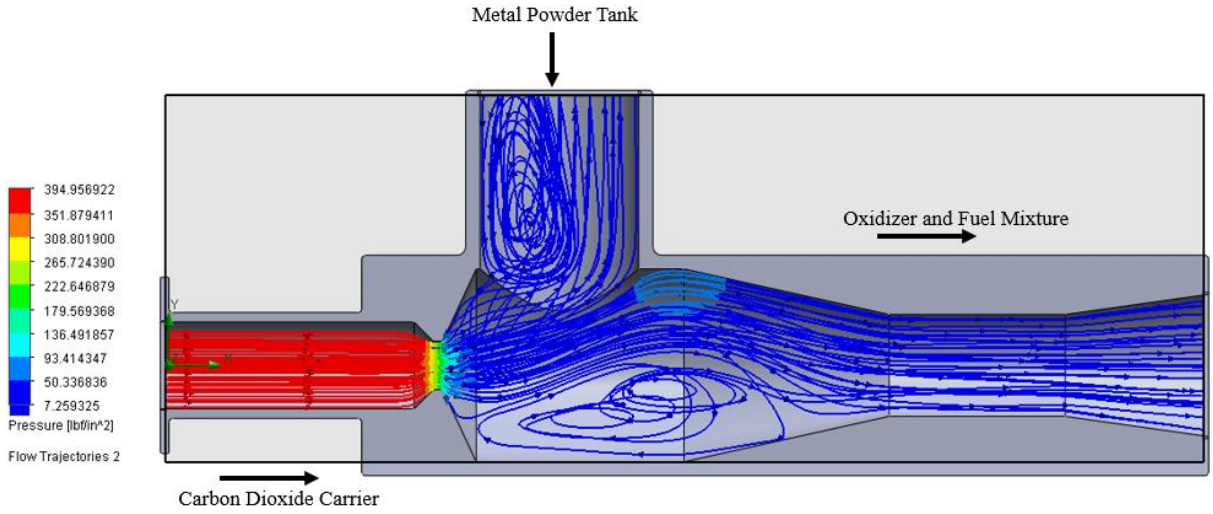

(a)

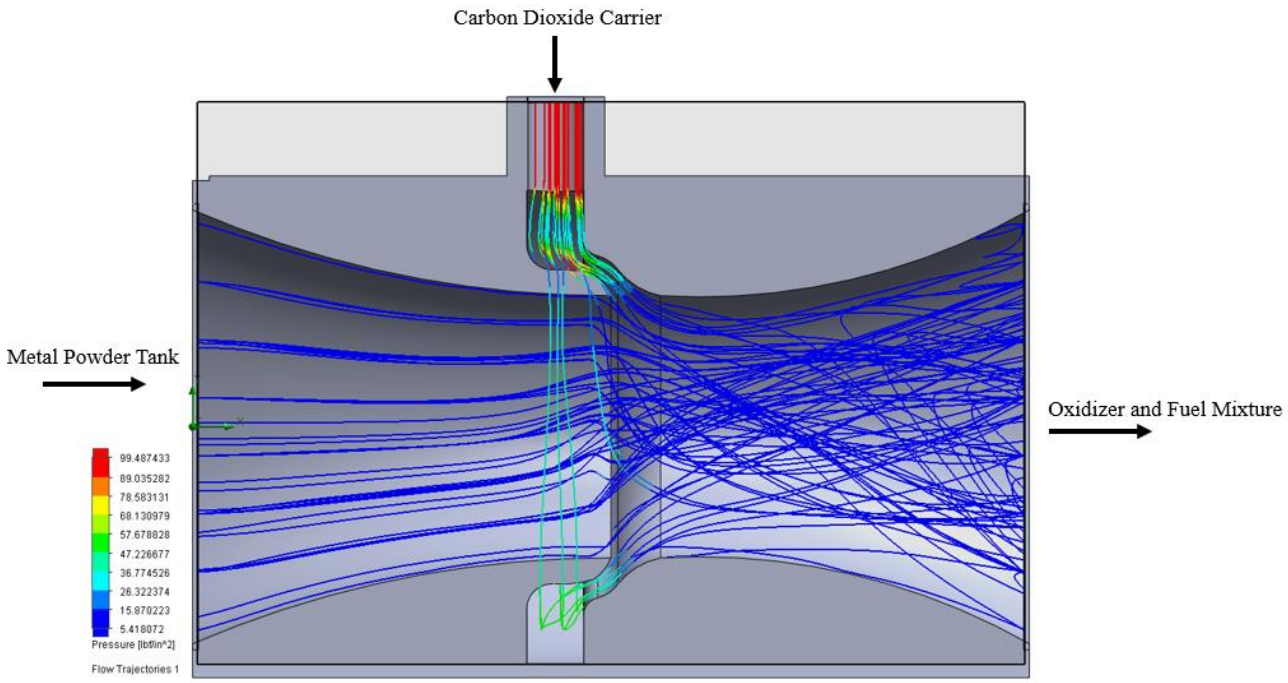

(b)

Figure 2-4. Venturi design (a) and annulus design (b) displaying pressure differential.

Hybrid Design

The hybrid design comprises of the metal powder being encased in a matrix binder that contains a port that allows mixing between the fuel and oxidizer to occur for combustion (Figure 2-5). The design is simple in nature as the only two actions needed to start this kind of motor are the ignition of the fuel grain and actuation of a valve to flow oxidizer into the fuel grain port. Although it is not a true in situ propellant motor due to the use of a binder that could not be manufactured on Mars, the hybrid design offers several advantages over the powder design. The most obvious is clogging of the fuel due to coagulation is significantly reduced. There is also less hardware associated with a hybrid motor, which decreases the overall weight of the system.

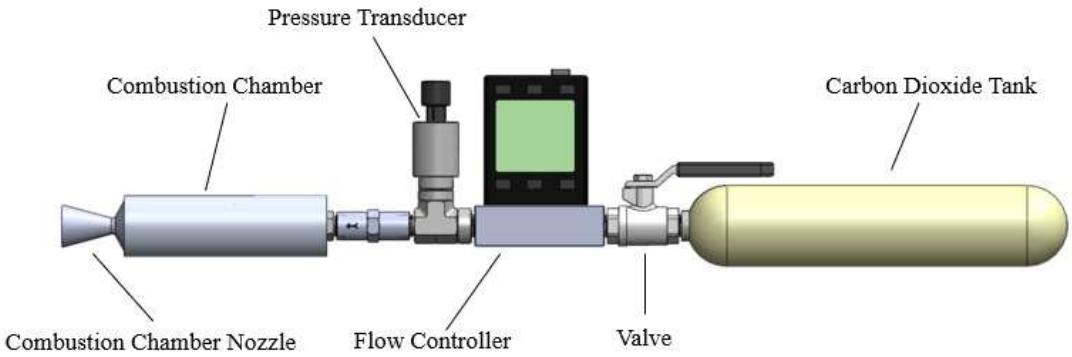

Figure 2-5. Traditional hybrid design.

The relationship between the combustion chamber pressure and the time of the burn is called burn profile, seen in Figure 2-6. It is graphed with the combustion chamber pressure or thrust on the Y-axis and the time on the X-axis. A regressive profile gradually decreases the pressure as time moves forward, while the progressive profile gradually increases the pressure as time moves forward. The neutral profile remains moderately constant in pressure throughout the burn. Hybrid rocket motors typically burn with a regressive burn profile. These profiles are useful in determining the total impulse and specific impulse of the motor.

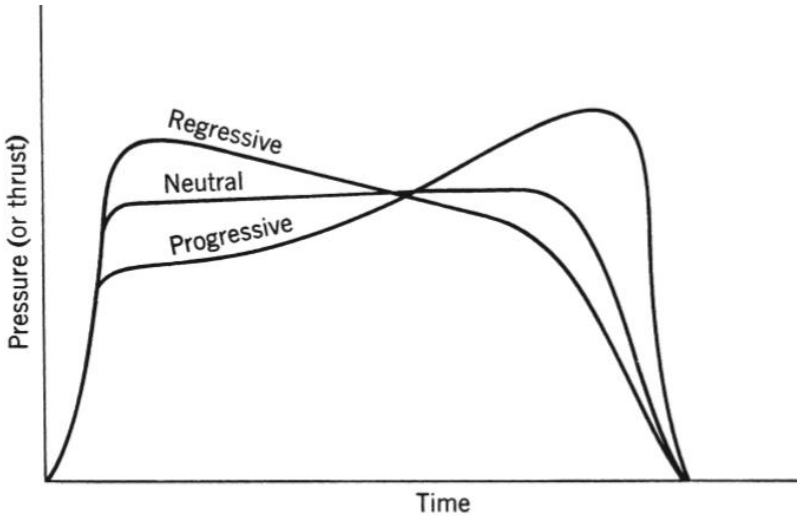

Figure 2-6. Burn profile for a progressive, neutral, regressive burn [4].

The regression rate (or burning rate) of propellant is the measure of how quickly the propellant gasifies for combustion. For solid rocket motors, the regression rate is primarily a function of the

combustion chamber pressure, and for hybrid rocket motors, the regression rate is largely a function of the oxidizer mass flux [4]. The direction of regression is typically orthogonal to the burning surface and is measured in inches per second [4]. Equation 2-1 displays the regression rate of a solid propellant where a is a coefficient based on the burning temperature, P_c is the combustion chamber pressure, and n is the burning rate, or pressure rate, exponent.

$$\dot{r}_{solid} = aP_c^n \tag{2-1}$$

$$\dot{r}_{hybrid} = aG_o^n \tag{2-2}$$

Equation 2-2 shows the regression rate for a hybrid rocket motor with the oxidizer mass flux (G_o) replacing the pressure in the previous equation. The oxidizer mass flux can also be expressed as a function of the density (ρ_o) and velocity (v_o) of the oxidizer stream. A more applicable solution to calculating the oxidizer mass flux is to divide the mass flow rate of the oxidizer ($\dot{m}_o$) by the area of the fuel grain port (A_{port}) seen in equation 2-3.

$$G_o = \rho_o v_o = \frac{\dot{m}_o}{A_{port}} \tag{2-3}$$

When the oxidizer is fed into the combustion chamber where the fuel grain resides, a boundary layer forms that eventually runs parallel to the surface of the grain. Within the boundary layer is where vaporization of the fuel and mixing between the fuel and oxidizer occur. The heat of combustion causes the solid fuel to change phase allowing for the mixing and combustion to be a continuous process. This can be seen in Figure 2-7, where the border of the boundary layer encompasses the mixing and subsequent active combustion zone.

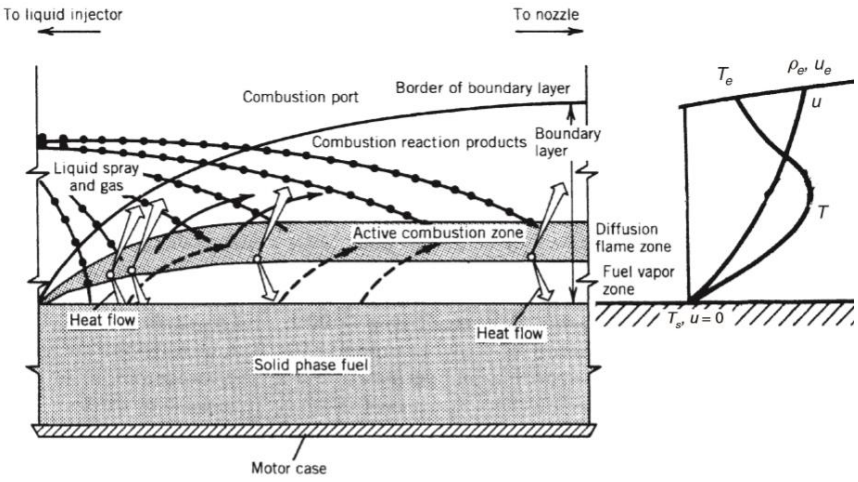

Figure 2-7. Interaction between oxidizer and fuel of a hybrid motor [4].

The regression rate explained above describes the regression of a hybrid fuel grain in which radiation can be neglected for fuels such as hydroxyl-terminated polybutadiene (HTPB), paraffin wax, polyethylene, ABS, PVC, and other polymers [4]. When metals are added to the fuel grain, the radiation and thus heat transfer to the grain can alter the overall regression rate. Previous testing that burned aluminum with HTPB showed that the radiation emitted from the aluminum oxide combustion product lowered the enthalpy of vaporization ($\Delta H_{v,eff}$) [17] The aluminum also appeared to increase the flame temperature, which in turn, could be responsible for the rise in regression rate [17]. Various forms of the equation for the regression rate of a hybrid rocket motor exist. They are dependent on many different variables, including grain composition, oxidizer composition, grain size, port size, port geometry, and injector design. Sutton gives the following equation (2-4) as an example of a relationship that could be used to account for the effect of radiation onto the regression rate [4]. It incorporates an initial pressure (P1) and port diameter for a cylindrical port geometry (D1) as well as a reference pressure (Pref) and port diameter (Dref) [4].

$$\dot{r}_{metal} \approx 2.5\, \dot{r}_{hybrid}\,(1-e^{-P1/Pref})(1-e^{-D1/Dref}) \tag{2-4}$$

Other relations (seen below) for regression rate include taking the mass flow rate of the fuel ($\dot{m}_f$), the density of the fuel (ρ_f), and various grain parameters like the length of the grain (L_g) and the diameter of the grain port (d_p) into account [17].

$$\dot{r}_{metal} = a G_o^n {L_g}^m \tag{2-5}$$

$$\dot{r}_{metal} = \frac{\dot{m}_f}{\pi \rho_f d_p L_g} \tag{2-6}$$

Additionally, the regression rate can be approximated by correlating the total heat flux (Q_{tot}) with the enthalpy of vaporization, or a total change in energy needed to heat the fuel grain to the temperature required for vaporization ($\Delta H_{v,eff}$)[17].

$$\dot{r}\rho_f = \frac{Q_{tot}}{\Delta H_{v,eff}} \tag{2-7}$$

The total heat flux can be equated to the summation of the convective heat transfer and radiative heat transfer from the combustion flame to the surface of the grain.

$$Q_{tot} = Q_{conv} + Q_{rad} \tag{2-8}$$

$$Q_{conv} = h_{conv} A_B (T_{flame} - T_{surface}) \tag{2-9}$$

$$h_{conv} = c_p \rho_o v_o S_t \tag{2-10}$$

In equation 2-10, the convective heat transfer coefficient is represented by h_{conv}, the fuel grain specific heat by c_p, the Stanton number as S_t, the density as ρ_o, and the velocity of the oxidizer as v_o [17]. The radiative heat transfer is calculated using

$$Q_{rad} = \sigma {T_{flame}}^4 (1 - e^{-k_g P_c d_p}) \tag{2-11}$$

where σ is the Stefan-Boltzmann constant, k_g is the gas phase absorption coefficient, and P_c is the combustion chamber pressure [17].

Chiaverini states that if the radiative heat transfer is one half or less than the convective heat transfer, the net result is a small change in the regression rate (approximately equal to or less than 10%). Additionally, there is a degree of disagreement in literature concerning the correlation between radiative heat transfer on regression rate [17].

Initial Hybrid Testing Predictions

Between the two options of the powdered metal design and the traditional hybrid design, the hybrid design was a better option for ease of testing and data acquisition. The testing of the transport of metal powders was beyond the scope of this work. Therefore, the hybrid design was selected as the focus of this project. The preliminary strategy for hot fire testing of a hybrid rocket motor was to have pure carbon dioxide as an oxidizer with a magnesium and aluminum alloy as the fuel grain. The tests would vary the percentage of aluminum and magnesium while keeping all other parameters constant. Preliminary burning tests, between carbon dioxide gas and magnesium powder, suggested that a secondary oxidizer added to the carbon dioxide would aid in ignition and sustaining combustion. The testing would proceed with having a majority of the oxidizer being this secondary, and more capable oxidizer while slowly adding carbon dioxide with each subsequent test to see the difference in performance. This changed the variable of testing to the oxidizer, instead of the fuel. Various "helping" oxidizers were considered with the main three being the following: liquid oxygen, nitric acid, and nitrous oxide. Liquid oxygen is the oxidizer of choice for many propulsion systems, especially for one that will see use on Mars. Its' high Isp with many different fuels makes it an attractive oxidizer; however, it is a cryogenic liquid and is difficult to procure in small quantities. Nitric acid was another option as a

secondary oxidizer as it easily prepared through the vacuum distillation of sulfuric acid and potassium nitrate seen below.

$$H_2SO_4 + 2KNO_3 \rightarrow 2HNO_3 + K_2SO_4 \quad (2\text{-}12)$$

A benefit that nitric acid possesses is its' hypergolic nature with certain fuels. This would eliminate the need for an ignition system, which would reduce overall weight while increasing reliability. Its toxicity, however, made it difficult to work with.

(a) (b)

Figure 2-8. Synthesis of nitric acid (a) and hypergolic ignition with turpentine (b).

Nitrous oxide is an oxidizer that is typically used with hybrid motors. In a sealed tank, it can be kept in a liquid state and fed into an injector using its own vapor pressure. Possibly the most significant benefit, in terms of this research, is the similarity in density to carbon dioxide. Carbon dioxide has a density of approximately 51 $\frac{lbs}{ft^3}$ at 725 pounds per square inch while nitrous oxide has a density of 49 $\frac{lbs}{ft^3}$ at the same pressure. This similarity in density meant that filling procedures would be identical for both fluids. Previous experience with nitrous oxide liquid rocket motors made it a familiar oxidizer to work with. Colorado State University's

Intercollegiate Rocket Engineering Competition (IREC) teams have built several nitrous oxide and ethanol motors in the past three years. These motors ranged from 100 pounds to 750 pounds of thrust.

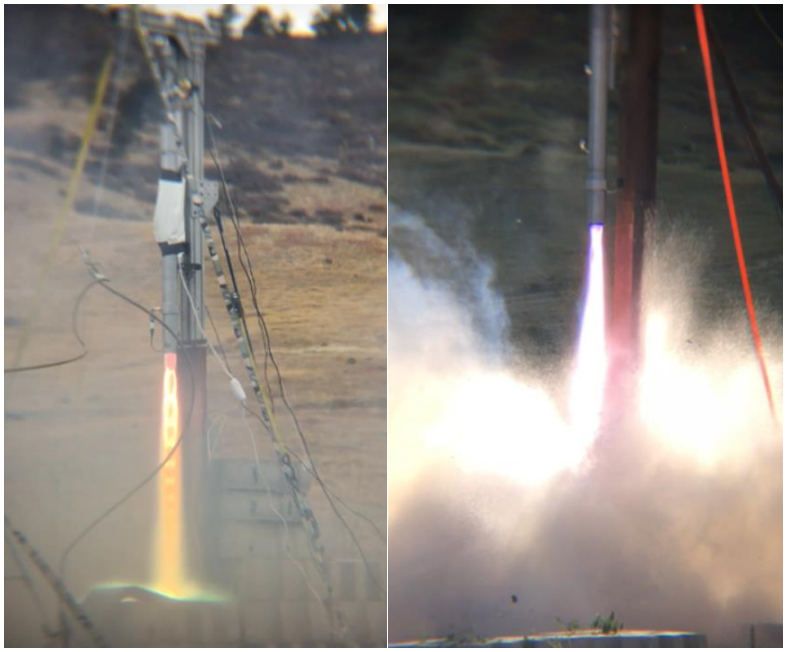

Figure 2-9. Hot test fires of previous motors using nitrous oxide at Colorado State University.

Due to the similarities in density, filling procedures, and previous experience in handling, nitrous oxide was chosen as the secondary oxidizer to add to the carbon dioxide. As previously stated, the testing regimen would start with solely nitrous oxide. The carbon dioxide would then be added in twenty-five percent increments by mass during each test. The fuel grain was decided to be composed of aluminum, magnesium, and a binder. Due to the high cost of nitrous oxide and magnesium powder, the testing would be conducted with a small motor with a liquid oxidizer mass of one pound and a fuel grain mass of 0.85 pounds.

An assumption was made early on that at the same temperature and pressure, carbon dioxide and nitrous oxide would be miscible due to their similar physical properties. To ensure that this

assumption was valid, a test setup (seen in Figure 2-10) was designed and manufactured to visually observe what occurs when the two fluids are brought together.

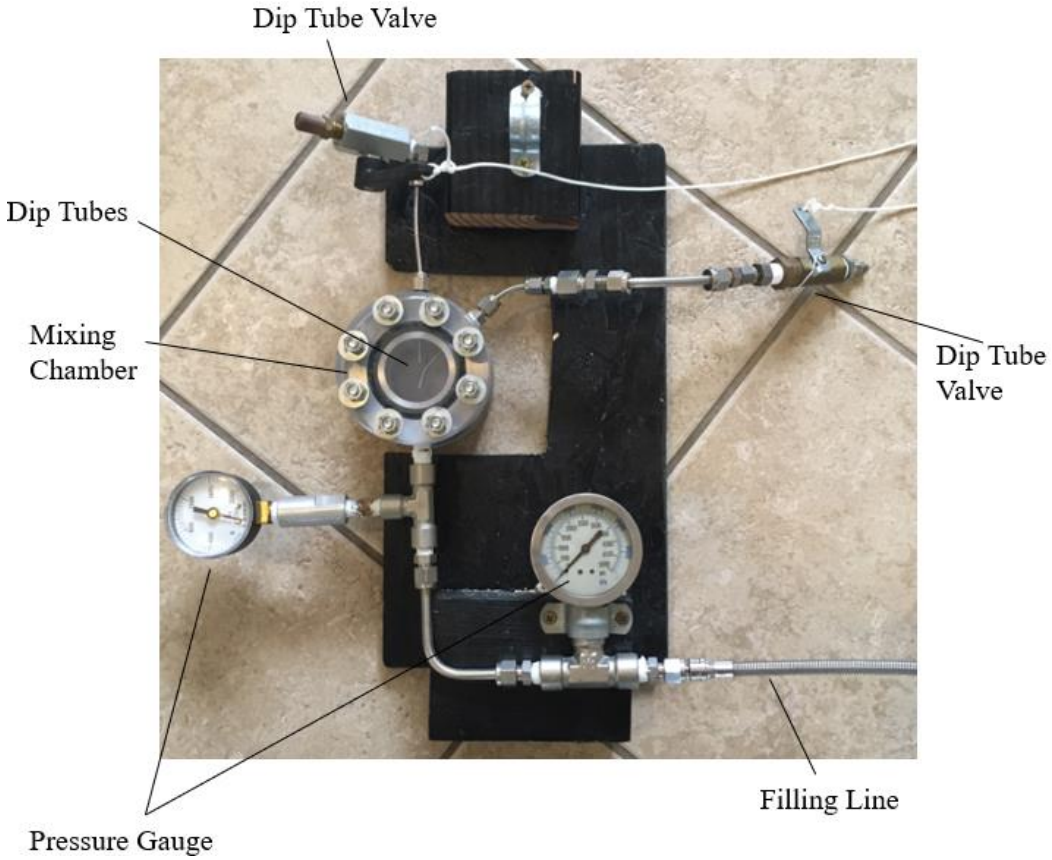

Figure 2-10. Carbon dioxide and nitrous oxide mixing chamber setup.

The mixing chamber was made of four pieces of polycarbonate that were stacked two on each side of an aluminum ring. The aluminum ring contained three ports; two for dip tubes and one for the filling line. The two 1/8 inch stainless steel dip tubes were used for venting headspace vapor and liquid when the liquid level reached the entrance of the dip tube. One was placed higher than the other allowing for venting of both fluids separately. The filling line was attached to a stainless steel tee in which the two sides were connected to the carbon dioxide and nitrous oxide fill tanks. The sequence of filling can be seen in Figure 2-11. Nitrous oxide filled the mixing chamber in sequence 1 and can be seen at steady state in sequence 2. Sequences 3 to 4

show the filling of carbon dioxide. Sequence 5 is the mixed product of both fluids. At this point during the test, turbulent gradient lines were visible until they settled a few seconds after the introduction of carbon dioxide. The start of the final venting of the mixing valve is shown in sequence 6.

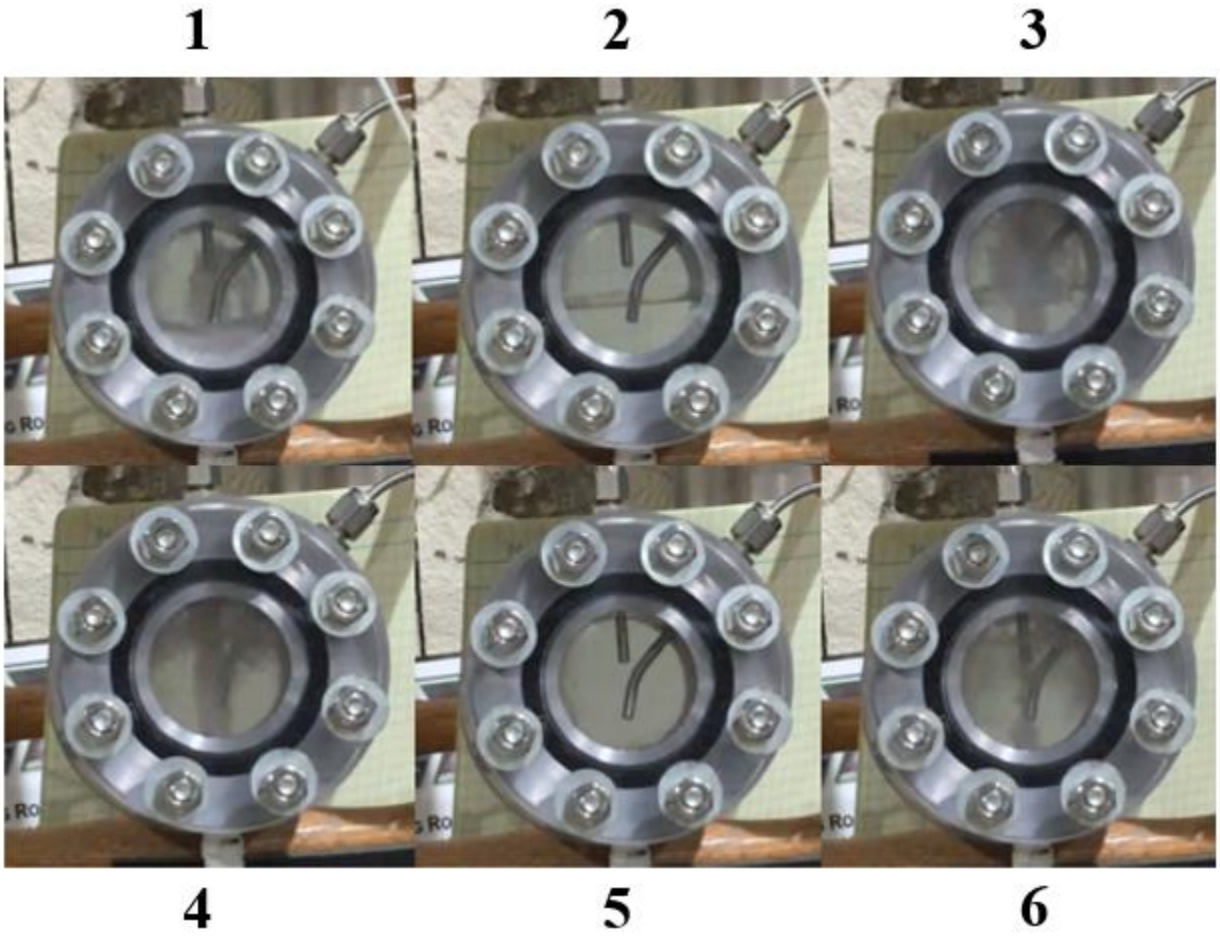

Figure 2-11. Carbon dioxide and nitrous oxide mixing sequence.

NASA's Chemical Equilibrium Analysis (McBride and Gordon, 1996), or NASA CEA, was used to find the theoretical characteristic velocity (C*) for various oxidizer to fuel ratios to observe the thermodynamic performance of the propellants. This was done for three different test cases for fuel composition. The first case used 100% HTPB as the fuel, the second was 50% HTPB, 40% aluminum powder, 10% magnesium powder, and the third was 25% HTPB, 65%

aluminum powder, and 10% magnesium powder. The combustion chamber pressure was kept at 200 pounds per square inch, and in each case, the oxidizer was tested at varying percentages of carbon dioxide and nitrous oxide.

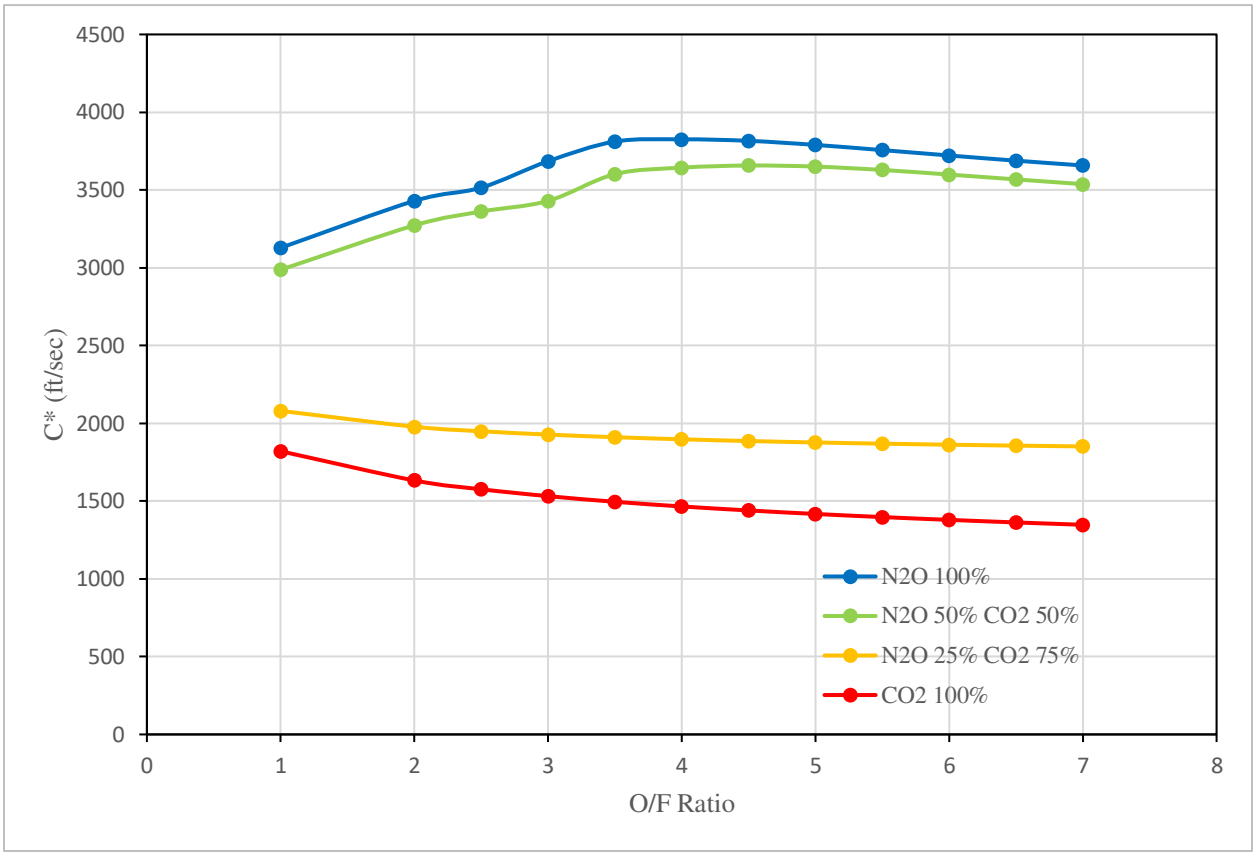

Figure 2-12. O/F ratio versus theoretical C* for 100% HTPB.

Figures 2-12, 2-13, and 2-14 show the characteristic velocity as a function of the oxidizer to fuel ratio for the three different test cases. The varying oxidizer composition is assumed as a mixture due to the similarities in density between carbon dioxide and nitrous oxide and the clear mixing chamber testing. As expected for all cases, the oxidizer mixture with the most nitrous oxide had the highest theoretical characteristic velocity, and the oxidizer mixture with the highest percentage of carbon dioxide had the lowest theoretical characteristic velocity.

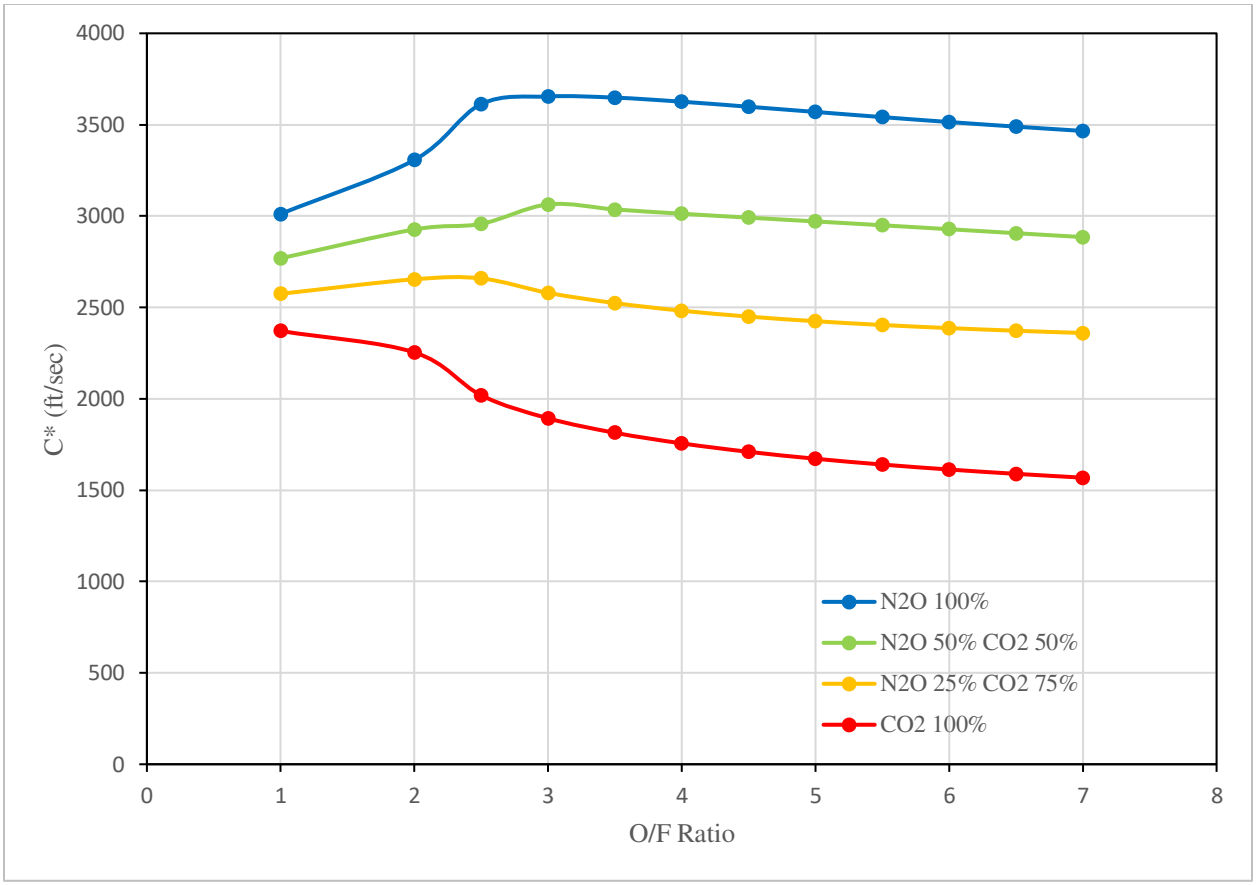

Figure 2-13. O/F ratio versus theoretical C* for 50% HTPB, 40% aluminum powder, 10% magnesium powder.

Additionally, for all three cases, the highest characteristic velocity appears to peak from an oxidizer to fuel ratio of 2.5 to 4 for any oxidizer mixture that contains nitrous oxide. For the pure carbon dioxide oxidizers, the highest characteristic velocity peaks at an oxidizer to fuel ratio of 1 and then begins to descend as the O/F ratio increases. The pure carbon dioxide oxidizer case for Figure 2-14 was not able to converge on NASA CEA. This could be due to the carbon dioxide not being able to oxidize or reduce the HTPB, even at low binder percentages.

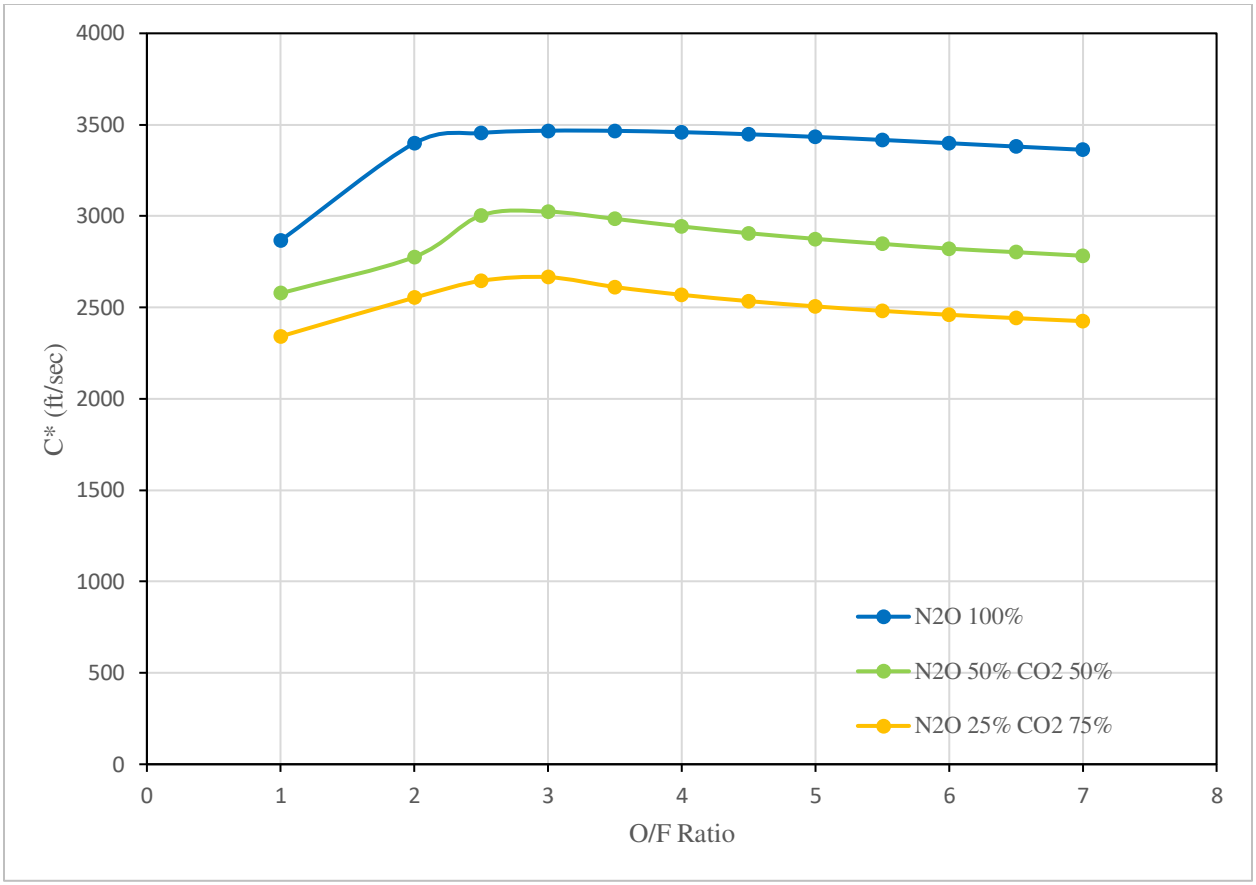

Figure 2-14. O/F ratio versus theoretical C* for 25% HTPB, 65% aluminum powder, 10% magnesium powder.

One of the challenges associated with metal and carbon dioxide combustion is the large amount of energy required to decompose the carbon dioxide in the first place. The enthalpy differences between carbon dioxide (ΔH_f = -393.5 kJ/mol) and nitrous oxide (ΔH_f = 82.1 kJ/mol) was thought to be an aid in reducing the overall energy needed. However, an ignition system would be needed that could provide enough energy to decompose the oxidizer, and deliver enough heat to raise the surface temperature of the fuel grain substantially, leading to the design and characterization testing of a preheater grain for the hybrid motor.

CHAPTER 3 – CHARACTERIZATION OF PREHEATER GRAIN

Preheater Grain Objectives

The preheater grain of a hybrid rocket motor heats the fuel grain and aids in decomposing the incoming oxidizer. It can be in the form of a compressed pellet composed of double-base propellant, or in the form of a solid propellant grain that utilizes the same fuel as the fuel grain with the addition of a solid oxidizer and binder. The goal for the preheater grain was to create a propellant that had a high adiabatic flame temperature to aid in the decomposition of the carbon dioxide oxidizer and possessed a similar regression rate to the hybrid fuel grain. The testing of the preheater grain, or characterization of the grain, is essentially testing the propellant in a traditional solid rocket motor. The testing sequence of the propellant results in the acquisition of regression rate values at their respective combustion chamber pressures. To acquire this data, a promising propellant is made into a grain with a specific port geometry and fired in a motor in which the only variable of each test is the nozzle throat diameter.

Preheater Grain and Ignitor Composition

Of the available solid oxidizers, ammonium perchlorate (NH_4ClO_4) and ammonium nitrate (NH_4NO_3) appeared to be best suited for the application. Ammonium perchlorate has had an extensive history in the use of solid propellants all the way from the Polaris and Minuteman missile systems to the space shuttle solid rocket boosters (SRBs). Unfortunately, its price and availability made it a difficult oxidizer to procure in the quantities needed. A less widely known oxidizer, ammonium nitrate, was utilized for its lower cost and higher availability. It has been used by Wickman Spacecraft and Propulsion Company to develop phase-stabilized ammonium nitrate

propellant (PSAN-1), a propellant that does not expand or contract in size due to variability in temperature. Wickman's ammonium nitrate propellant formulation appears below.

Table 3-1. Wickman Ammonium Nitrate Propellant [18].

Composition	Percent by Mass
Ammonium Nitrate	60.0
Magnesium	20.0
R20LM Binder (HTPB)	20.0

In 2004, Nakka found that a chlorine donor could assist in the combustion of ammonium nitrate with aluminum as early ignition attempts proved difficult [19]. Instead of using HTPB as a binder, he opted for polychloroprene (also known as chloroprene) which contained a high chlorine content (approximately 39% by mass) and could be easily found in the form of contact cement. Several small test propellants (based on Nakka's results) were mixed to conduct open-air burn testing to visually observe ignitability.

Table 3-2. Polychloroprene binder based test propellants [19].

	AN	S	Al	Mg	NaCl	MnO_2	CuO	Binder
A14	41	15	24	0	2	0	0	18
A20	49.1	2.3	19.2	0	0	0	0	29.4
A24	48	2.8	12	0	0	0	0	37.2
A201	44.5	2.1	17.4	8.3	0	1	0	26.7
A202	40.5	2.7	15.7	15.7	0	0	1.1	24.3

Table 3-2 shows three of Nakka's propellant formulations (designated as A14, A20, and A24) and two formulations that were alterations to the A20 propellant (designated as A201 and A202). A201 and A202 incorporated magnesium, manganese dioxide, and copper (II) oxide to increase the adiabatic flame temperature, while all formulations utilized sulfur to reduce overall ignition temperature.

(a) (b) (c)

Figure 3-1. Ignition testing of A20 (a), A201 (b), and A202 (c).

Each propellant formulation was timed to observe how long it took for the slug to fully ignite using a standard electronic match (E-match). Under these conditions, it was determined that propellant formulations with an ammonium nitrate oxidizer took a lengthy amount of time (approximately 2.5-3 seconds average) to ignite. Therefore, three ignitor compounds were evaluated to observe the time delay of ignition. These compounds were thermite based to promote high-temperature exhaust products to contact the propellant grain. Their compositions are below in Table 3-3.

Table 3-3. Thermite ignitor compositions.

Ignitor-1	**Ignitor-2**	**Ignitor-3**
55% Teflon (PTFE)	77% CuO	82% CuO
22.5% Al	23% Mg	18% Al
22.5% Mg		

It appeared that the aluminum-based igniter compositions took longer to ignite than ones that contained magnesium. This could be due to a combination of the aluminum oxide layer on the particles and relatively their large size (30 micron). Thus, the copper (II) oxide and magnesium thermite composition was chosen for the ignitor compound.

(a) (b) (c)

Figure 3-2. Ignition testing of Ignitor-1 (a), Ignitor-2 (b), Ignitor-3 (c).

Solid Motor and Test Stand Design

Based on the time delay of ignition, ease of ignition, and ease of manufacturing, A202 was the propellant composition chosen for the first hot fire test. The motor design was then completed in Solidworks. Figure 3-3 shows the detail of this design. The aluminum casing held all components and acted as the pressure vessel. The PVC liner was held the propellant grain and acted as a thermal liner once the regressing propellant finally reached its outer radius. The forward closure contained a tapped hole with a pressure port to read combustion chamber pressure, and the graphite nozzle directed the hot exhaust gases. The equation for thrust is given below in equation 3-1 where P_c.is the combustion chamber pressure, A_t is the area of the nozzle throat and C_F is the thrust coefficient.

$$F = C_F \, A_t P_c \tag{3-1}$$

The thrust coefficient is a measure of how well the nozzle accelerates the expanding exhaust flow and typically resides between 0.8 to 1.9 [4]. For the characterization of the propellant, it was decided that the nozzle would have a straight throat profile and not a divergent exhaust

section. This reduced any variability that the thrust coefficient could add by having a diverging nozzle.

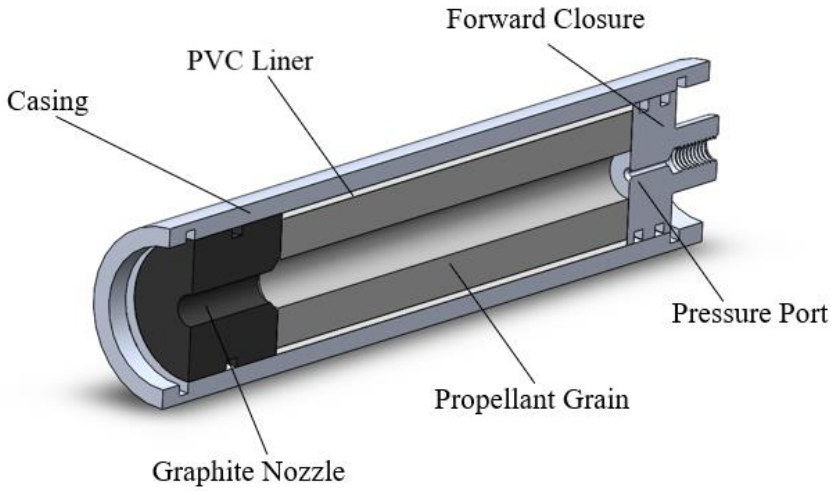

Figure 3-3. Solidworks model of solid propellant test motor.

Before the motor components were machined, a small test stand was designed and built. The stand was made from angle iron and was fitted with an aluminum C channel to allow for variability in testing solid motors of different sizes. Additionally, the aluminum C channel was attached to a T-slot rail, which could have permitted a load cell to be mounted if needed. Figure 3-4 displays the CAD drawing of the test stand with the assembly model of a possible hybrid motor for scale.

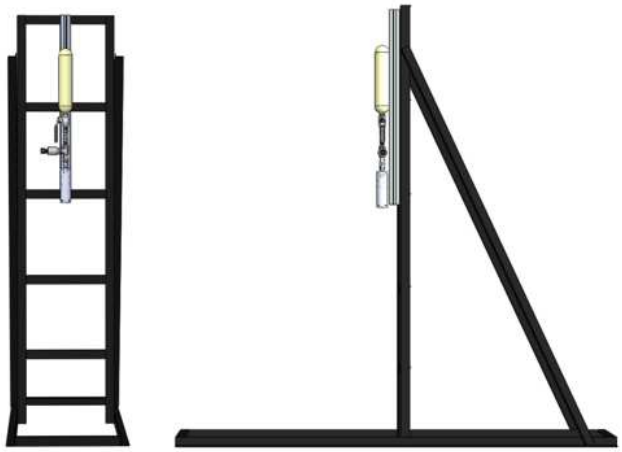

Figure 3-4. Solidworks model of the test stand.

The propellant was made by adding the metals to the polychloroprene binder and mixing slowly to prevent any metal dust being lofted in the air. The copper (II) oxide and sulfur were then added in and mixed thoroughly. Lastly, the ammonium nitrate was sifted into the mixture and mixed until a homogenous mixture was attained. The resultant mixture was laid out onto wax paper to cure (Figure 3-5). During curing, the propellant was torn into smaller pieces to increase surface area for faster curing. Once the propellant was fully cured, it was ground to a powder using a commercial grinder and sifted to achieve a uniform particle size of approximately 200 micron. This powder was then placed into the PVC liner and compressed with a 20-ton hydraulic press. The powder was compressed in stages to achieve an overall higher density in the grain. Once the desired amount of propellant was compressed into the PVC liner, the grain port was machined using a lathe. Polychloroprene's commercial use as a contact cement requires applying it to the bonding surfaces and then allowing it to partially cure. The surfaces are then brought together under compression until curing is complete. As a result, the high compression on the powdered grain made the end material easily machinable.

Figure 3-5. Curing A202 propellant.

Initial performance characteristics on the A202 propellant was acquired with Propellant Evaluation Program (PROPEP). The propellant constituents, and estimated combustion chamber pressure were input into the program to retrieve an approximate characteristic velocity, and specific impulse. Figure 3-6 displays the input propellant constituents and the estimated specific impulse, characteristic velocity, density, molecular weight, combustion chamber specific heat ratio, and combustion chamber temperature outputs. The estimated characteristic velocity and specific impulse were 3876.7 ft/sec and 147.7 sec, respectively. The entire output file, which included the combustion exhaust species, frozen and shifting specific impulses, chamber temperatures, and characteristic velocities, can be viewed in Appendix Figure A-1. Some of the combustion products can change from the combustion chamber to the nozzle exit. This can be in the form of phase changes and secondary chemical reactions and is known as shifting equilibrium[4]. Shifting equilibrium usually tends to overestimate the performance parameters (specific impulse and exhaust velocity) anywhere from 1% to 4% [4]. Frozen equilibrium is the term given for no change in phase or secondary reactions occurring from the chamber to the nozzle exit [4]. It underestimates the performance by approximately 1% to 4%. For the purposes of the solid motor testing, a frozen equilibrium was assumed due to the decrease in temperature and pressure as the combustion products travel through the divergent portion of the nozzle.

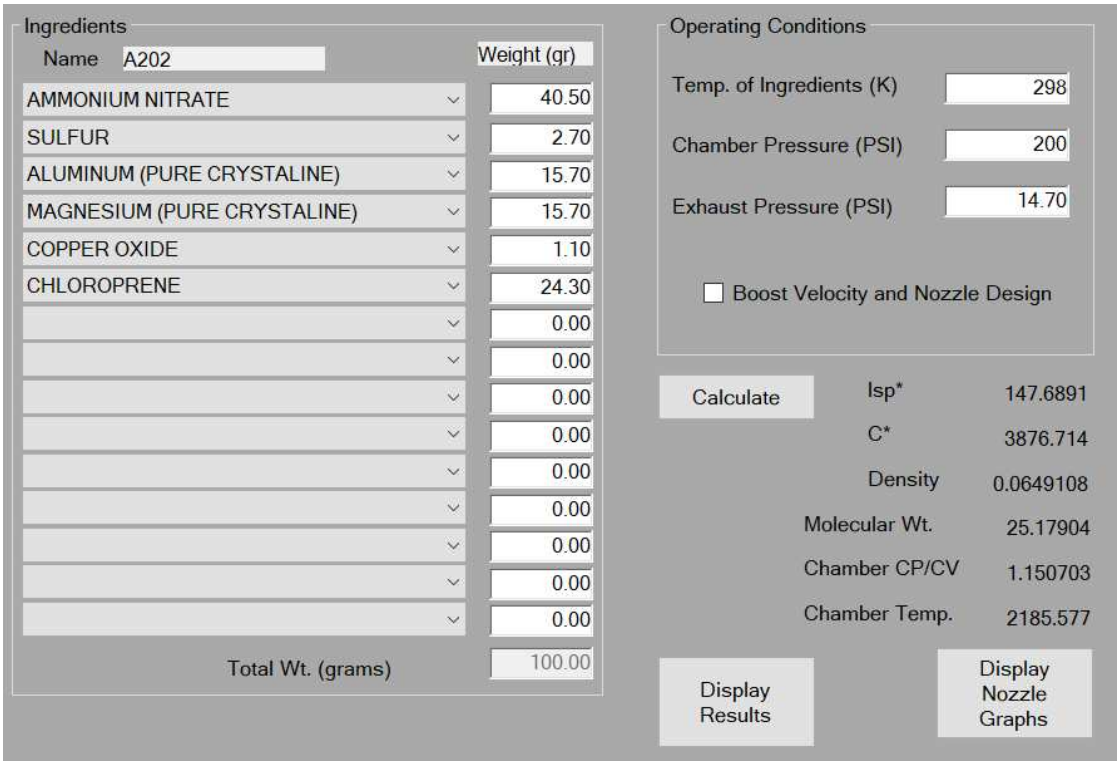

Figure 3-6. PROPEP simulation of A202 propellant.

The data acquisition system (DAQ) used to record combustion chamber pressure was a DATAQ DI-1110 USB Data Acquisition Starter Kit. An external 12-volt power supply provided power to the transducer, and the output signal line and ground was wired to the DAQ. The DAQ was connected to a USB to Ethernet adapter and fed into 150 feet of Ethernet cable. The end of the Ethernet cable finally connected to a laptop which then stored the data received from the transducer. The initial 110-volt power line was connected via an extension cord to a power outlet box and routed to the computer/arming circuit and the 12-volt power supply. The site chosen for the hot fire testing of both solid and hybrid motors was the Engineering Research Center (ERC). The ERC was an ideal location for testing as it was remote. The layout of the power, arming, ignition, and DAQ lines can be viewed below in Figure 3-7.

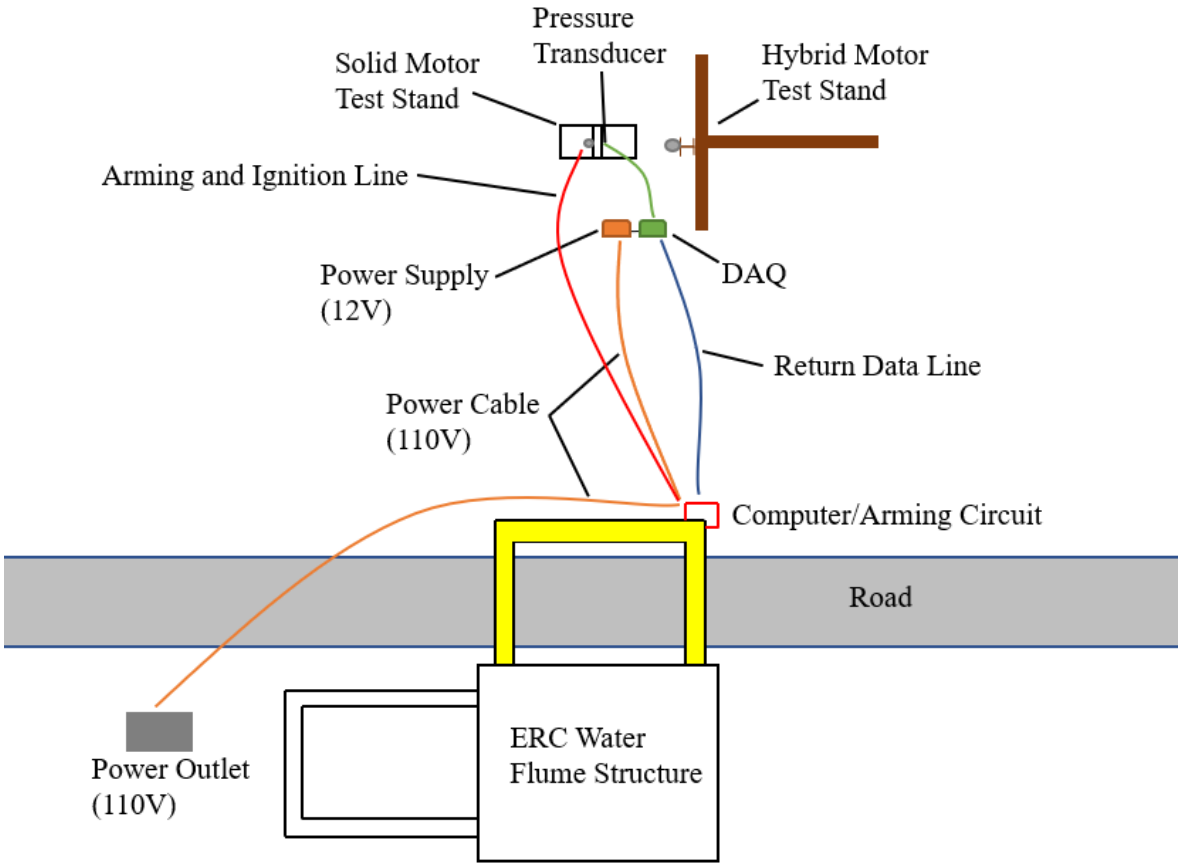

Figure 3-7. Layout of hot test fire components at the Engineering Research Center.

First Hot Test Fire

After the A202 grain was machined to achieve the proper length and core diameter (3.75 inches and 0.42 inches, respectively), it was placed into the casing, along with the graphite nozzle, forward closure. The motor assembly was then attached to the test stand. Once all of the power, arming, ignition, and DAQ lines were laid out and tested for continuity, the copper (II) oxide and magnesium thermite ignitor was placed through the nozzle and fed into the motor until it contacted the forward closure. The resulting combustion chamber pressure data from the hot test fire can be seen in the figure below.

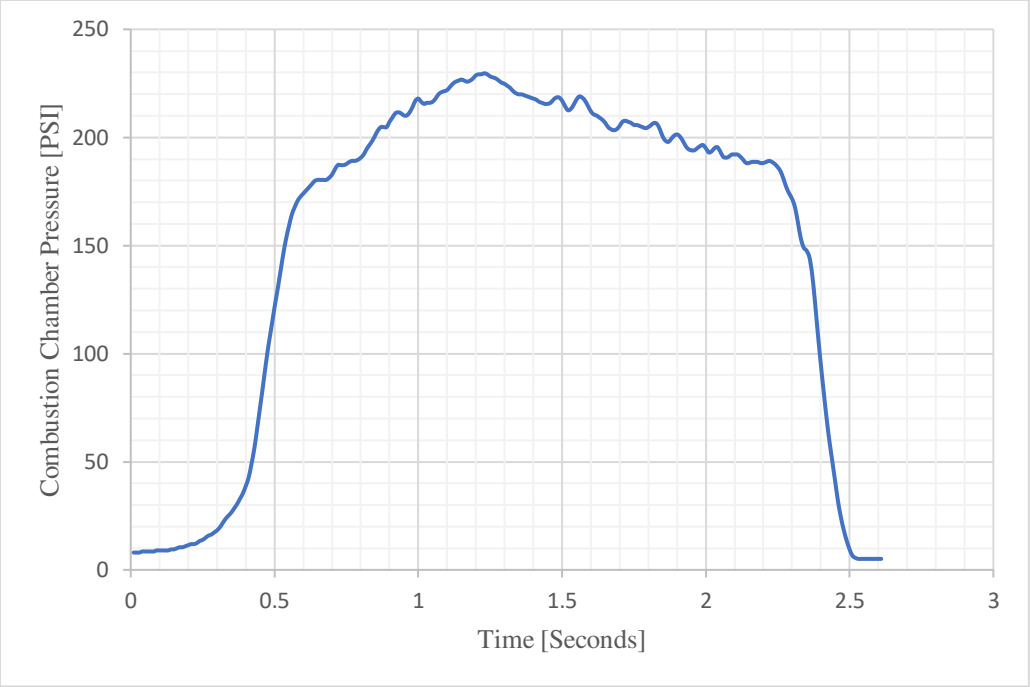

Figure 3-8. A202 solid motor with 0.25" nozzle diameter chamber pressure data.

The motor burned for an average of two seconds and reached an average combustion chamber pressure of 175 psi. From the pressure data in Figure 3-8, an actual characteristic velocity was calculated using equation 3-2 and compared with the PROPEP data.

$$C^* = \frac{A_t\, \Delta t}{m_p} \sum_{i=1}^{n} P_i \tag{3-2}$$

The characteristic velocity calculated was based on the area of the nozzle throat (A_t), the mass of the propellant (m_p), the time interval (Δt), and combustion chamber pressure increment (P_i) [20]. Taking the sum of each pressure value with its corresponding time interval and multiplying by the throat area divided by the propellant mass yielded a characteristic velocity of 2840 ft/sec. This value was then put back into BurnSim, a simulation program for estimating performance parameters of solid propellant rocket motors, to observe if the performance could be replicated. This can be seen below in Figure 3-9. The red line indicates the ratio of the total burning surface area (A_B) to the area of the nozzle throat and is denoted as Kn (equation 3-3). Typical values for

Kn range from 180 to 250 [21]. The initial Kn can be indicative of how well the start of combustion occurs in a motor.

$$Kn = \frac{A_B}{A_t} \tag{3-3}$$

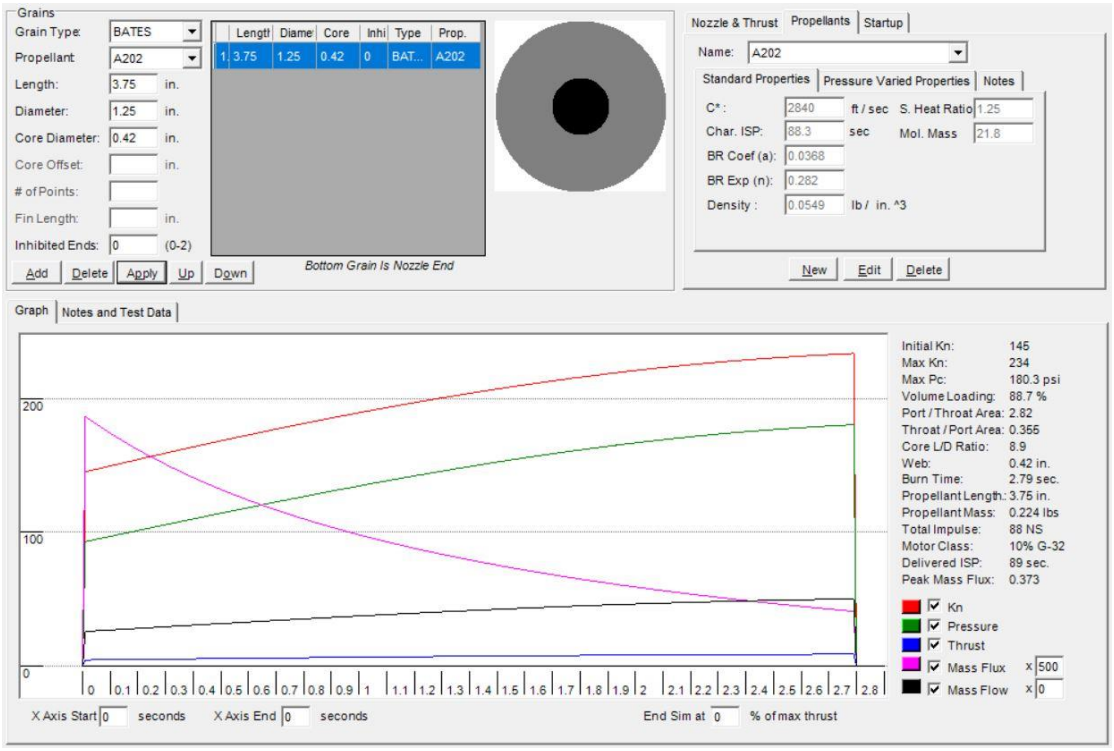

Figure 3-9. BurnSim evaluation of A202 solid motor with 0.25" nozzle.

BurnSim predicted a specific impulse of 89 seconds. A manual calculation was performed to check the accuracy of the simulation. A modified version of equation of 3-1 was used to acquire the thrust data from the combustion chamber pressure. This modified thrust equation simply excluded the thrust coefficient, C_F, as the solid motor nozzles used in testing did not possess divergent exits (i.e., the throat diameter was constant throughout the entire length of the nozzle).

$$F = A_t P_c \tag{3-4}$$

The thrust curve in Figure 3-10 was used to determine the total impulse of the motor, equivalent to the total area under the thrust curve. The total impulse was found by taking the sum of the

thrust values, then multiplying by the time interval, shown in equation 3-5. This resulted in a calculated total impulse of 19.46 lb-sec.

$$I_{tot} = \Delta t \sum_{i=1}^{n} F_i \tag{3-5}$$

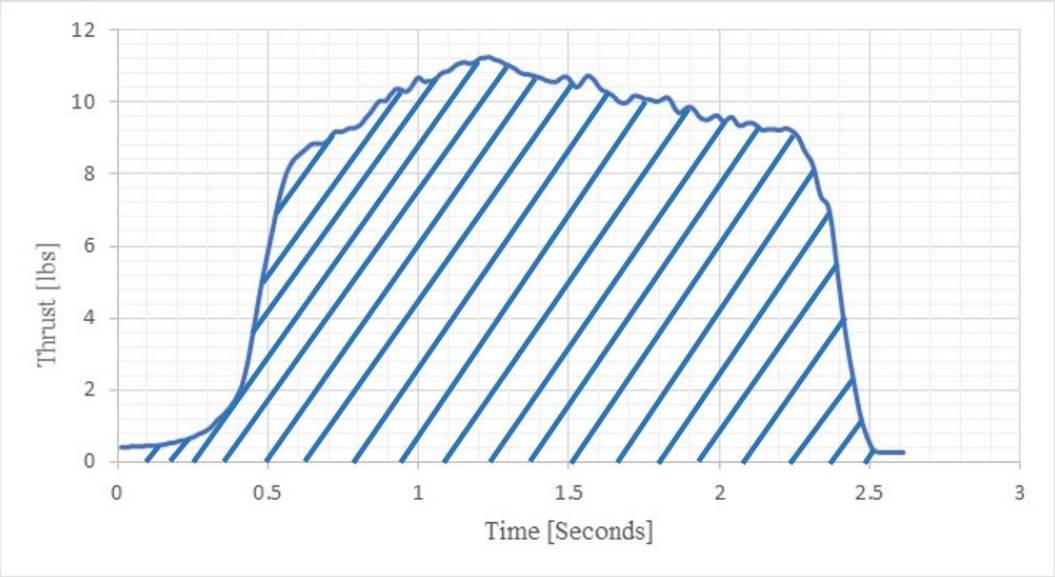

Figure 3-10. A202 solid motor with 0.25" nozzle diameter thrust data.

The specific impulse was then found through dividing the total impulse by the mass of the propellant burned, shown in equation 3-6. A calculated specific impulse value of 88.5 seconds appeared to be very similar to the predicted BurnSim specific impulse of 89 seconds.

$$Isp = \frac{I_{tot}}{m_p} \tag{3-6}$$

Figure 3-11. First hot fire test of A202 propellant.

Second Solid Hot Test Fire

The second hot test fire utilized the same configuration as the first, the only difference being in the size of the nozzle throat. The diameter was reduced from 0.25 inches to 0.2031 inches. The BurnSim simulation presented a progressive chamber pressure profile with a starting and maximum Kn of 220 and 354, respectively.

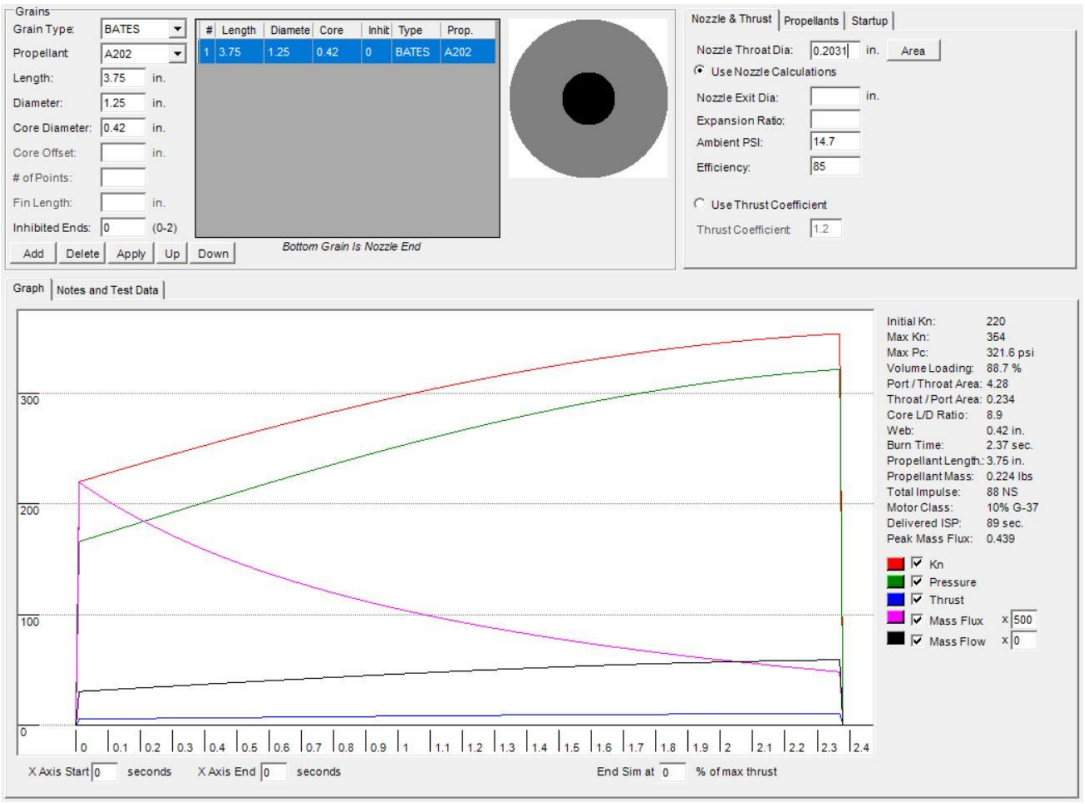

Figure 3-12. BurnSim evaluation of A202 solid motor with 0.2031" nozzle.

The same setup for the January 19th hot test fire was adopted for the second test in which the ignitor was placed through the nozzle and extended to the forward closure.

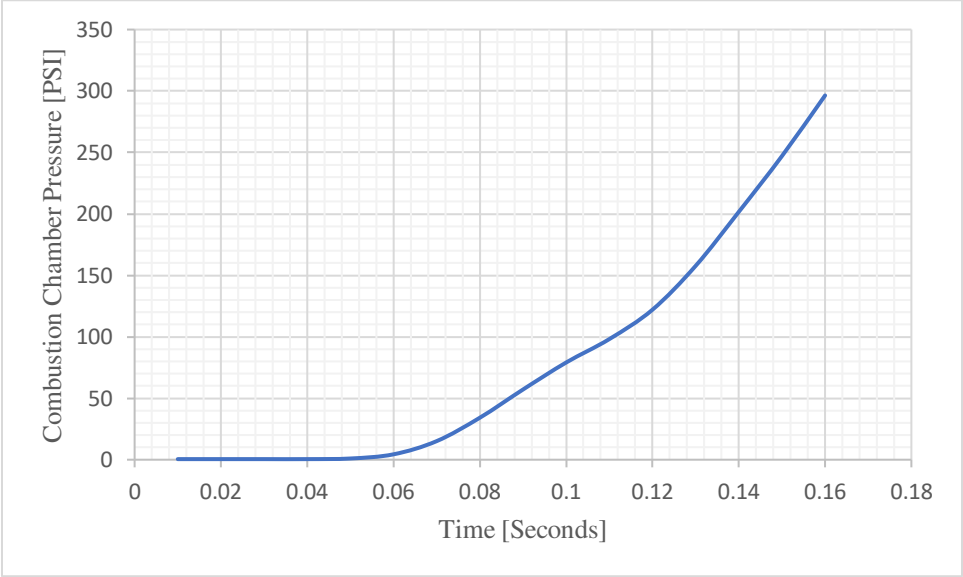

Figure 3-13. A202 solid motor with 0.2031" nozzle diameter chamber pressure data.

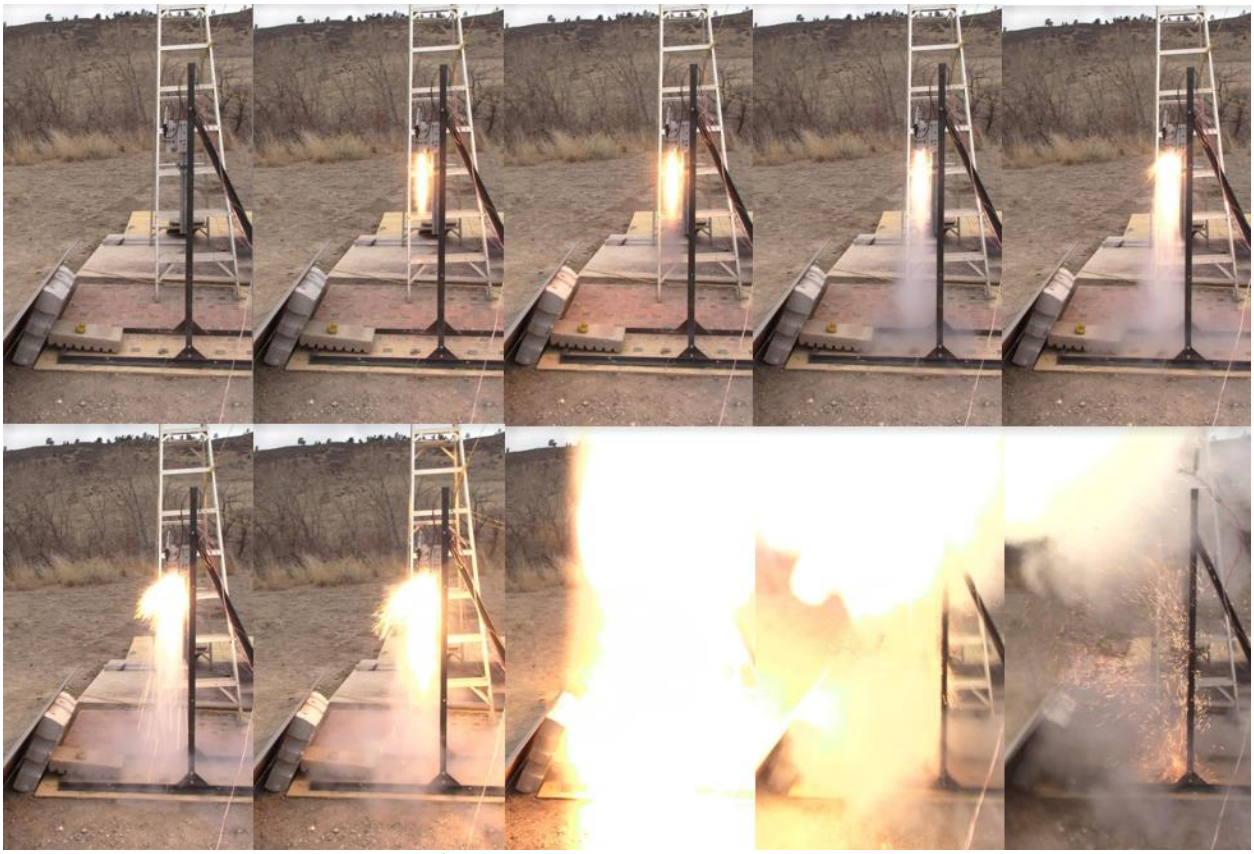

Figure 3-14. February 16th test of A202 propellant with 0.2031" diameter nozzle.

As seen in Figures 3-13 and 3-14, the combustion chamber pressure exceeded the structural limitations of the motor casing. The combustion chamber catastrophically failed at 300 psi resulting in the forward closure being expelled from the main casing. The rapid increase in chamber pressure indicated that the motor burned too progressively.

Third Solid Hot Test Fire

Two BurnSim files were compared to observe the difference in burn profile. In an attempt to achieve a more neutral burn profile, a Bates grain configuration was incorporated into the design. A Bates grain simply consists of a long grain that has been cut into segments. The segments increase the total burning surface area (additionally increasing the Kn) and result in a

more neutral burn profile. A diagram showing the segmented Bates grain motor is shown in Figure 3-15.

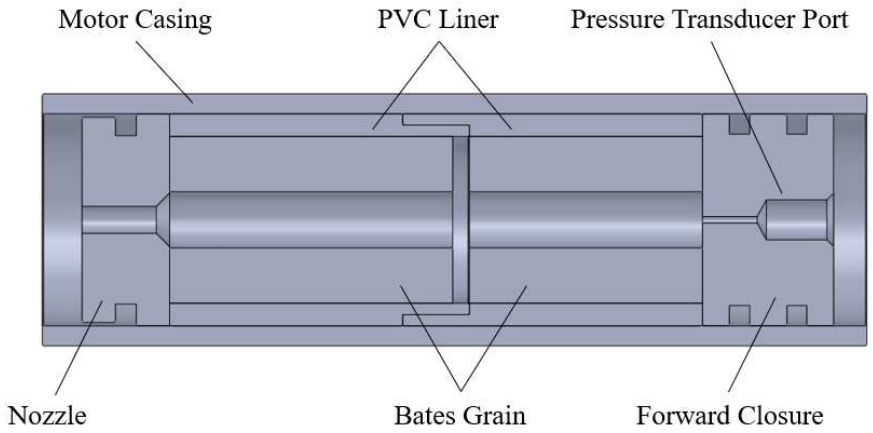

Figure 3-15. Solidworks model of solid motor with Bates grains.

Figures 3-16 and 3-17 show the simulation of a single and two grain solid motor with a 0.25 inch nozzle throat diameter. The maximum Kn for the single grain motor was 145, while the two-grain motor had a maximum Kn value of 212. The two-grain configuration simulation displayed a more neutral burn profile when compared to the single grain. This was the main motivation for switching to a two-grain motor.

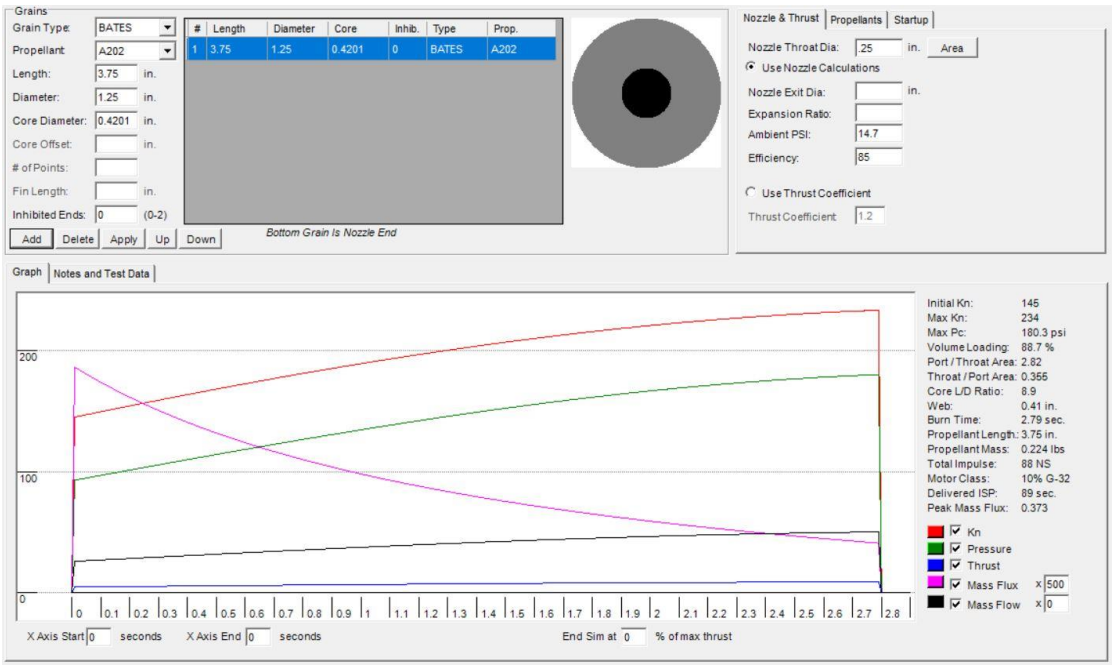

Figure 3-16. Single grain BurnSim prediction with 0.25” diameter nozzle.

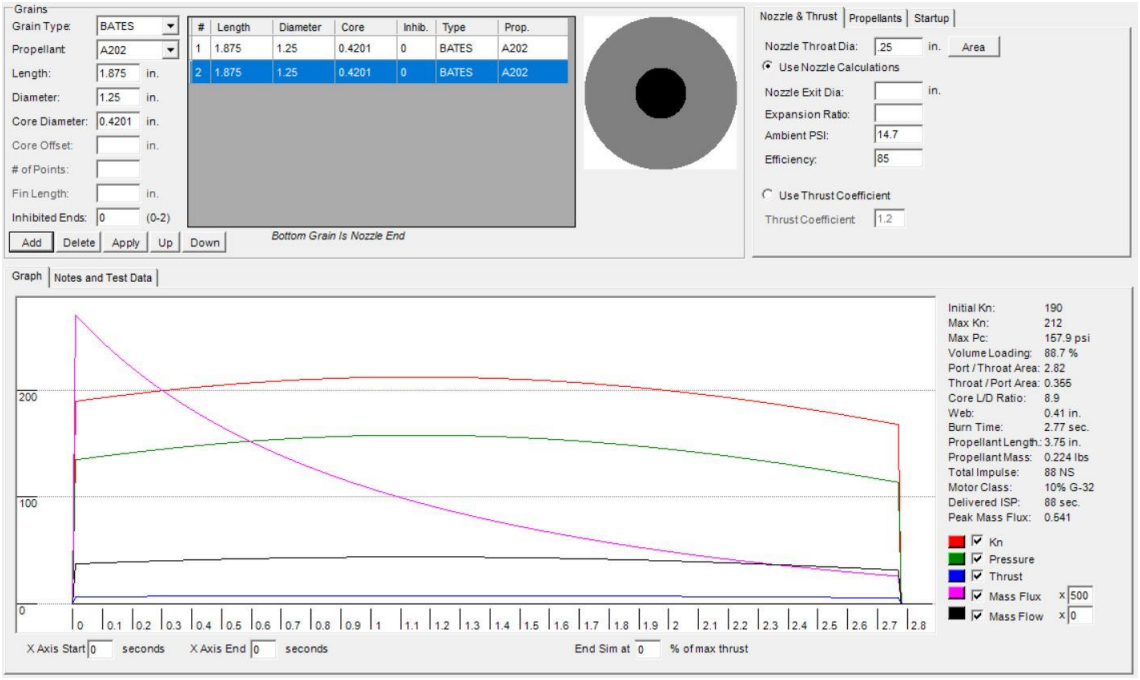

Figure 3-17. Two grain BurnSim prediction with 0.25” diameter nozzle.

The motor was fired (Figure 3-19), and the data were retrieved (Figure 3-18). When compared to the data of the first test fire in Figure 3-8, the chamber pressure increased by an average of 50

psi. This was expected due to the higher surface area, and thus higher Kn, even as the nozzle throat diameter was kept constant. The change in combustion chamber pressure was not, however, observed in the BurnSim simulation. This was determined to be associated with the exhaust velocity of the propellant being higher than the PROPEP code predicted.

The fourth hot test fire would have the same two grain configuration but would have a reduced nozzle throat diameter to increase the Kn and combustion chamber pressure.

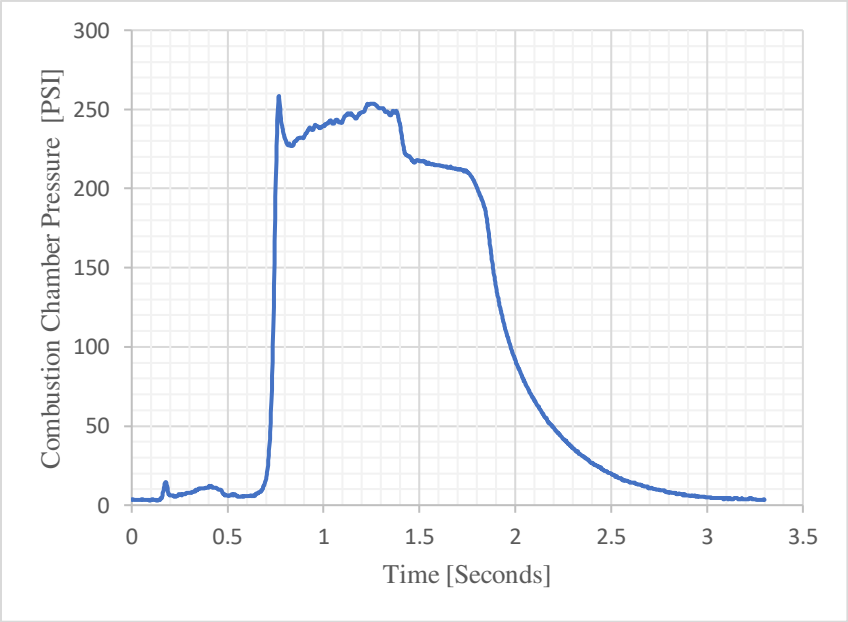

Figure 3-18. March 1st test of Bates grain chamber pressure data.

Figure 3-19. March 1st test of Bates grains.

Fourth Solid Hot Test Fire

The fourth test contained the same two grain configuration as the third test with the exception of the reduced nozzle throat diameter of 0.2031 inches. The BurnSim model that was created showed that the highest combustion chamber pressure the motor would produce was 281.7 psi with an initial and maximum Kn of 287 and 322, respectively. The model in Figure 3-20 additionally displays a shorter burn duration, which is indicative that the regression rate of the propellant increased with the increase in chamber pressure.

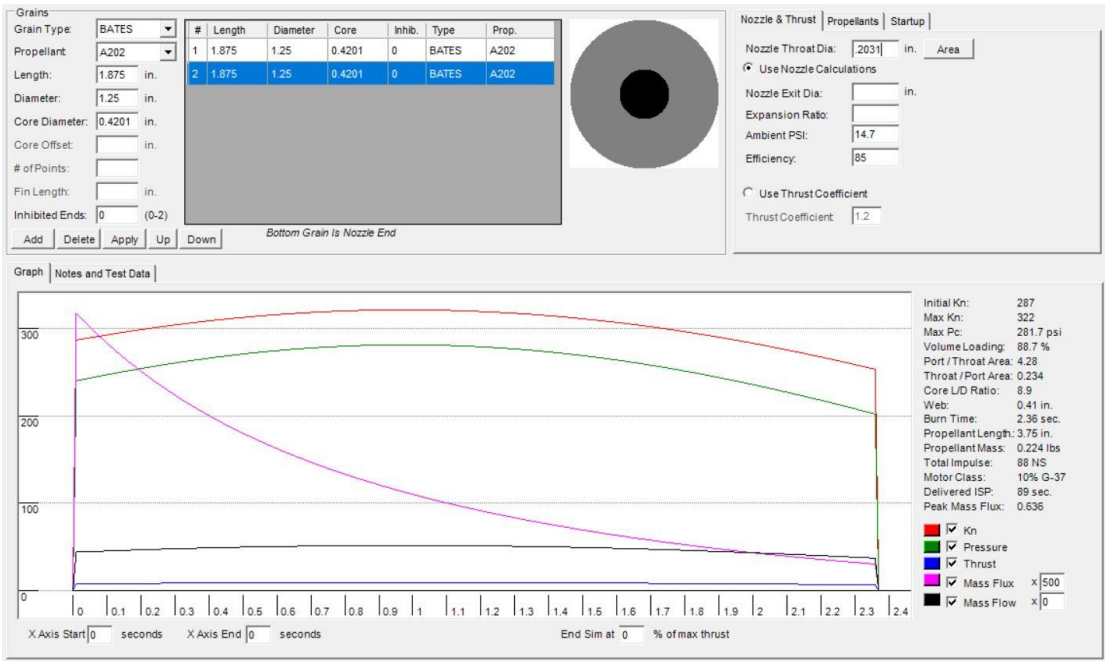

Figure 3-20. Two grain BurnSim prediction with 0.2031" diameter nozzle.

The motor was fired, and another over-pressurization occured. The data that was retrieved (Figure 3-21) was analyzed to determine the cause of failure. For 0.05 seconds, the motor was in a ramp up phase to a pressure of approximately 300 psi. From there, it reached steady state for 0.04 seconds until a secondary increase in pressure resulted in a breach in the casing. After the test, the inspection of the motor remains yielded many fragmented pieces of both the PVC liner and unburned propellant that were laying near the test stand. The remainder of the PVC liner that was still in the aluminum casing had a thin crack that propagated along the length of the grain. This crack (seen in Figure 3-22) was identified as the likely cause of the propellant cracking just after steady-state burning at 300 psi. The cracks that propagated during the burn increased the burning surface area, which caused the dramatic increase in pressure. As a result of this test and prior hot fire tests, it was determined that the A202 propellant was too brittle at combustion chamber pressures above 250 psi.

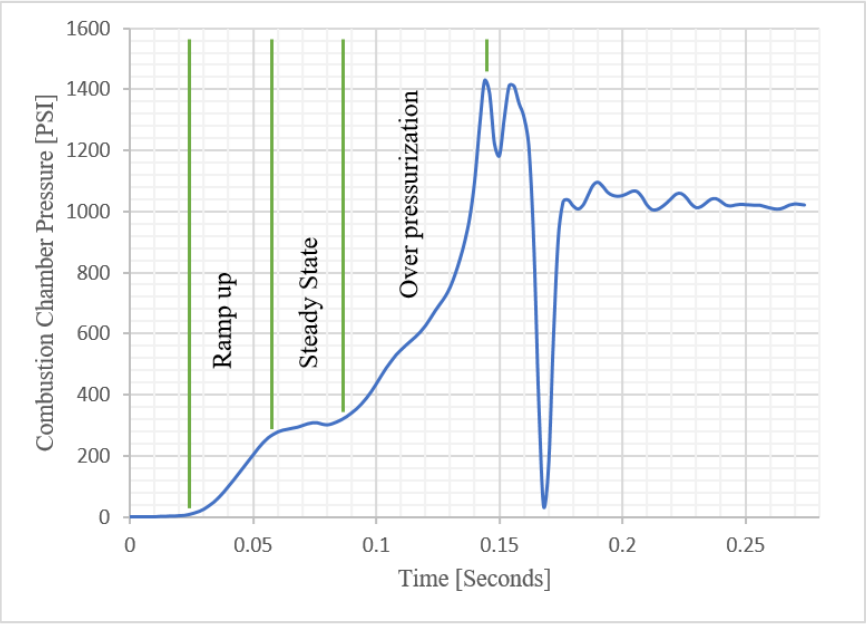

Figure 3-21. March 6th test of two grain motor chamber pressure data.

(a) (b)

Figure 3-22. March 6th test of two grain motor (a) and crack within PVC liner (b).

A203-A206 Solid Hot Test Fires

Due to the brittle nature of the A202 propellant, a more pliable propellant that could take the structural stress of a motor firing was sought for the continued development of a preheater grain for the hybrid rocket motor. The obvious choice on which component of the propellant to alter was the binder. The two additive binders that were considered were polybutadiene acrylonitrile (PBAN) and the previously mentioned, hydroxyl-terminated polybutadiene (HTPB). Depending on the other components of the propellant, both of these compounds become elastic once cured, similar to the rigidity of tire rubber. HTPB was chosen based on availability as the additive to the A202 propellant. The new A203 was mixed with a binder ratio of 50% polychloroprene and 50% HTPB with PAPI 94 curative. The results of this propellant were not favorable, as the mixture did not cure as a homogenous mixture. The next test propellant, A204, used solely HTPB and PAPI 94 as the binder. The PROPEP results are in Appendix Figures A-2 and A-3, and the composition is displayed in the table below:

Table 3-4. A204 propellant mass composition.

A204	
Ammonium Nitrate	54.5
Aluminum	20.0
Magnesium	5.0
Sulfur	0.5
Teflon (PTFE)	1.0
Copper (II) Oxide	1.0
R45 Binder (HTPB)	15.68
PAPI 94	2.32

Open air burn tests revealed that the A204 propellant could not sustain a flame sufficient enough for further testing. This led to increasing the chlorine production during burning to improve the regression rate by introducing Saran powder (polyvinylidene chloride). Table 3-5 shows the alterations made to the A204 propellant to form A205-A and A205-B.

Table 3-5. A205-A and A205-B propellant composition.

A205-A		**A205-B**	
Ammonium Nitrate	59.0	Ammonium Nitrate	68.0
Aluminum	10.0	Aluminum	5.0
Magnesium	5.25	Magnesium	3.0
Sulfur	0.75	Sulfur	1.0
Saran (PVDC)	3.0	Saran (PVDC)	2.0
Copper (II) Oxide	3.0	Copper (II) Oxide	2.0
Iron Oxide	1.0	Iron Oxide	1.0
R45 Binder (HTPB)	15.68	R45 Binder (HTPB)	15.68
PAPI 94	2.32	PAPI 94	2.32

The A205-B propellant was used for the next hot fire test as it had a slightly higher burn rate than A205-A when two samples of each propellant of the same mass were burned in open air. The grains were prepared and arranged in a two grain configuration with a 0.28125 inch (9/32”) diameter nozzle throat. The nozzle throat diameter was increased to decrease the Kn to an initial value of 150 and a max value of 168 in a conservative approach after the previous over-pressurizations of the motor. The motor was fired and immediately experienced a phenomenon known as chuffing. Chuffing occurs when rapid combustion of propellant cannot be sustained due to a lack of combustion chamber pressure. This exhibits itself as rapid bursts of pressure that may exit the nozzle at a supersonic velocity but quickly diminishes to atmospheric burning [22].

The motor then builds up enough pressure to initiate rapid burning once again, and the cycle repeats itself until all the propellant is depleted. Chuffing can be seen in the combustion chamber pressure data in Figure 3-23.

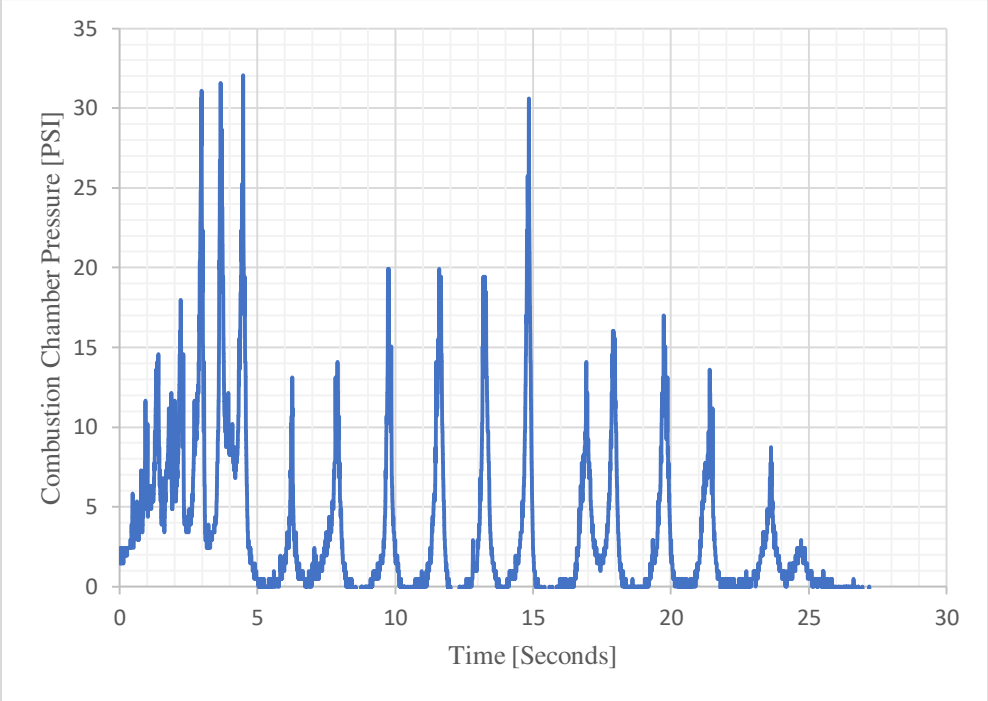

Figure 3-23. March 21st chamber pressure data.

In an attempt to increase the decomposition of the ammonium nitrate, copper chloride was synthesized to act as an additional catalyst as it was more easily prepared than other chlorine donors. The synthesis utilized copper metal, hydrogen peroxide, and hydrochloric acid as the reactants and produced copper chloride and water as the products (3-7).

$$Cu + 2HCl + H_2O_2 \rightarrow CuCl_2 + 2H_2O \quad (3\text{-}7)$$

Figure 3-24. Copper chloride synthesis.

The addition of 2% copper chloride, unfortunately, did little to improve the burning rate of the A205-B propellant. Open-air tests showed a negligible decrease in the time for a test sample piece (0.75 inch diameter, 1 inch length) to burn. The decision was then made to acquire a small quantity of ammonium perchlorate to add to the oxidizer mixture to support the decomposition of the ammonium nitrate. The new propellant, designated as A206-A, was prepared for open-air tests to observe the viability adding a small percentage of ammonium perchlorate as the oxidizer.

Table 3-6. A206-A propellant composition

A206-A	
Ammonium Nitrate	48.0
Ammonium Perchlorate	18.0
Aluminum	6.0
Magnesium	3.0
Copper (II) Oxide	2.0
Saran	1.0

Iron Oxide	1.0
R45 Binder (HTPB)	15.68
PAPI 94	2.32
Isodecyl Pelargonate (IDP)	3.0

A206-A additionally incorporated a plasticizer called Isodecyl Pelargonate (IDP). The plasticizer aided in the mixing and casting, making the propellant less viscous and easier to work with while maintaining the same density. Several test pieces that were burned in open-air (Figure 3-25) showed promise as the burn time was reduced, indicating a higher regression rate. This propellant was then cast into a PVC liner, machined, and was prepared for the next hot test fire in a two grain motor configuration. The nozzle throat diameter was kept at 0.2813 inches to maintain a conservative Kn and combustion chamber pressure.

Figure 3-25. A206-A open air burn test.

The motor was ignited and did not reach the desired the combustion chamber pressure. Chuffing occurred again in a similar fashion as the previous test but it occurred at an increased average chamber pressure (Figure 3-26).

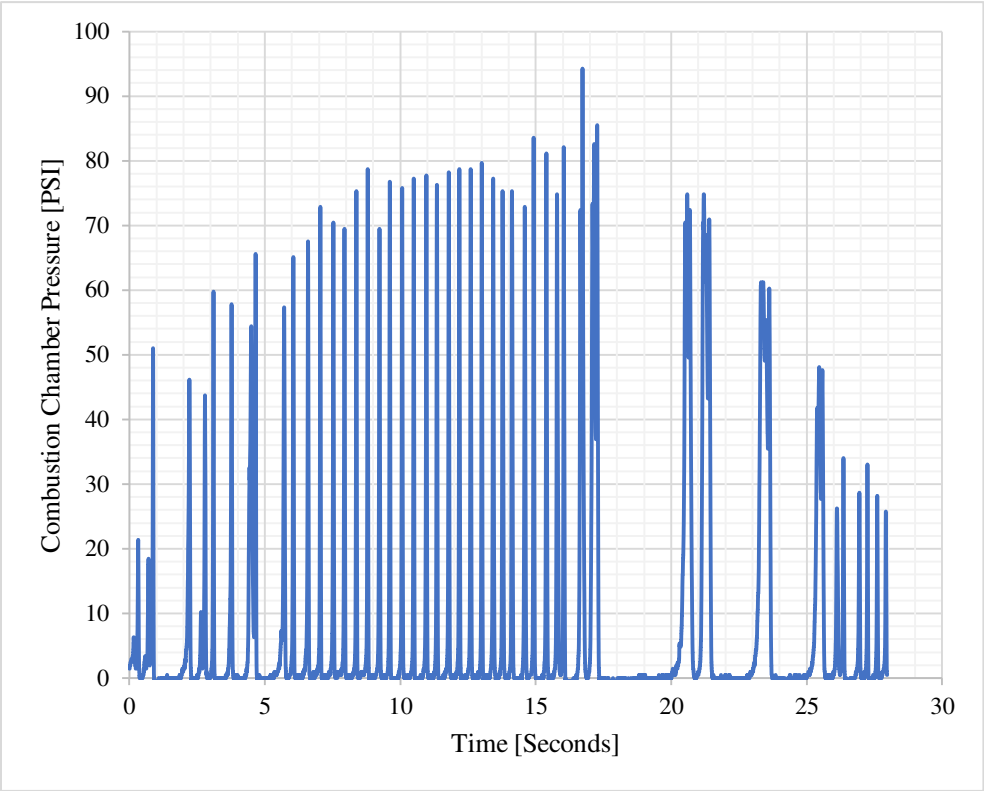

Figure 3-26. April 5th chamber pressure data.

The next alteration increased the Kn by increasing the burning surface area and reducing the nozzle throat diameter. The nozzle throat diameter was reduced from 0.28125 inches to 0.25 inches, and the third grain was added, increasing the total length of the motor by 1.875 inches. Additionally, the final changes were made to the A206 propellant. The A206-B propellant incorporated an increase in ammonium perchlorate to aid in raising the combustion temperature and increase the chlorine output to help decomposition of the ammonium nitrate (Appendix Figures A-6 and A-7).

Table 3-7. A206-B propellant composition

A206-B	
Ammonium Nitrate	41.0
Ammonium Perchlorate	26.0
Aluminum	7.0
Magnesium	3.0
Copper (II) Oxide	4.0
Iron Oxide	1.0
R45 Binder (HTPB)	14.0
PAPI 94	2.0
Isodecyl Pelargonate (IDP)	2.0

The three grain motor was fired, and the data were gathered. The chuffing produced was yet again higher in chamber pressure (Figure 3-27). Each pulse that developed progressively increased in duration, an indication that the increased initial Kn ratio was closer to the value needed to sustain combustion chamber pressure. This was encouraging as the nozzle throat diameter could be reduced further, and the burning surface area could be increased without overt concern of over pressurization to the motor casing.

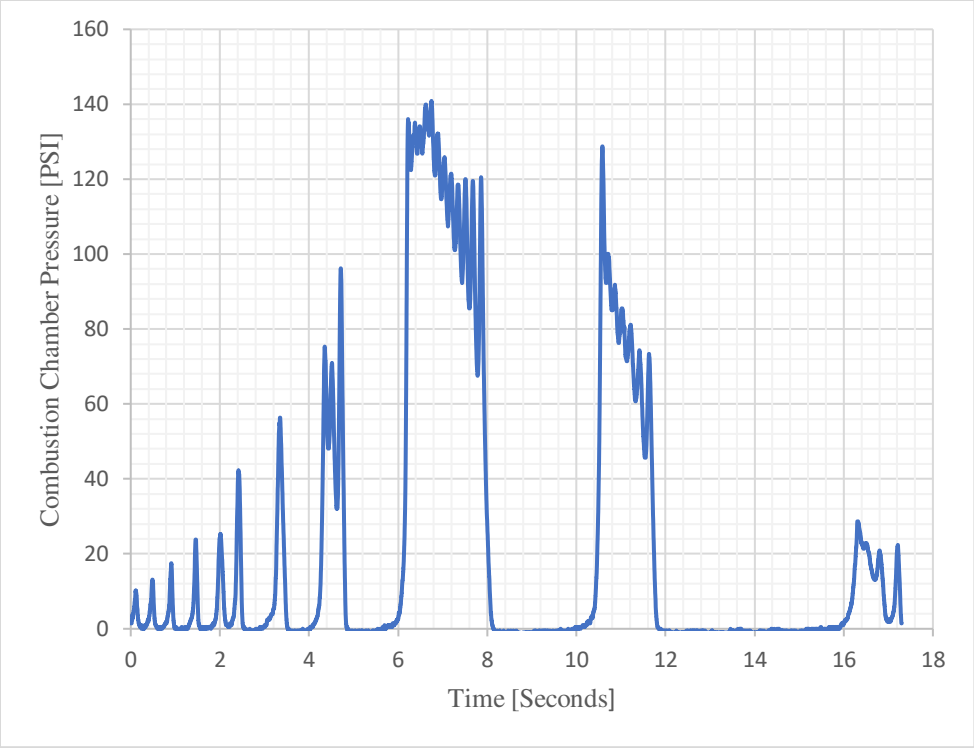

Figure 3-27. April 7th chamber pressure data.

Eighth Solid Hot Test Fire

The next motor design utilized a 0.25 inch nozzle throat diameter. It also contained four grains to increase the burning surface area. All other geometrical parameters remained constant. The four grain configuration can be viewed in Figure 3-28. The ends of each grain were beveled to five degrees to ensure adequate flame propagation for ignition.

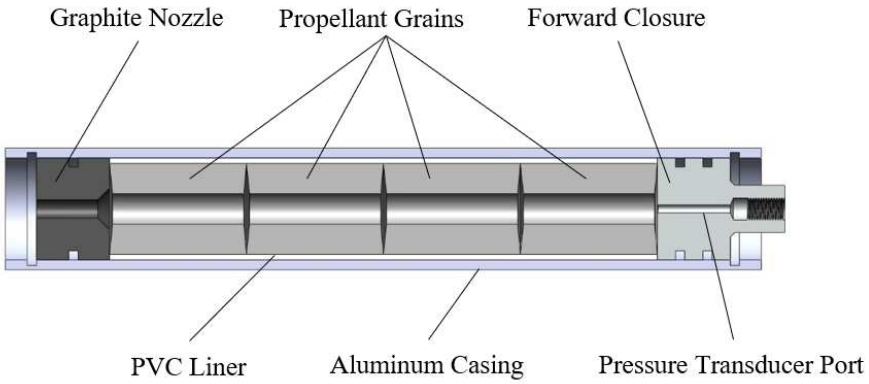

Figure 3-28. Four grain motor configuration.

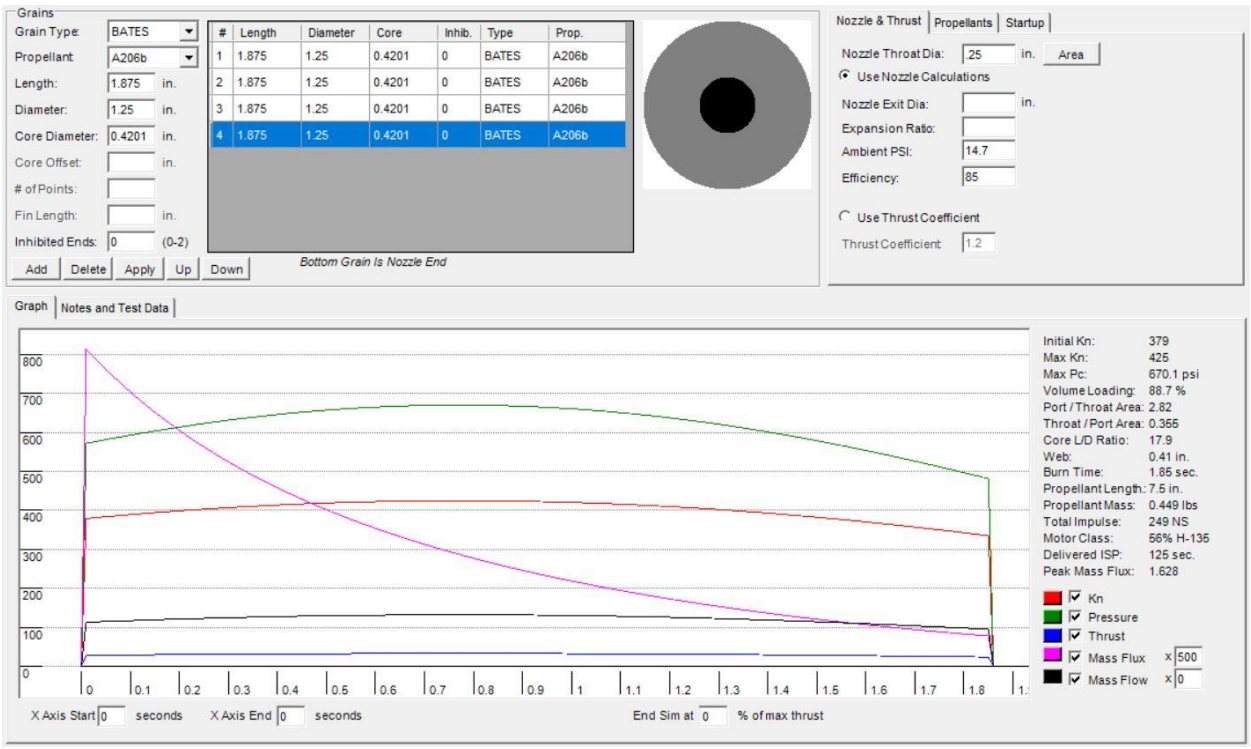

Figure 3-29. BurnSim simulation of A206-B four grain motor with 0.25 inch nozzle.

The BurnSim simulation (Figure 3-29) projected an initial Kn of 379 and a maximum Kn of 426. The maximum combustion chamber pressure was predicted to be 670.1 psi.

The motor was ignited and successfully burned for approximately two seconds at an average combustion chamber pressure of 550 psi and a maximum chamber pressure of 610 psi (Figure 3-30). This result corresponded well with the BurnSim predictions. The Kn values from the hot fire test reinforced the notion that the polychloroprene binder based propellants may have been too brittle to handle the structural loading from elevated chamber pressure conditions.

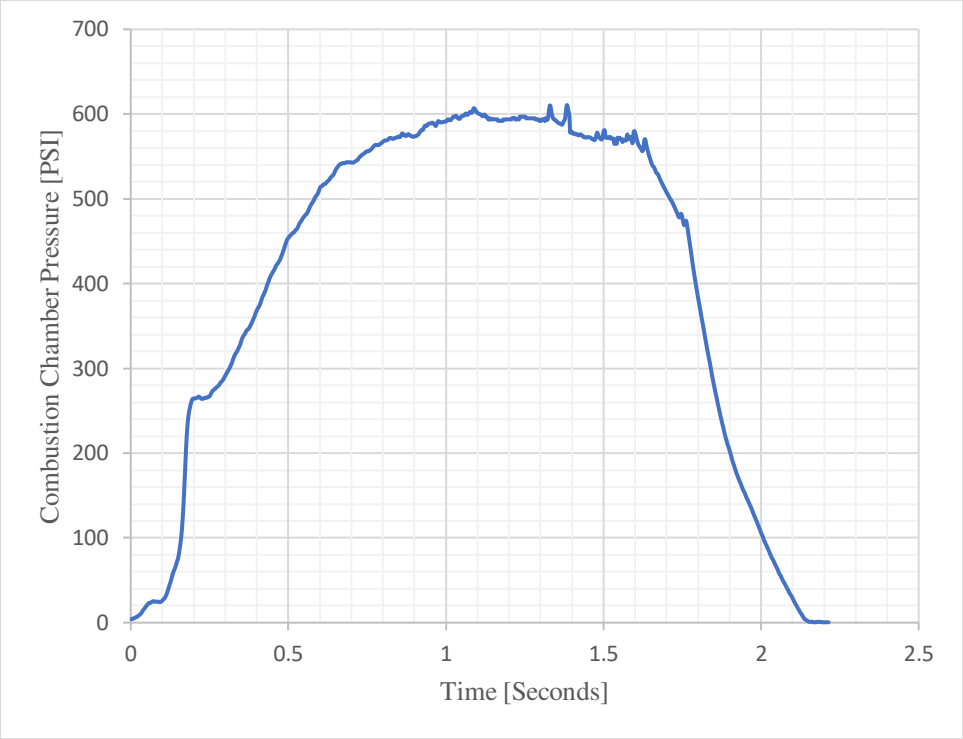

Figure 3-30. April 12th chamber pressure data.

Figure 3-31. April 12th hot fire test.

Ninth and Tenth Solid Hot Test Fire

The next test utilized the A206-B propellant and had an identical grain configuration as the previous test. A new graphite nozzle was designed and machined with a throat diameter of 0.21875 (7/32) inches to increase the initial Kn to 495 and the maximum Kn to 555. Figure 3-32 displays the BurnSim prediction for the reduced nozzle throat.

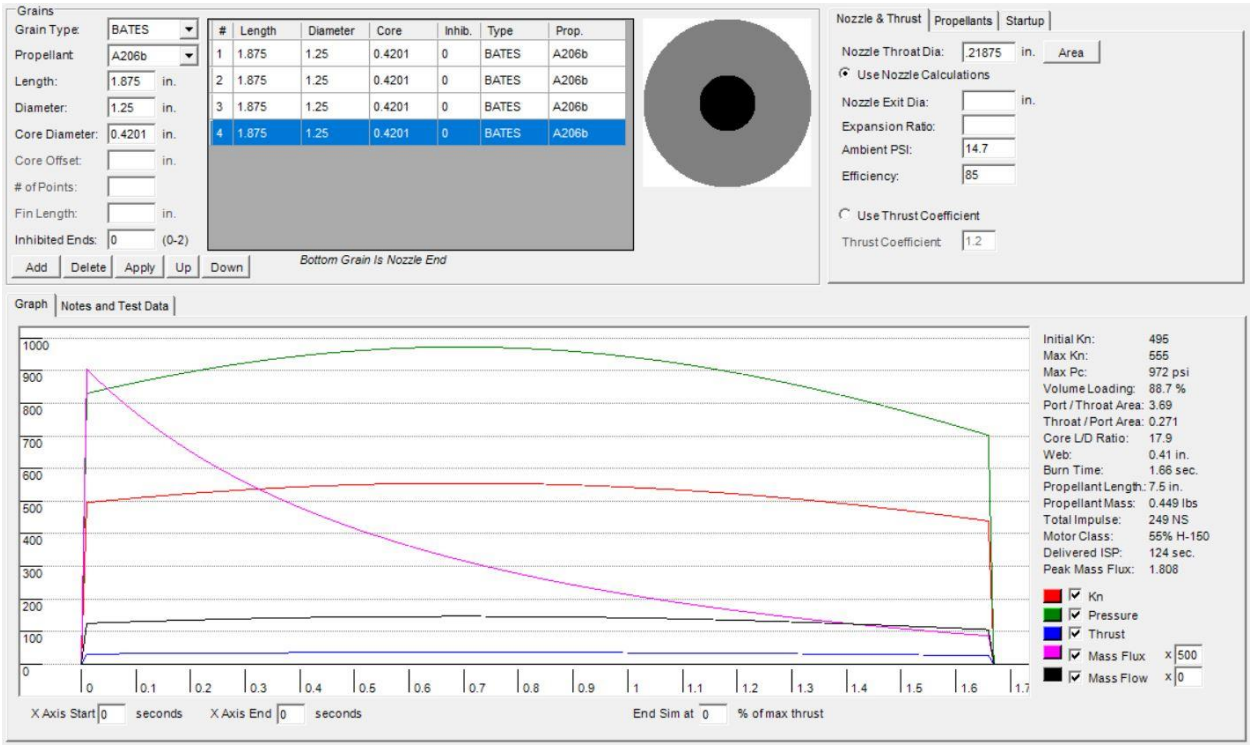

Figure 3-32. BurnSim simulation of A206-B four grain motor with 0.21875 inch nozzle.

The motor was ignited and fired successfully (Figure 3-33). However, the data were not retrieved. It was determined that an exposed wire in the ignition line might have been close enough to the DATAQ input terminal block to have contacted, causing a reset to the data acquisition system during the burn. More propellant was cast and machined to perform an identical test with the 0.21875 inch nozzle throat diameter.

Figure 3-33. April 14th hot fire test at moment of ignition.

While taking more precautions with cable management, the motor was cleaned and reassembled for another hot test fire. The motor was then ignited, and the data were successfully retrieved. The combustion chamber pressure data (Figure 3-34) showed a progressive burn for the first second of firing, then leveled to a more neutral burn profile for the last 0.6 seconds. Though not exact in matching the BurnSim prediction in Figure 3-32, the data were similar enough in chamber pressure and duration of burn to validate predictions using different parameters of burning surface area and nozzle throat diameter.

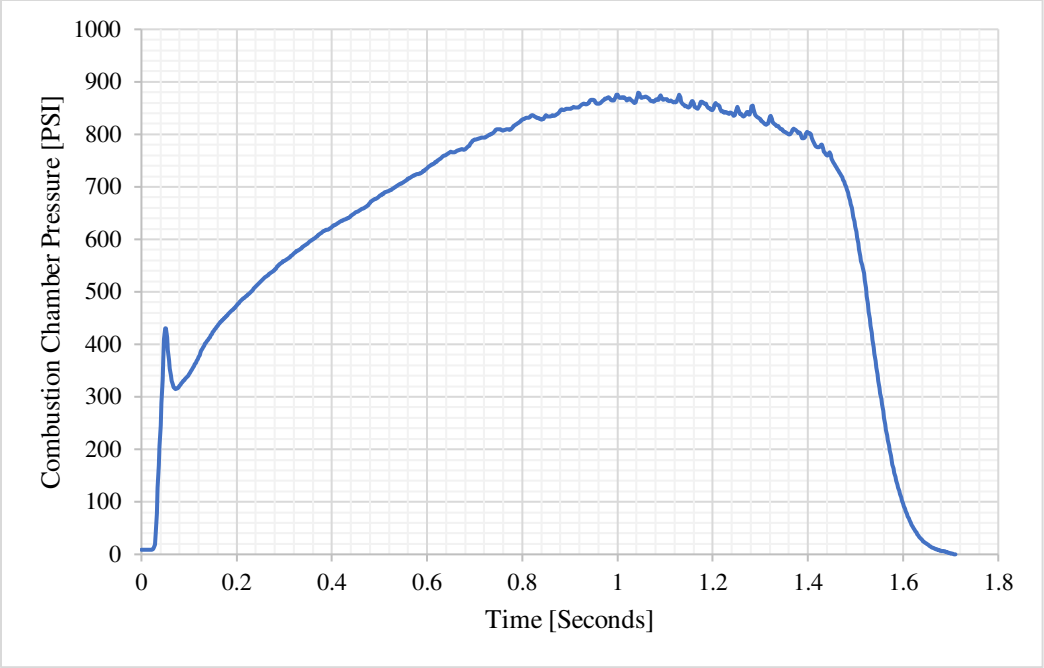

Figure 3-34. April 20th chamber pressure data.

Figure 3-35. April 20th hot fire test.

Determination of A206-B Regression Rate

Due to limited time and resources, it was decided to use the previous two tests with A206-B propellant to determine a theoretical regression rate rather than casting another propellant grain and machining a new 0.28125 (9/32) inch nozzle. PROPEP calculations were completed to determine the regression rate from the mass of the propellant grains, average thrust, combustion chamber pressure, burn time, and nozzle throat diameter.

Figure 3-36. PROPEP grain dimension and mass input.

Figure 3-36 shows the first window input parameters for the grains' geometry, number of grains, and the mass of each grain. At the bottom of the window, an output density per grain was given. The next window, seen in Figure 3-37, required the average thrust, average, combustion chamber pressure, burn time, total impulse, and nozzle throat diameter.

	Burn 1 Avg.	Burn 2 Avg.
Thrust	21.84	25.52
Pressure	445.06	678.98
Burn Time	2.00	1.60
Impulse	43.69	40.83
Nozzle Throat	0.2500	0.2188

Figure 3-37. PROPEP burn parameters input.

In order to find the average thrust and average combustion chamber pressure, the total impulse was first calculated using equation 3-5. This was then divided by the time duration of steady-state burning (labeled Burn Time in Figure 3-37) to get the average thrust [20]. The average thrust and the diameter of the nozzle throat were then used in conjunction with the average thrust to achieve the average combustion chamber pressure. For both test fires, the average combustion chamber pressure can be viewed in Figure 3-38.

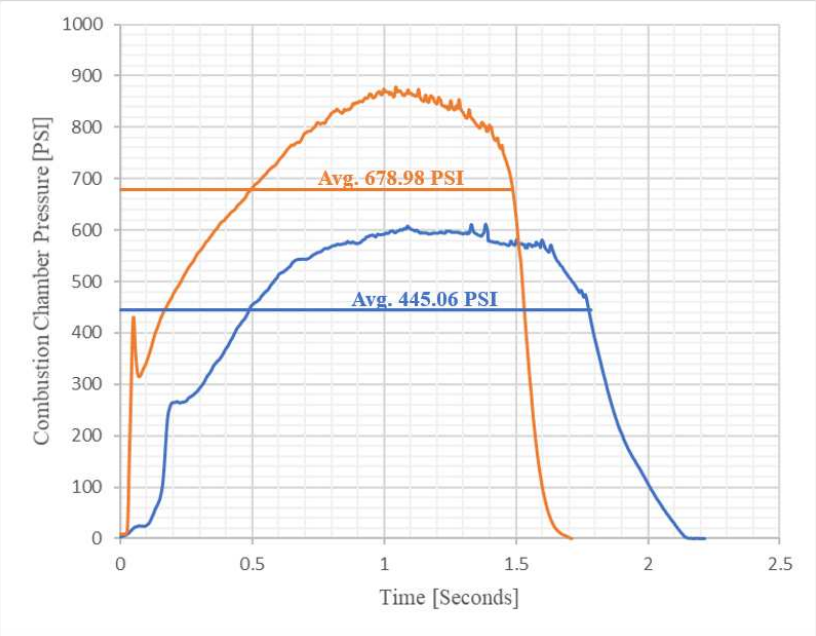

Figure 3-38. April 14th and 20th test fires with respective average chamber pressures overlaid.

After these values were placed in the PROPEP input windows, the output burn rate coefficient (a) and burn rate exponent (n) were given Figure 3-39. The equation for the regression was given as the following:

$$Y = 0.008275\ X^{0.52832} \tag{3-7}$$

where Y is the regression rate in inches per second, and X is the combustion chamber pressure.

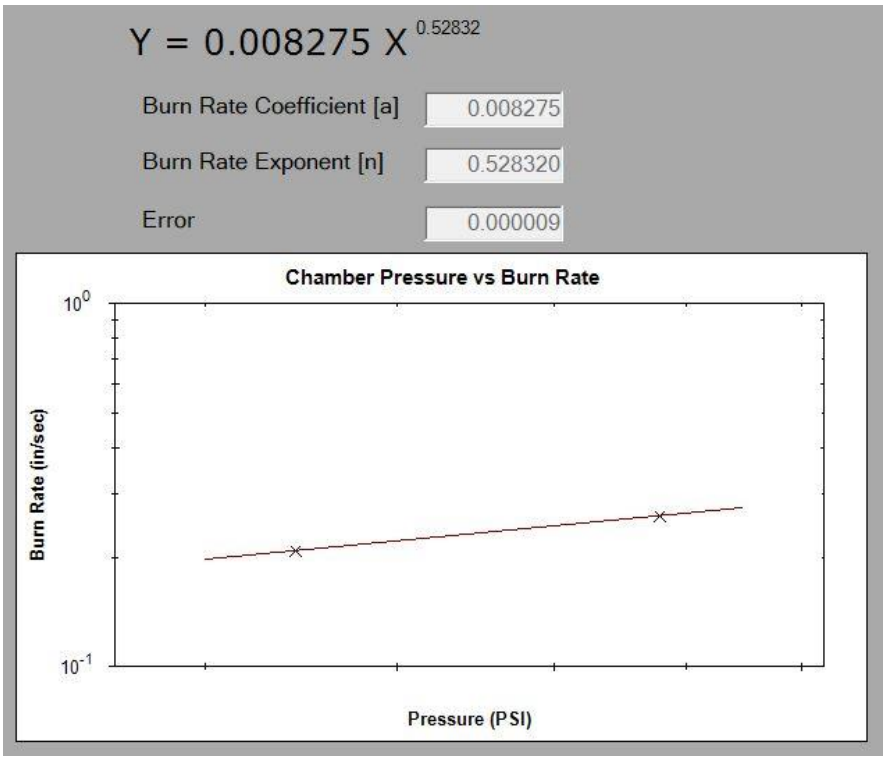

Figure 3-39. PROPEP regression rate output.

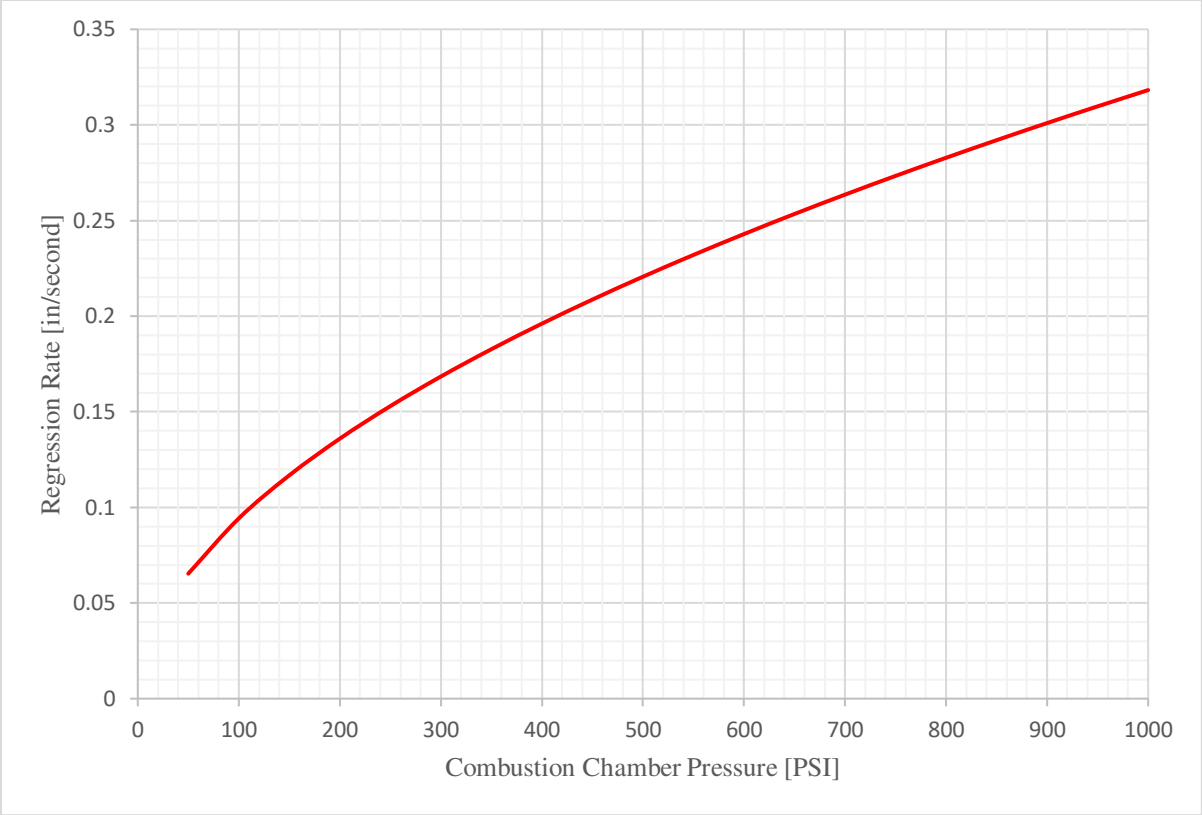

Figure 3-40. Regression rate of A206-B propellant.

This result was then graphed over a combustion chamber pressure range of 50 to 1000 psi (Figure 3-40). A simulated third test fire was added into PROPEP to observe the differences between the calculated regression rate equation from two test fires to three test fires. A BurnSim prediction (Appendix Figures A-9, A-10, and A-11) was made with the same grain geometry as the previous two tests, with a new nozzle throat diameter of 0.28125 inches. The average combustion chamber pressure and average thrust were calculated to be 277.19 psi and 17.22 lbf, respectively. This was then used to find the regression rate equation, seen below.

$$Y = 0.018409\ X^{0.402876} \tag{3-8}$$

This result was then graphed against the first regression rate equation to observe if there was enough of a difference to warrant a third test fire (Figure 3-41).

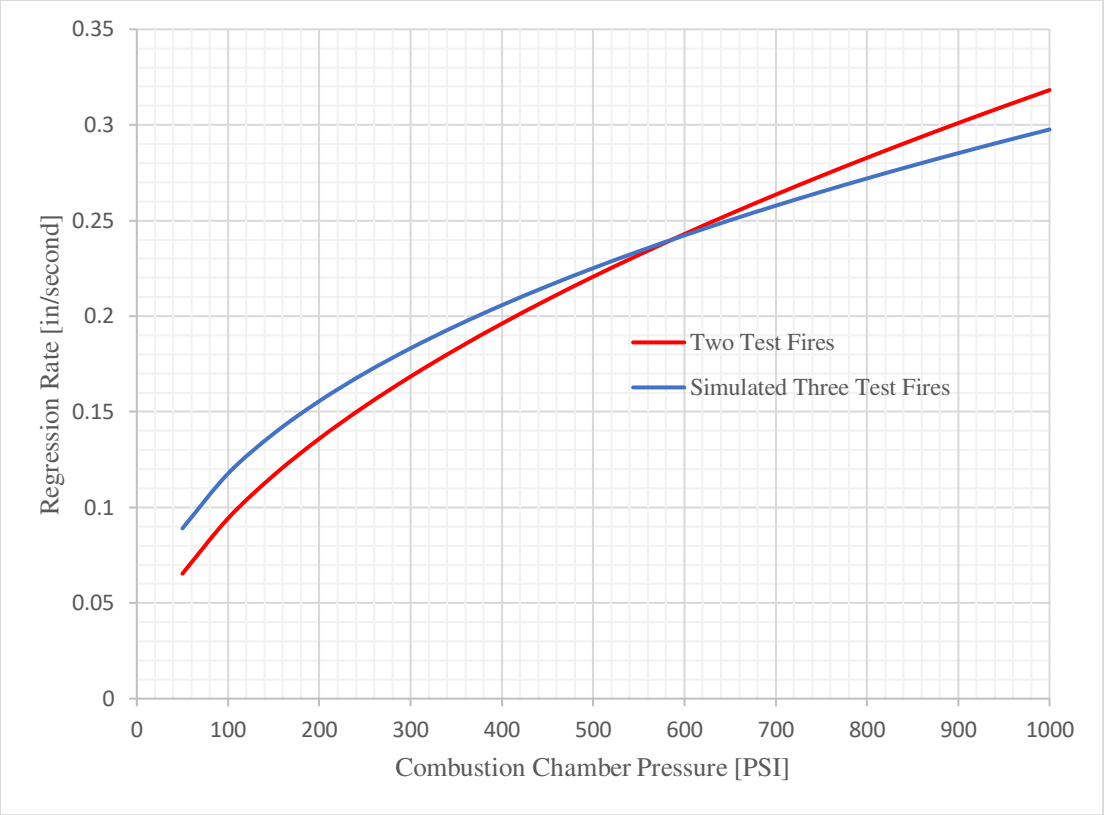

Figure 3-41. Regression rate of A206-B propellant with simulated three test fire regression rate.

The two regression rate profiles looked similar enough to be confident in further predictions in use as a hybrid preheater grain. The difference in regression rate at 200 psi was only 0.0197 inches per second, an acceptable difference for using the two test data.

CHAPTER 4 – DESIGN, MANUFACTURING, AND TESTING OF HYBRID SYSTEM

Parameters and Nozzle Design

The design parameters of the hybrid motor started with setting limits on cost and ease of manufacturing. A Microsoft Excel spreadsheet (Appendix Figures B-1 and B-2) was utilized to model the behavior of a simple hybrid rocket motor with various geometrical and physical input parameters. The starting design parameter was a combustion chamber pressure of 200 psi. From this, the thrust coefficient was calculated using equation 4-1 below where P_e represents the exit pressure, and γ is the ratio of specific heats. The coefficient of thrust was now included in the calculations as nozzle used for the hybrid motor was a De Laval nozzle with a convergent flow entry and a divergent flow exit.

$$C_F = \sqrt{\left[\left(\frac{2\,\gamma^2}{\gamma-1}\right)\left(\frac{2}{\gamma+1}\right)\right]^{\frac{\gamma+1}{\gamma-1}}\left(1-\left(\frac{P_e}{P_c}\right)^{\frac{\gamma-1}{\gamma}}\right)} \tag{4-1}$$

The coefficient of thrust was then fed back into equation 3-1, rearranged to attain the nozzle throat area.

$$A_t = \frac{F}{C_F\,P_c} \tag{4-2}$$

The throat area equated to an approximated 0.5 inch throat diameter. To achieve the exit area (A_e), the following equation was used:

$$\frac{A_t}{A_e} = \left(\frac{\gamma+1}{2}\right)^{\frac{1}{\gamma-1}}\left(\frac{P_e}{P_c}\right)^{\frac{1}{\gamma}}\sqrt{\left(\frac{\gamma+1}{\gamma-1}\right)\left(1-\left(\frac{P_e}{P_c}\right)^{\frac{\gamma-1}{\gamma}}\right)} \tag{4-3}$$

The nozzle was designed with a 45 degree convergent angle and 15 degree divergent angle. The design incorporates a two part construction comprised of a steel carrier with a graphite insert (Figure 4-1).

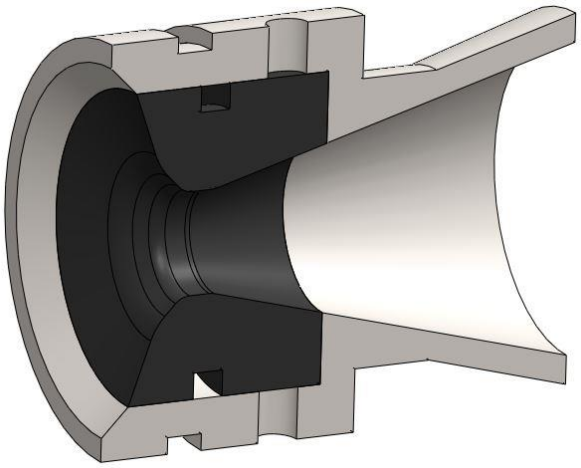

Figure 4-1. CAD rendering of hybrid motor nozzle assembly.

A total oxidizer mass of one pound was decided used in the calculations. The average density between the carbon dioxide and nitrous oxide was used to determine the oxidizer tank dimensions. A mass flow rate ($\dot{m}_o$) of 0.25 pounds per second was used to further calculate the characteristic velocity to check against the NASA CEA code.

$$C^* = \frac{P_c A_t}{\dot{m_{tot}}} \tag{4-4}$$

where

$$\dot{m_{tot}} = \dot{m}_o + \dot{m}_f \tag{4-5}$$

$$\dot{m}_f = \dot{r}\ \rho_f\ A_B \tag{4-6}$$

$$\dot{r}_{hybrid} = a\left(\frac{\dot{m}_o}{A_{port}}\right)^n \tag{4-7}$$

To find the mass flow rate of the fuel, $\dot{m}_f$, the regression rate was calculated using known values for the burning rate coefficient and exponent a and n from Chiaverini, M. J., & Kuo, K. K. [17].

The oxidizer to fuel ratio (O/F) was predicted to be approximately a value of three from Figures 2-13 and 2-14. As the mass flow rate of the oxidizer and O/F ratio was known, the mass flow rate of the fuel and mass of the fuel were then found using equation 4-8. Approximately 15% more mass was added to the fuel grain design to allow the remainder of the fuel to act as a passive thermal insulative layer for the combustion chamber.

$$O/F = \frac{\dot{m}_o}{\dot{m}_f} \tag{4-8}$$

Injector Design

The area of the injector port (A_{inj}) was determined by the mass flow rate of the oxidizer, coefficient of discharge (C_d), the density of the oxidizer, and the change in pressure from the oxidizer tank to the combustion chamber.

$$A_{inj} = \frac{\dot{m}_o}{C_d\sqrt{2\rho_o\,(P_t - P_c)}} \tag{4-9}$$

The discharge coefficient is a dimensionless value used to describe how well fluid flows through an orifice. Values close to one describe more laminar fluid movement, while values close to 0.1 describe more turbulent flow through an orifice [4]. A value of 0.175 was chosen for the discharge coefficient as previous tests with liquid motors using nitrous oxide showed possible mixed-phase flow through the injector.

The design of the pintle injector chosen was a baffled pintle injector due to its ease of manufacturing, and simplicity of tuning. This type of injector housed a single pintle with three orifices, which added to the equivalent the calculated area of the injector. The pintle was made

from a hex piece of brass and machined to thread into the housing of the injector body (Figure 4-2).

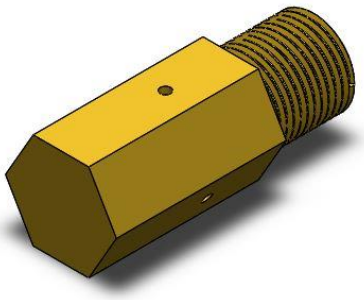

Figure 4-2. CAD rendering of hybrid motor pintle.

The injector body possessed a baffled face that extended past the pintle orifices on the pintle to induce turbulence for decreasing the size of the oxidizer droplets traveling into the fuel grain port. The baffle induced this turbulence through redirecting the flow orthogonally to the pintle orifices (Figure 4-3).

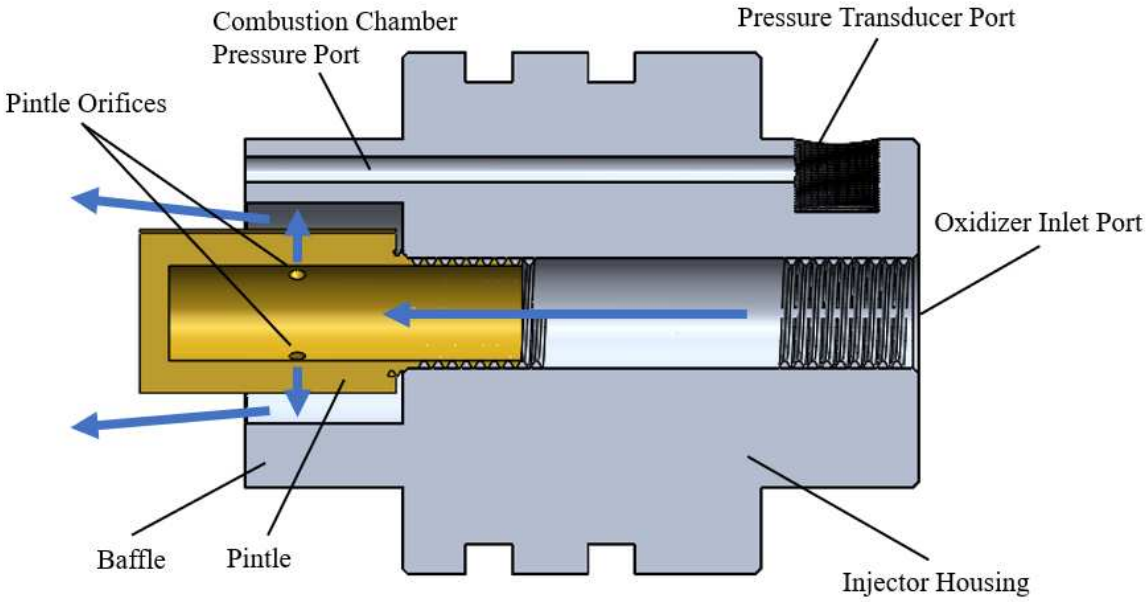

Figure 4-3. Diagram of hybrid motor injector.

Pyrotechnic valve Design

The valve design selected for delivering the oxidizer through the injector and to the combustion chamber was a pyrotechnic valve. This type of valving offered simplicity and reliability. The design of the pyrotechnic valve was based on the helium valve used on the Mueller XLR-50 rocket in 1994 [23].

The valve was actuated from a single pyrotechnic squib placed at the front of the piston. This squib consisted of an E- match fed into the forward cap and filled with 0.75 grams of recrystallized potassium nitrate-based propellant.

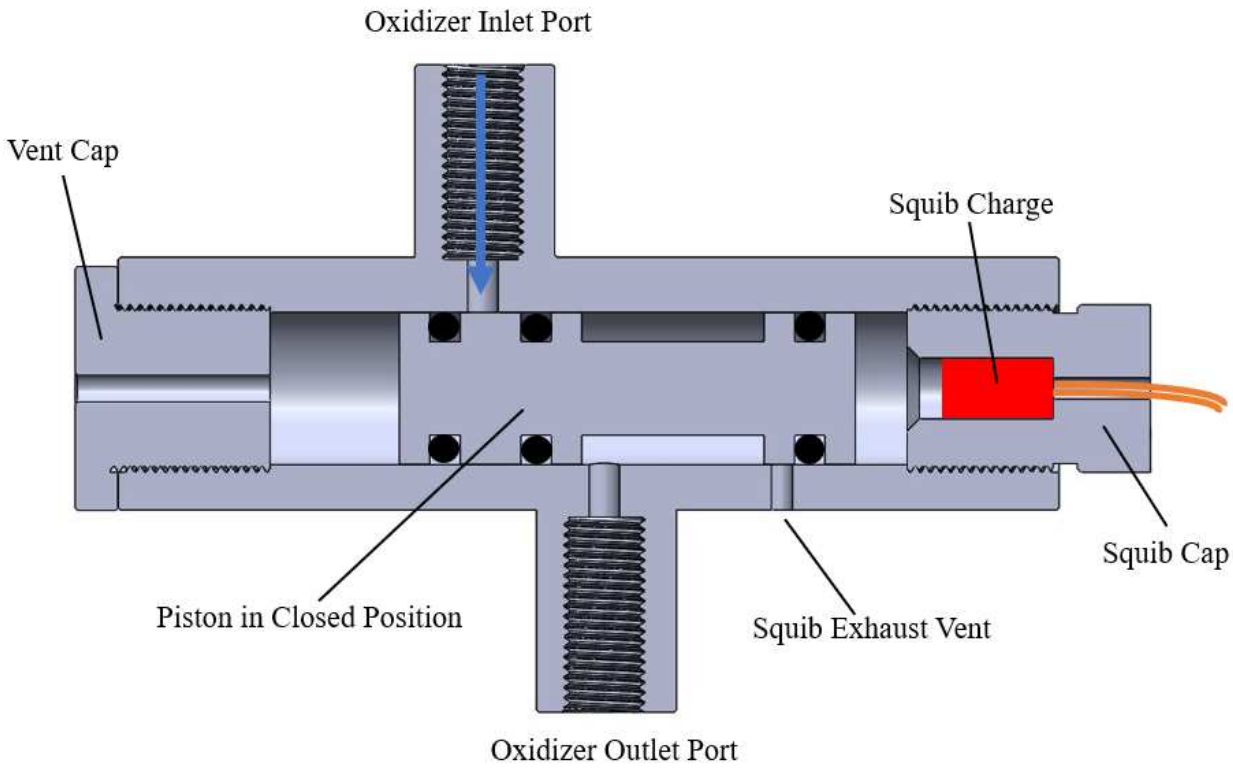

Figure 4-4. Diagram of hybrid motor pyrotechnic valve in the closed position.

When the squib charge ignited, the expanding gas pushed the piston past the oxidizer inlet port, which allowed the oxidizer to flow around the piston into the oxidizer outlet port (Figure 4-4).

The exhaust gases from the squib charge exited an exhaust vent, and the air that was present forward of the piston was vented out of the vent cap.

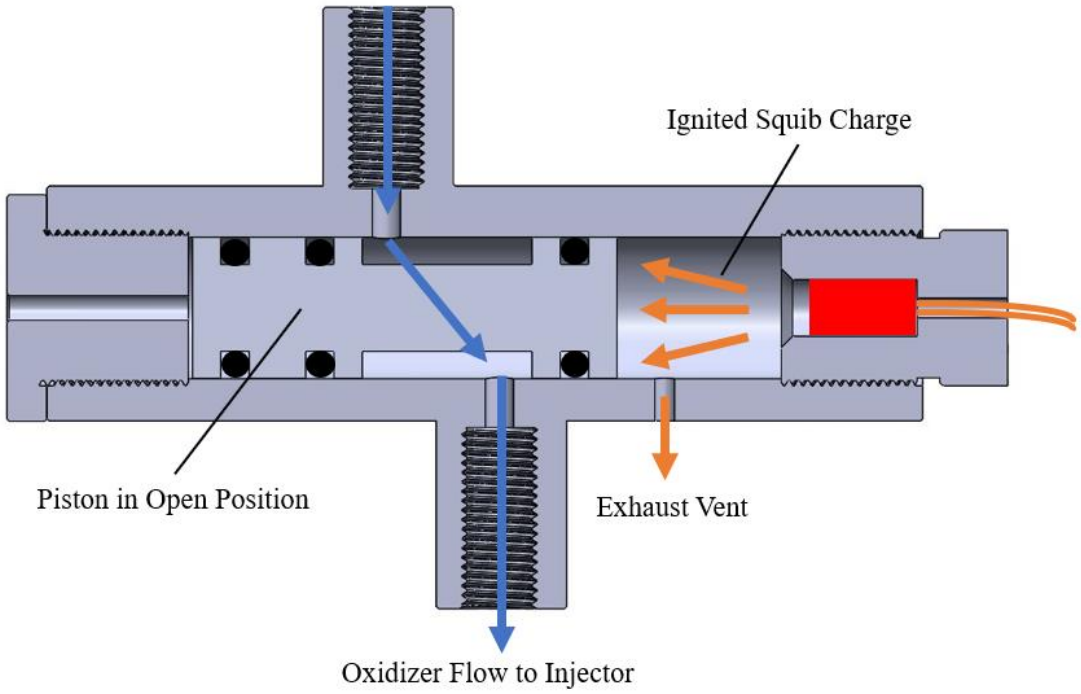

Figure 4-5. Diagram of hybrid motor pyrotechnic valve in the open position.

Fuel Grain Composition

The first hybrid motor hot test fire was decided to be a systems test to ensure that the oxidizer filling sequence, ignition sequence, and DAQ system were working properly. Therefore, the starting fuel grain composition of the hybrid motor consisted of aluminum and HTPB binder with a cylindrical core (Table 4-1).

Table 4-1. Hybrid Motor Fuel 1.

Composition	Percent by Mass
Aluminum	50.0
PAPI 94	6.0
R20LM Binder (HTPB)	44.0

For subsequent hot test fires in which carbon dioxide was added, the fuel grain was altered to include more metal fuels and increase the surface area of the grain port. Two different sizes of aluminum powder were employed to achieve a higher packing density for the metals. Aluminum particles that were 30μ and 5μ were placed under a microscope to see the relative difference in size (Figure 4-5).

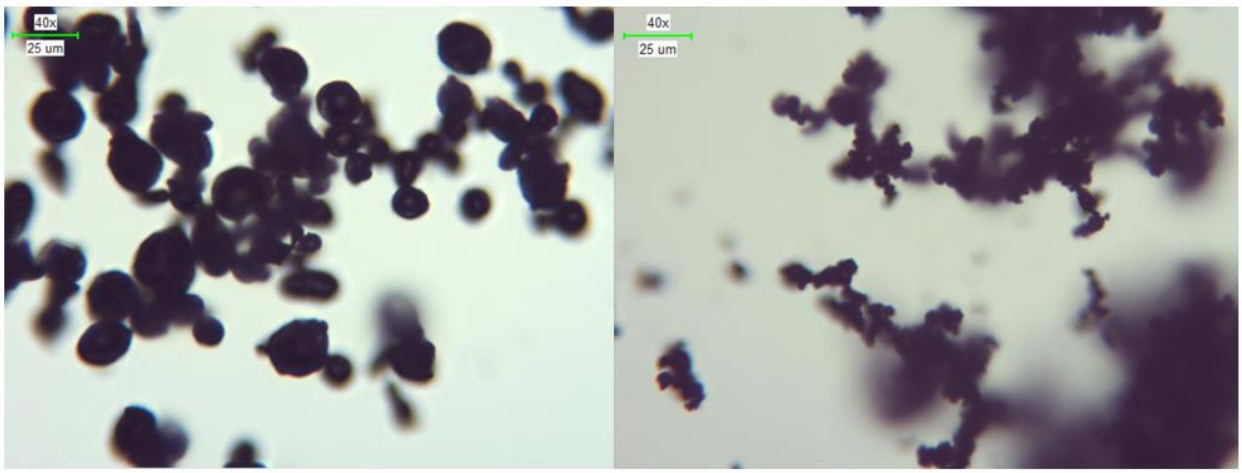

Figure 4-6. Optical microscope images of 30μ on the left, and 5μ on the right.

Styrofoam beads and paraffin wax pellets were tested in small test aluminum, and HTPB fuel grains as two possible solutions to observe how well mixing and casting into a grain configuration would occur. The addition of either of these components was to increase the grain port surface area during combustion. The Styrofoam would be melted away after casting by flowing acetone through the grain, exposing the metal and binder. At the same time, the paraffin wax pellets would remain in the grain until the heat of combustion would melt and evaporate the pellets, thus leaving voids in the fuel grain. The test fuel grain consisted of an HTPB and aluminum mixture amounting to 70% of the total mass. The 30% remainder was filled by the Styrofoam beads, and was cast into a PVC liner seen in Figure 4-6.

Figure 4-7. Styrofoam beads in test fuel grain.

After the test grain was cast, acetone was applied to the exterior surfaces to dissolve away the Styrofoam beads. This was unsuccessful due to the thin layer of HTPB and aluminum that coated all of the beads. The next test was replacing the 30% Styrofoam beads with paraffin wax. The wax provided a more homogenous mixture when cast, and appeared to leave a large number of voids when heated by an external flame, as seen in Figure 4-6.

Figure 4-8. Paraffin wax in test fuel grain.

With the addition of multimodal metals and paraffin wax pellets, the final fuel grain composition for the carbon dioxide and nitrous oxide hybrid motors was developed (Table 4-2).

Table 4-2. Hybrid Motor Fuel 2.

Composition	Percent by Mass
Aluminum (5μ)	10.0
Aluminum (30μ)	32.0
Magnesium (30μ)	10.0
Paraffin Wax	30.0
R20LM Binder (HTPB)	14.0
PAPI 94	2.0
IDP	2.0

Fuel Grain Port Geometry

As stated above, the port geometry for the first test of the hybrid system was to be a cylindrical port design. To find the length required for the correct O/F ratio, the mass flow rate of the fuel ($\dot{m}_f$) was found using equation 4-8. Equation 4-6 was then rearranged to solve for the burning area, A_B. The density of the fuel grain, ρ_f , was found by weighing a one cubic inch volume of the grain, and the theoretical regression rate was approximated using equation 2-2 using known values for the burning rate coefficient and exponent (a and n) [17].

$$A_B = \frac{\dot{r}\ \rho_f}{\dot{m}_f} \tag{4-10}$$

The length of the port was then found to be approximately 9 inches by using the circumference of the port. The diameter for the cylindrical port was calculated to be 0.625 inches.

For the carbon dioxide and nitrous oxide hybrid motors, a finocyl port geometry was selected as its increase in surface area was advantageous. A propellant grain simulator called GrainsCAD was used to visualize the cylindrical and finocyl fuel grains seen below.

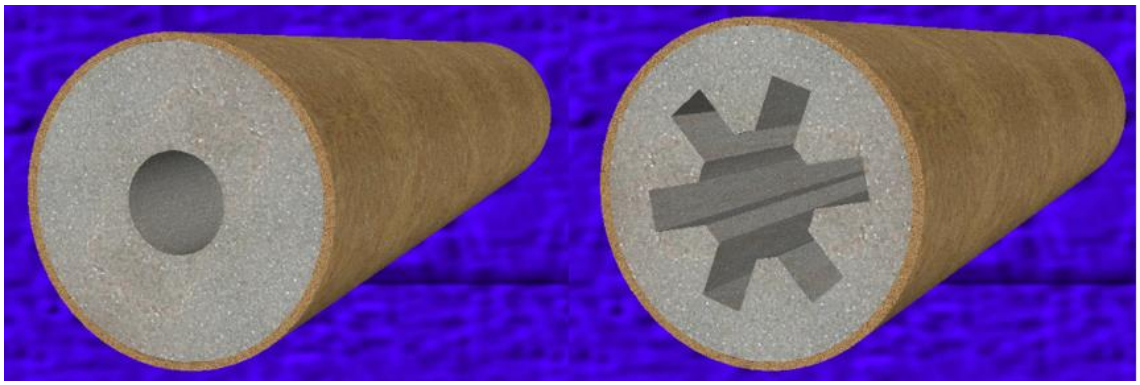

(a) (b)

Figure 4-9. GrainsCAD simulation of a cylindrical grain port (a) and finocyl grain port (b).

Overall Design and Initial Testing

The design of the hybrid motor was assembled in Solidworks to visualize the placement of where each component would reside in hot test firings (Figure 4-10).

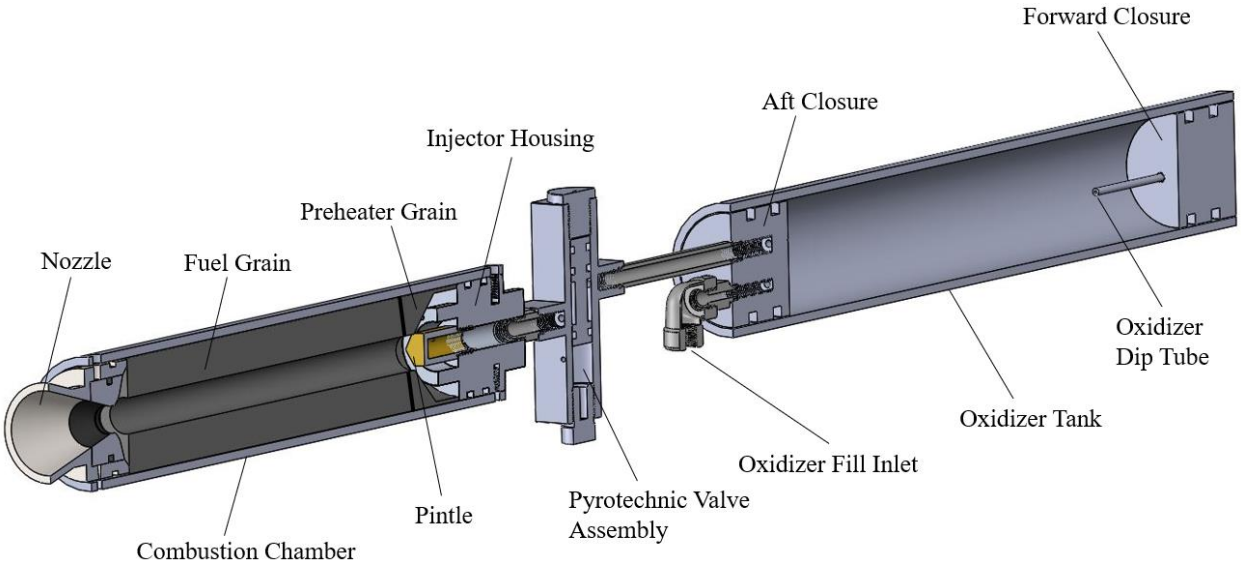

Figure 4-10. Diagram of hybrid motor with cylindrical fuel grain.

The pyrotechnic valve was the first component to be manufactured and tested. The valve housing, piston, vent cap, and squib cap were machined from 6061 T6 aluminum. A hydrostatic pump pressurized water to two times the maximum operating pressure into the inlet of the valve assembly. After a period of five minutes, the squib charge was remotely ignited, and the water

successfully drained from the outlet port. The oxidizer tank assembly and combustion chamber assembly were then manufactured and hydrostatically tested to two times the maximum operating pressure and held for five minutes. The next and final initial test of the equipment was a preheater ignition and cold flow test. This test was intended to provide valuable data for the timing of the preheater grain burn, the filling sequence with additional associated hardware, the testing of the DAQ system, and the testing of the ignition circuit (Figure 4-11).

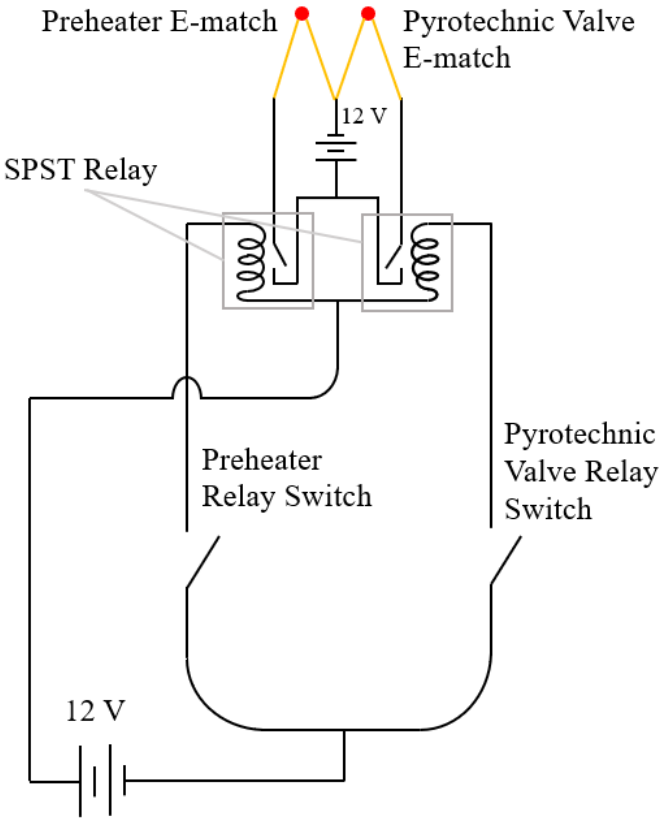

Figure 4-11. Circuit diagram of preheater and pyrotechnic valve ignition system.

The test began by filling the oxidizer tank with liquid carbon dioxide until the liquid started flowing out of the dip tube, indicating that the tank was entirely filled. This was followed with the ignition of the preheater grain. The combustion chamber and nozzle were not attached to the injector to take high-speed video of the cold flow exiting the baffled pintle. Three seconds after

preheater grain ignition, the pyrotechnic valve relay switch was thrown, and the carbon dioxide immediately flowed rapidly out of the baffled pintle (Figure 4-12).

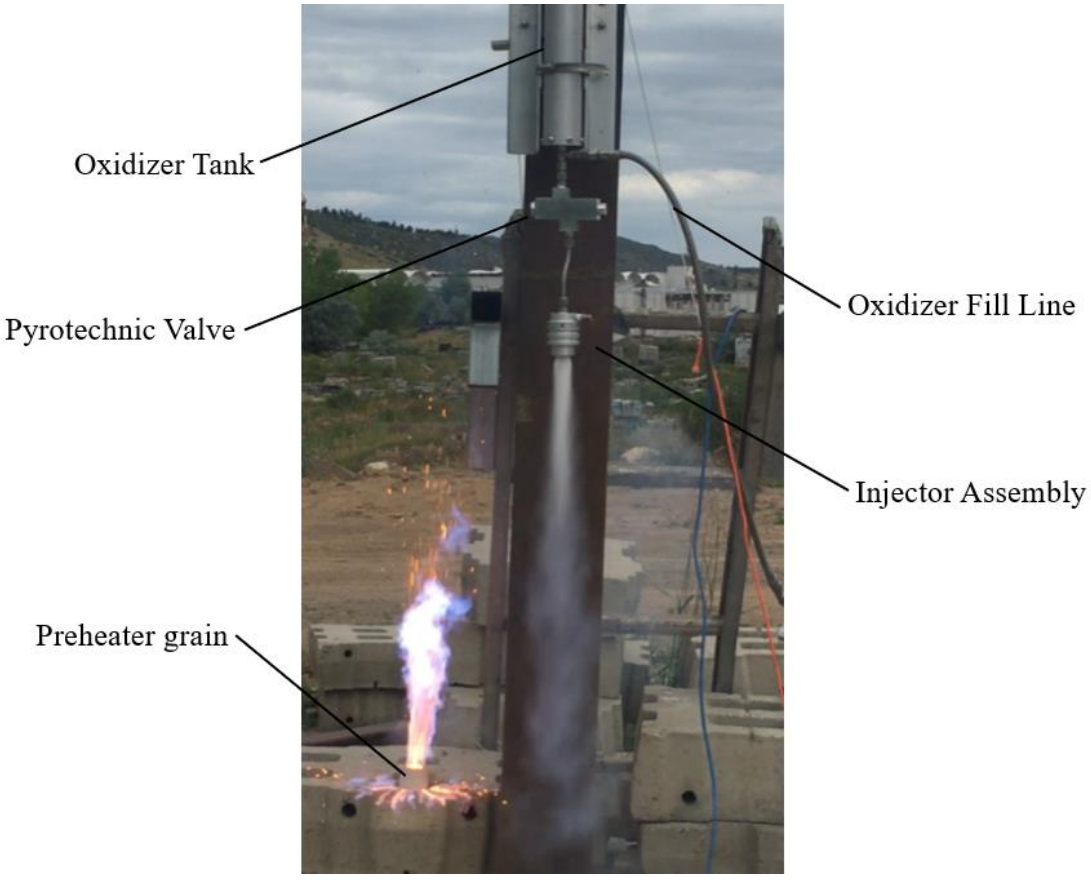

Figure 4-12. Cold flow and ignition system test.

As the carbon dioxide was being injected into ambient atmosphere, the difference in pressure (ΔP) was just the starting pressure subtracted from the ambient pressure. This meant that the expected time for all the carbon dioxide to flow out of the injector was expected to be smaller than the time of a hot fire test due to the decrease in mass flow rate from the smaller ΔP contributed from the 200 psi combustion chamber pressure. The liquid carbon dioxide took approximately two seconds to fully drain from the tank through the injector. This was expected as the predicted time for the hot test fires was approximately three seconds.

First Hot Fire Test – 100% Nitrous Oxide

After the completion of the cold flow and preheater grain test, the cylindrical fuel grain was cast and machined to length. The preheater grain was installed near the base of the baffle on the injector. The ambient temperature on the day of the hot test fire was approximately 90 degrees Fahrenheit, therefore, cooling of the nitrous oxide tank was necessary to retain the pressure from exceeding 900 psi. The filling of the nitrous oxide (from the fill tank to the oxidizer tank) was conducted after several attempts to cool the fill tank. The oxidizer fill tank contained a ball valve that was used to manually fill the oxidizer tank on the test stand.

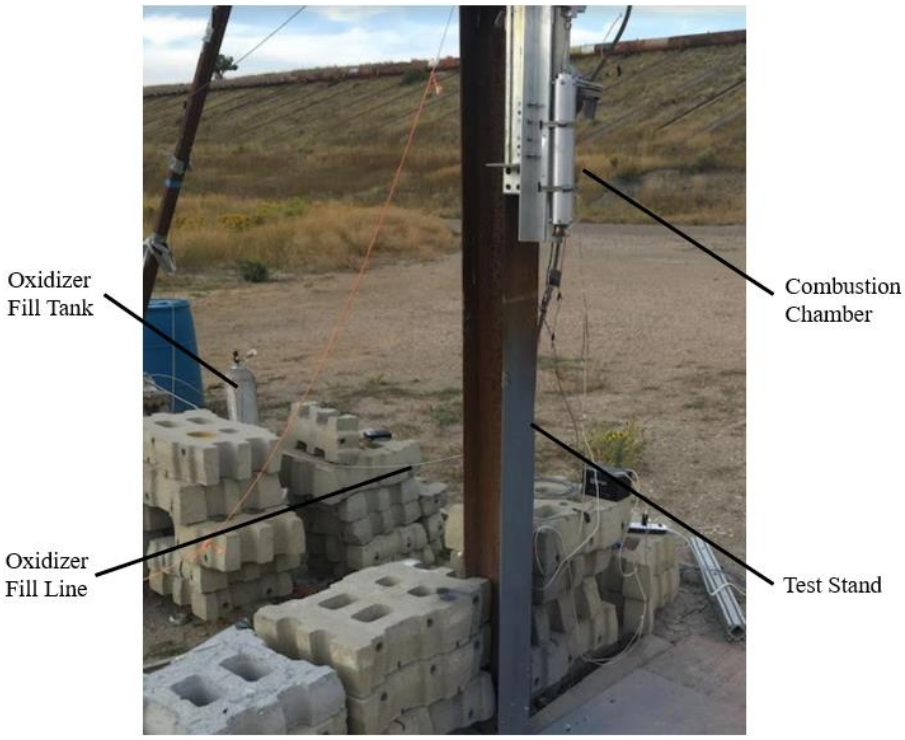

Figure 4-13. Filling setup for August 9th hot fire test.

The E-matches for the preheater grain and pyrotechnic valve were armed, and the DAQ was set to record the combustion chamber pressure and oxidizer tank data. The preheater grain was ignited, and three seconds later, the signal to the pyrotechnic valve E-match was sent. The motor fired successfully, and the data were retrieved. The graph below displays the pressure versus

time for the combustion chamber and oxidizer tank. The vertical green line displays the point at which the liquid nitrous oxide was depleted, and mainly gaseous nitrous oxide was flowing through the injector. This inflection point occurs when the negative slope of the combustion chamber increases to a larger value. This holds true only for pressure-fed rocket motors as the oxidizer tank pressure is continuously decreasing.

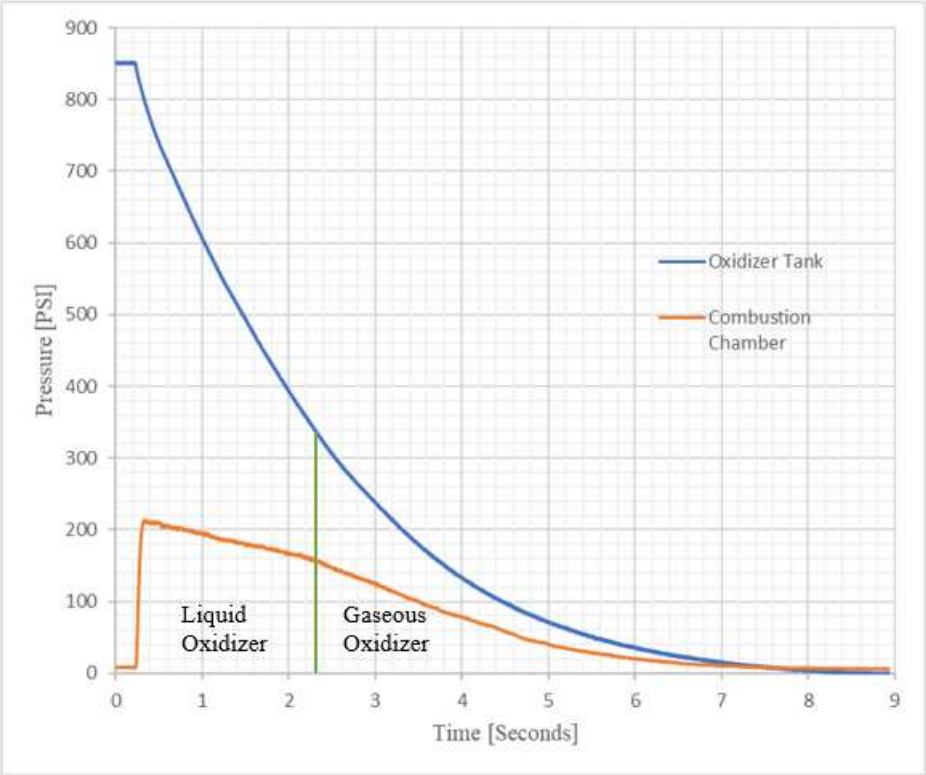

Figure 4-14. August 9th hot fire test data.

An estimated regression rate was then calculated with the time that the liquid oxidizer flowed into the chamber and the change in the fuel grain port area. The fuel grain port diameter (d_p) was cast at 0.625 inches and ended at an average diameter (D_p) of 1 inch after the firing. The radii of these diameters were then subtracted from each other to attain the distance evaporated and burned that was perpendicular to the port axis (Figure 4-15). This was then divided by the burn

duration (T_b) during liquid oxidizer flow to achieve an approximated regression rate for the fuel grain (equation 4-11).

$$\dot{r} = \frac{\frac{1}{2}(D_p - d_p)}{T_b} \tag{4-11}$$

An experimental regression rate of 0.085 inches per second was calculated. This value was similar to the predictive values of 0.110 inches per second and 0.097 inches per second calculated using equations 2.2 and 2.4, respectively.

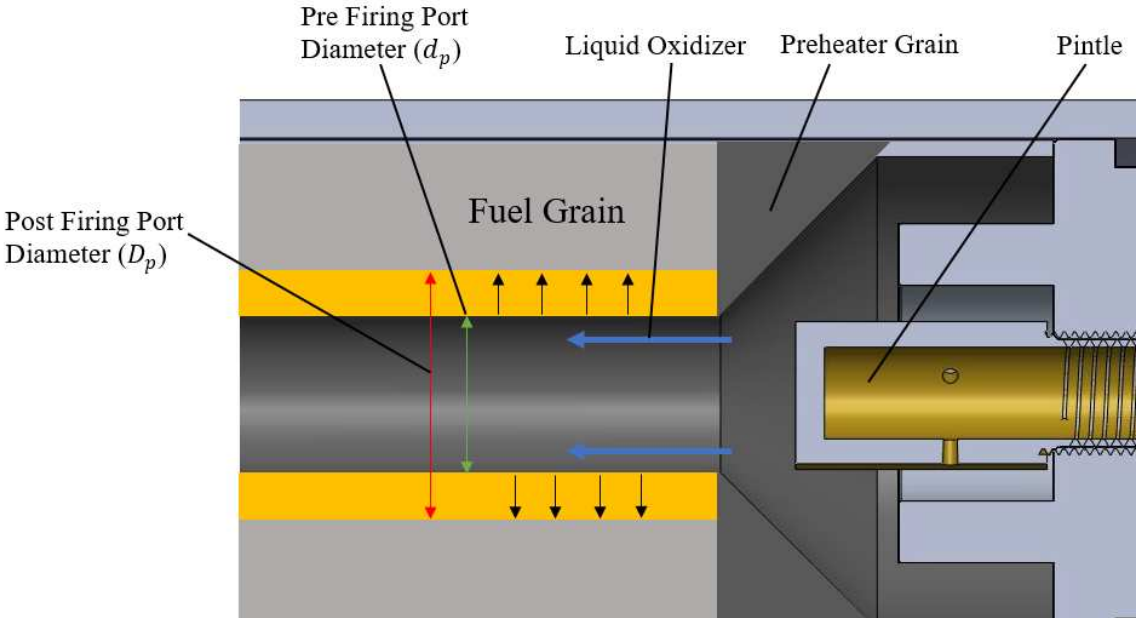

Figure 4-15. Fuel grain regression diagram.

The grain post-firing is shown below in Figure 4-16. The post-firing port diameter, D_p, was measured by measuring the diameter in multiple locations on both ends and averaging the result. The post-firing mass of the grain was subtracted from the initial mass and was recorded as 0.217 pounds burned. This was utilized to find the experimental fuel mass flow rate ($\dot{m}_f$) of the fuel grain; 0.090 pounds per second.

Figure 4-16. Injector side (left) and nozzle side (right) of the grain post-firing.

Knowing an approximate regression rate for the fuel having a fifty percent metals mass ratio aided in progressing in the next series of tests in which the oxidizer composition was the only variable across all tests.

Figure 4-17. August 9th hot fire test: 100% nitrous oxide.

Second Hot Fire Test – 100% Nitrous Oxide

The second hot fire test was a repeat of the first firing with the exception of replacing the cylindrical fuel grain port with a finocyl port and changing to the second fuel composition (Table

4-2). The purpose of these changes was to increase the port area and to introduce magnesium into the fuel composition.

Figure 4-18. View of preheater grain looking towards the finocyl fuel grain.

The motor was assembled, filled with nitrous oxide, fired, and the data were retrieved successfully (Figure 4-19). The result of the change in fuel composition and port geometry appeared to produce a more desirable neutral burn profile throughout the liquid oxidizer portion of the burn. The gaseous oxidizer segment of the burn seemed similar to the previous test fire in which a gradual decay in oxidizer tank pressure mimicked the combustion chamber decay. The mass of the fuel grain burned was recorded as 0.198 pounds, a similar value to the previous hot test fire.

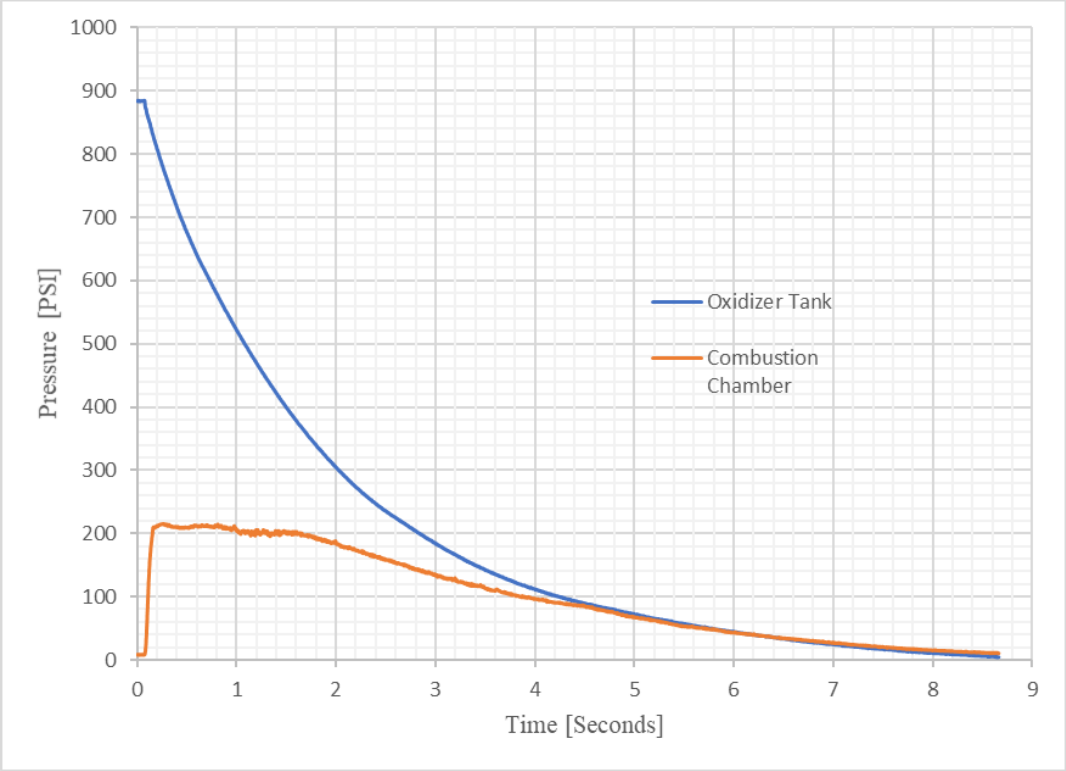

Figure 4-19. August 19th hot fire test data.

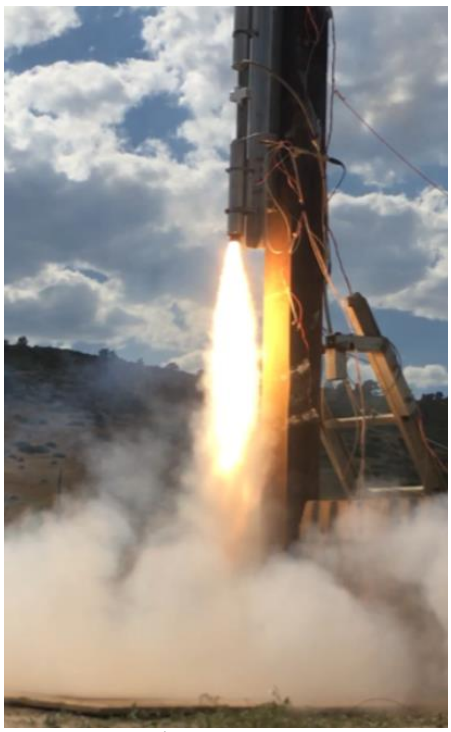

Figure 4-20. August 19th hot fire test: 100% nitrous oxide.

Third Hot Fire Test – 75% Nitrous Oxide and 25% Carbon Dioxide

The third hot test fire of the hybrid motor was the first to change the oxidizer composition by introducing carbon dioxide. The mixture ratio was set to be 75% nitrous oxide and 25% carbon dioxide by volume. This was accomplished through the use of two dip tubes set at different lengths at the forward closure. Figure 4-21 showcases this design for mixing the carbon dioxide and nitrous oxide. During the filling procedure, carbon dioxide first entered through the oxidizer fill inlet. The headspace gas exited through the carbon dioxide dip tube until the liquid level reached the lowest point in the dip tube. As soon as capillary forces caused liquid carbon dioxide to flow through the dip tube and it was visually observed to flow outside of the tank, the carbon dioxide vent valve was closed remotely by exerting tension on a rope that was attached to the valve handle. The carbon dioxide fill tank valve was then closed off. The nitrous oxide fill tank valve was then opened and also filled through the oxidizer fill inlet. The purpose of using a single inlet for both fluids was to encourage turbulent mixing. Once the nitrous oxide began to exit the nitrous oxide fill valve through its own dip tube, that valve was then closed off with a different rope leading back to the remote filling station. If the ambient temperature was too high to maintain a moderately constant tank pressure, the nitrous oxide vent valve would be opened to relieve headspace pressure until the pressure reading on the DAQ was within acceptable limits. If the ambient temperature was too low, a heater blanket was attached to both the fill tank and the oxidizer tank to warm them to the desired pressure.

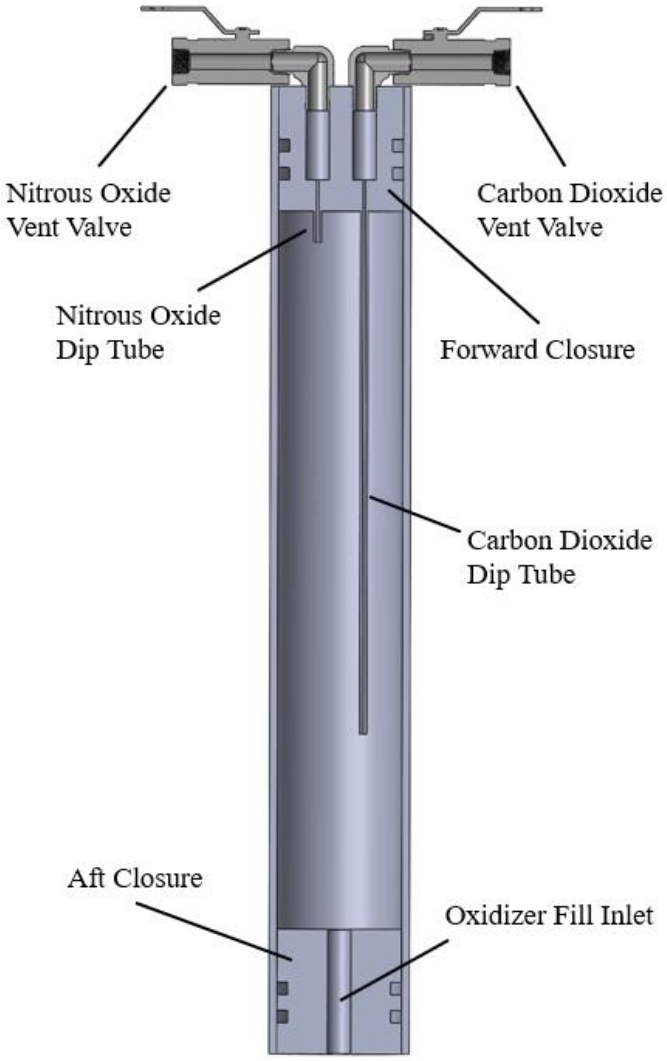

Figure 4-21. Oxidizer tank dip tube assembly.

The motor was filled and fired successfully, however, the data did not look as promising as the previous test fires. Figure 4-22 shows the combustion chamber pressure climbing to a maximum pressure of 154 psi and then gradually decreasing in a regressive burn profile. The outcome was expected to be the combustion chamber pressure profile mimicking the previous test in which a neutral profile was present during the liquid oxidizer phase before regressing under gaseous oxidizer flow, but shifted down to a lower average pressure. As the ambient temperature on the day of the hot test fire was approximately 90 degrees Fahrenheit, this outcome in the data could have been the result of venting too much headspace gas pressure to relive the tank to a suitable

pressure just before firing. The average time of the burn was additionally substantially less than that of the previous tests. Although the C* versus O/F graph (Figures 2-11 through 2-13) presented the oxidizer mixture having a lower exhaust velocity as the amount of carbon dioxide increased, the result of the third test was deemed to be less based on the combustion interactions of the 25% carbon dioxide and 75% nitrous oxide and more on the filling procedure. Additionally, the mass of the fuel grain burned was 0.149 pounds, which was the lowest value at that point in the testing. As the mass flow rate of the oxidizer directly influences the mass flow rate of the fuel in a hybrid rocket motor, it was assumed that since the fuel mass flow rate was lower than expected, the oxidizer mass flow rate was also most likely lower than expected (equations 4-6 and 4-7).

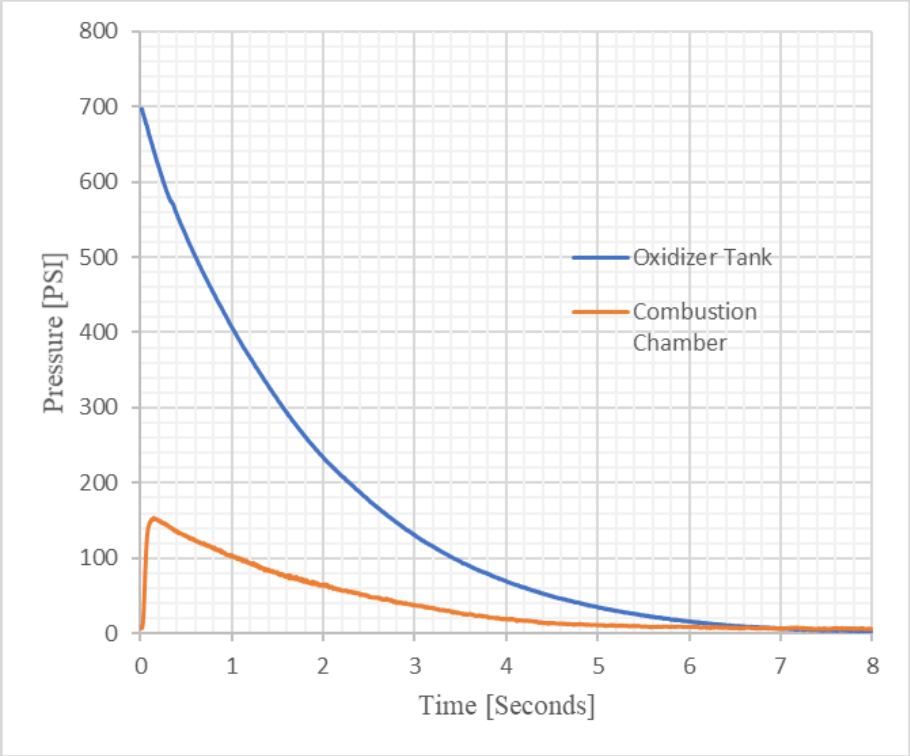

Figure 4-22. September 15th hot fire test data.

Figure 4-23. September 15th hot fire test: 75% nitrous oxide and 25% carbon dioxide.

Fourth Hot Fire Test – 50% Nitrous Oxide and 50% Carbon Dioxide

It was decided to move forward with the testing regime to a mixture of 50% carbon dioxide and 50% nitrous oxide due to time and cost constraints. The only changes made for the fourth test was altering the lengths of the dip tubes to equate an equivalent mixture ratio within the oxidizer tank. The motor was filled and fired successfully. Upon inspection of the recorded high-speed video footage at 960 frames per second, an odd phenomenon was observed that had not taken place in any of the previous hot test fires. The exhaust gases appeared to pulsate rapidly as they were exiting the nozzle. This visual occurrence was then confirmed by the recorded pressure data in Figure 4-24.

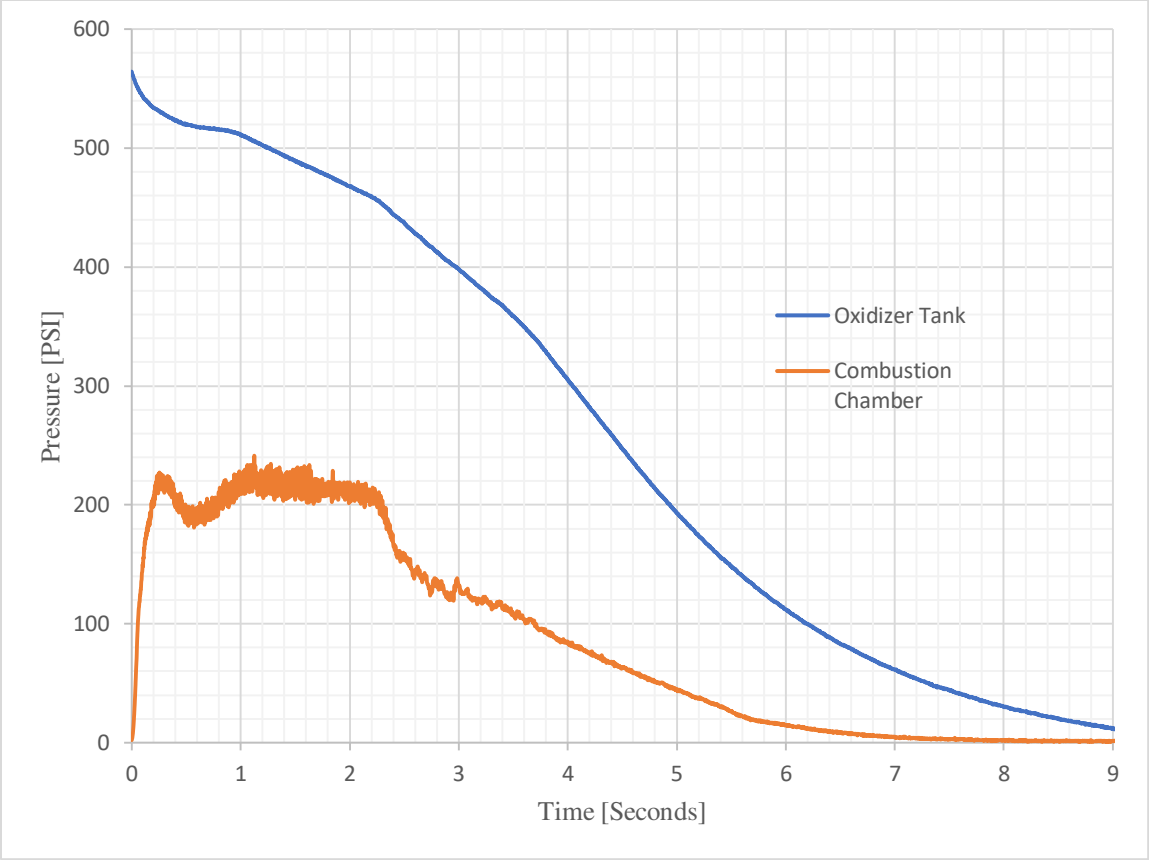

Figure 4-24. October 3rd hot fire test data.

The data in Figure 4-24 show a restively neutral burn profile for the liquid portion of the oxidizer until subsiding at 2.35 seconds to a regressive profile for the remainder of the burn. Within that neutral portion, the combustion chamber pressure oscillated as initially indicated by the high-speed video. A closer view of the neutral burn portion can be viewed below in Figure 4-25. From this graph, an oscillating frequency of approximately 80 Hz was determined. Combustion instability of this nature is described by Sutton in the following statement: "hybrid motors have exhibited two basic types of instabilities in static test environments: oxidizer feed system-induced instability (nonacoustic), and flame holding instability (acoustic). Oxidizer feed system instability is essentially a chugging type as described in Chapter 9 and arises when the feed system is sufficiently soft" [4]. As the oscillations appear harmonic, it was determined that the

instability was more likely a oxidizer feed system induced instability, and not a flame holding instability.

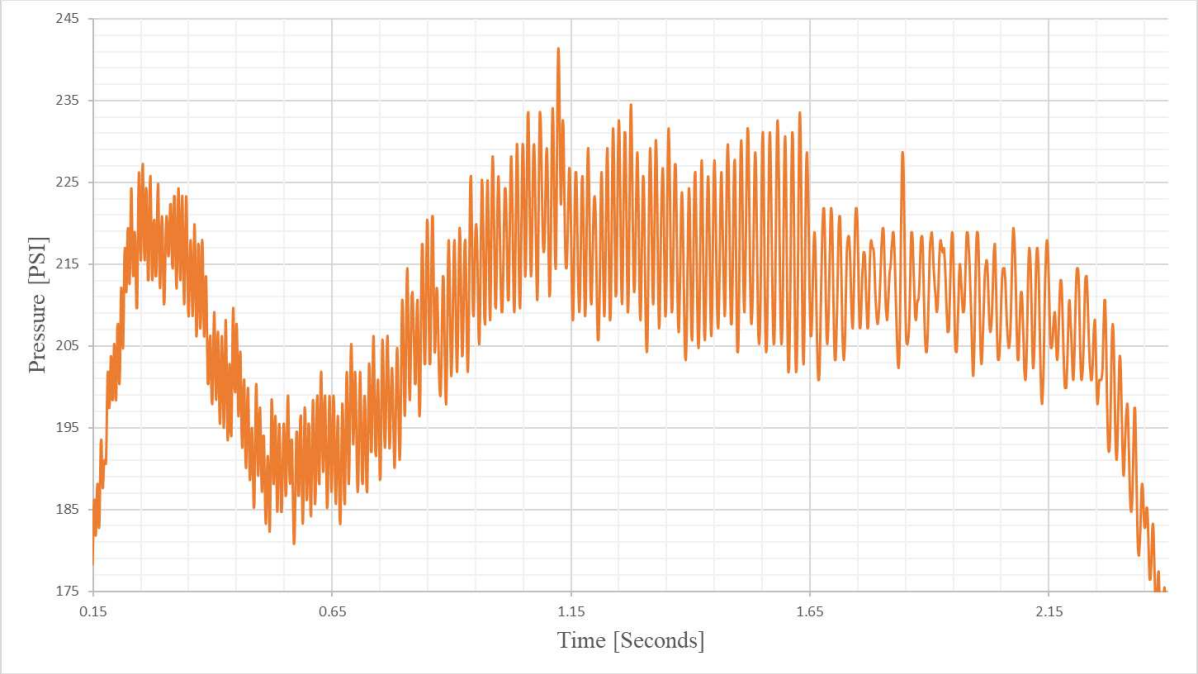

Figure 4-25. Enlarged October 3rd combustion chamber data.

Figure 4-26 below is combustion chamber pressure data gathered from a 24 inch diameter liquid oxygen and HTPB hybrid rocket motor that experienced oxidizer feed system induced instability [4]. The data appeared quite similar to the pressure data in Figure 4-25.

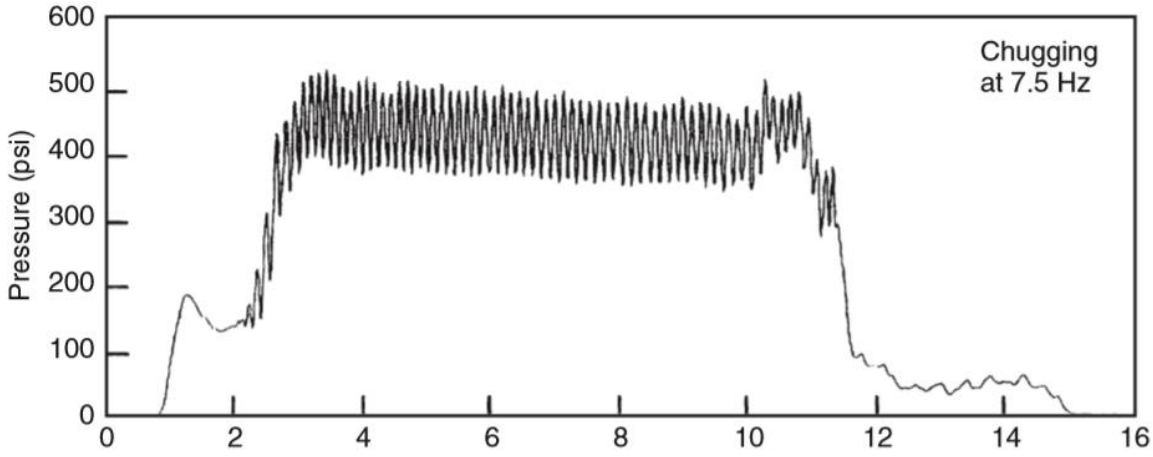

Figure 4-26. Low frequency, high amplitude combustion chamber pressure oscillation [4].

The ramifications of the oxidizer feed system induced instability could have meant that either the pressure drop (ΔP) between the oxidizer tank and combustion chamber was too small, or that undesirable physical interactions were occurring between the carbon dioxide and nitrous oxide. Since the pressure drop had consistently been over 400 psi as of all the tests thus far with no indication of combustion instability, the source of the instability was most likely an interaction between the two oxidizers that occurred during the burn. Even as the results given by the clear mixing chamber (Figure 2-11) seemed quite promising, there might have either been slight differences in miscibility between the two oxidizers, or the turbulent mixing achieved through the filling process was inadequate to ensure a homogeneous mixture. A combination of these two inadequacies may have been amplified during the pressure drop, which affected the concentration of either oxidizer flowing into the combustion chamber.

Figure 4-27. October 3rd hot fire test: 50% nitrous oxide and 50% carbon dioxide.

Fifth Hot Fire Test – 50% Nitrous Oxide and 50% Carbon Dioxide

Due to the instability experienced in the previous test, a new testing arrangement was developed. In an attempt to mitigate the oscillations in the combustion chamber pressure, it was decided to contain the carbon dioxide and nitrous oxide in two separate oxidizer tanks. These separated tanks contained their own filling lines and dip tubes. As the tanks were different geometrically, the dip tubes were cut to specific lengths to equate the two volumes. The volumes were calculated to hold the same mass of oxidizer as the previous test- 0.5 pounds of nitrous oxide and 0.5 pounds of carbon dioxide. Figure 4-28 shows the separated oxidizer tank arrangement on the test stand.

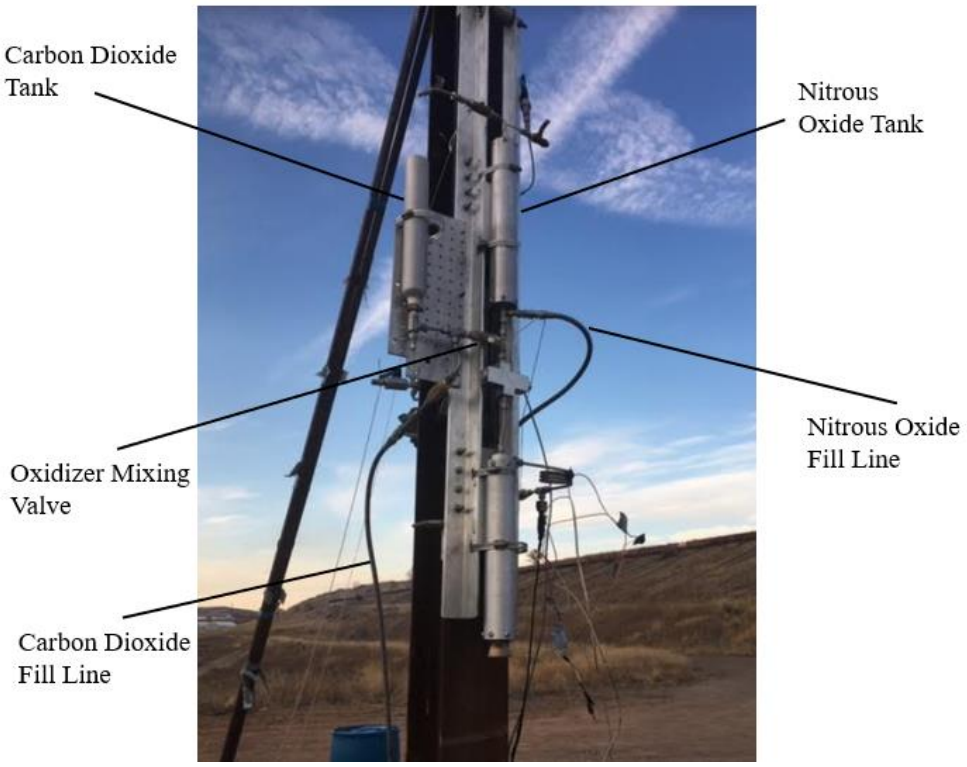

Figure 4-28. Dual oxidizer tank setup.

A closer view of the dual oxidizer tank arrangement is below. The filling sequence for the hot test fire was altered to accommodate the second tank. First, the oxidizer mixing valve was closed

to ensure that no carbon dioxide would enter the nitrous oxide tank before filling of the nitrous oxide. Then the carbon dioxide vent valve was opened to allow the headspace gas to vent. Next, the carbon dioxide fill tank valve was opened to allow flow into the carbon dioxide tank. Once liquid carbon dioxide was observed flowing out of the vent valve port, the vent valve was closed. The same process was then performed with the nitrous oxide. Finally, the oxidizer mixing valve was opened to allow both oxidizers to share an open port above the pyrotechnic valve. When the time for the hot fire test came, the preheater grain was ignited, and three seconds later, the pyrotechnic valve was ignited.

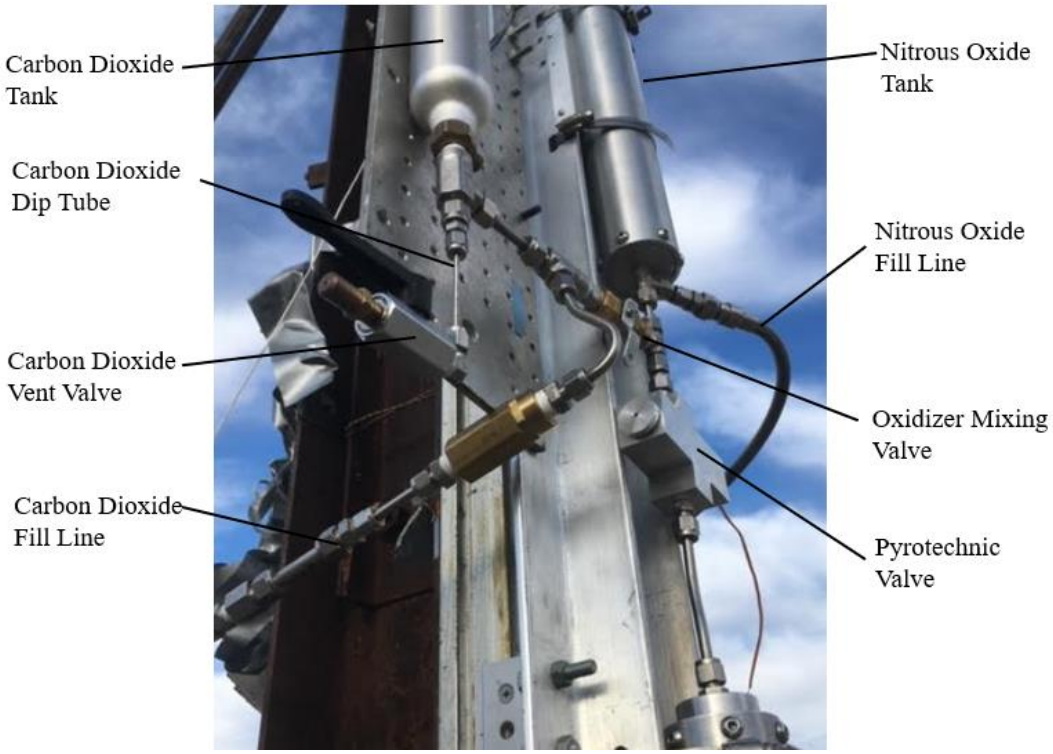

Figure 4-29. Close up view of dual oxidizer tank setup.

After the test, the high-speed footage was viewed, and no large oscillations were observed. The data was then reviewed and confirmed that no combustion chamber oscillations were as large in

amplitude or frequency as the previous test, but erratic changes in the chamber pressure were present during the firing (Figure 4-29).

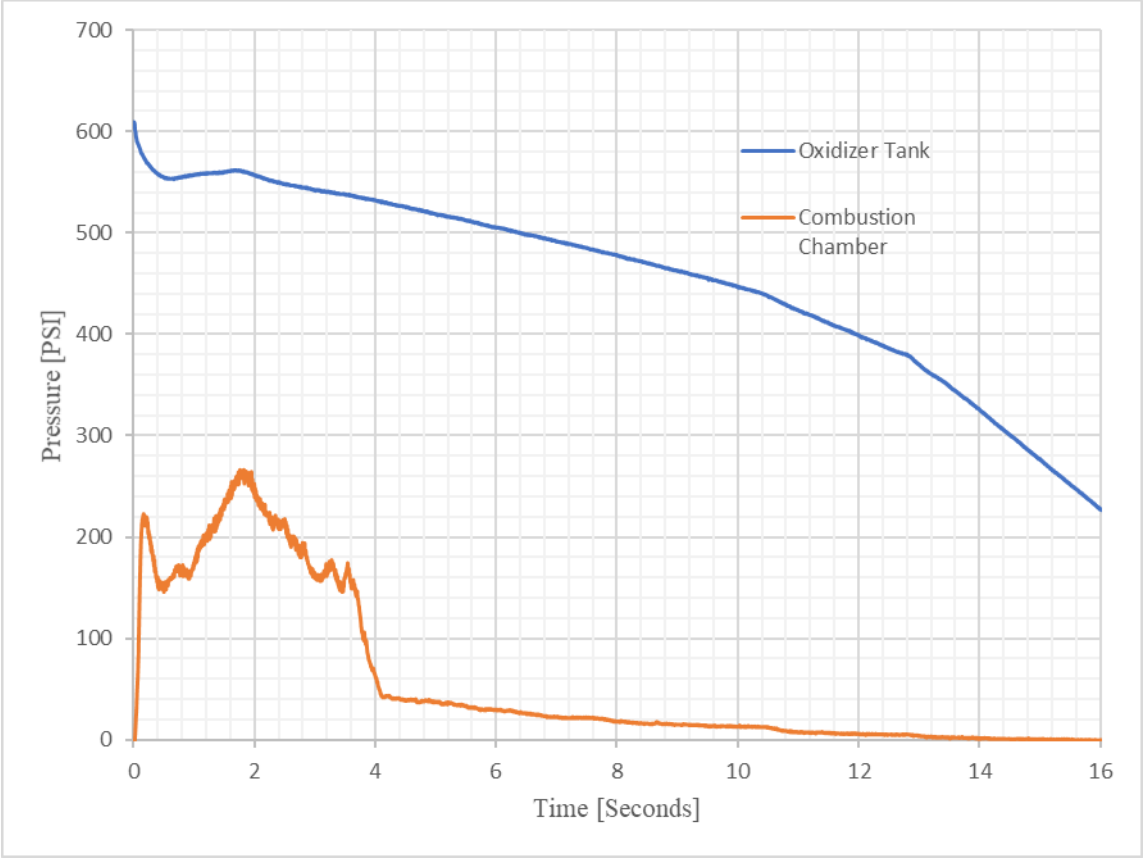

Figure 4-30. November 14th hot fire test data.

These peaks seen in the combustion chamber pressure data were most likely due to differences in the flow of carbon dioxide and nitrous oxide. As the nitrous oxide had an unimpeded flow direction to the injector, it appears as though it may have been leading the combustion. The carbon dioxide had two 90 degree turns before it mixed with the nitrous oxide directly above the injector, which could have caused turbulent Eddies to form (Figure 4-30).

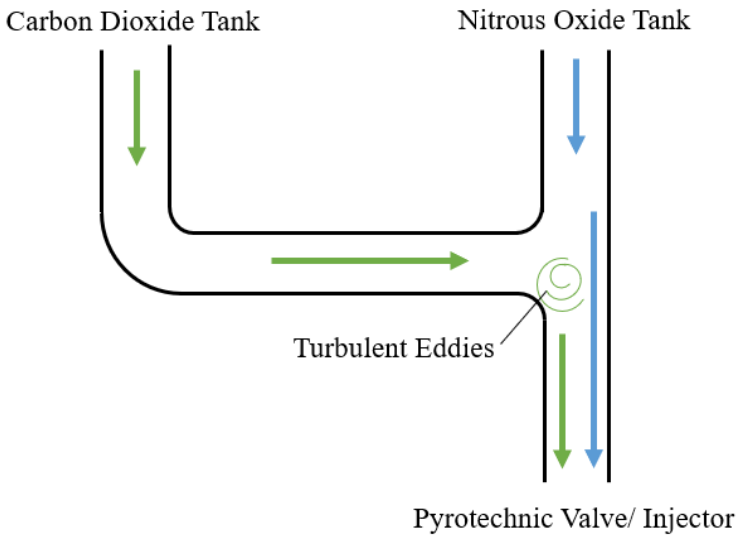

Figure 4-31. Diagram of CO2 and N2O routing.

The oxidizer tank pressure remained relatively high (525 psi) after the combustion chamber pressure receded to approximately 50 psi. This was most likely residual carbon dioxide left in its tank and evaporated through the piping until it eventually exited the injector.

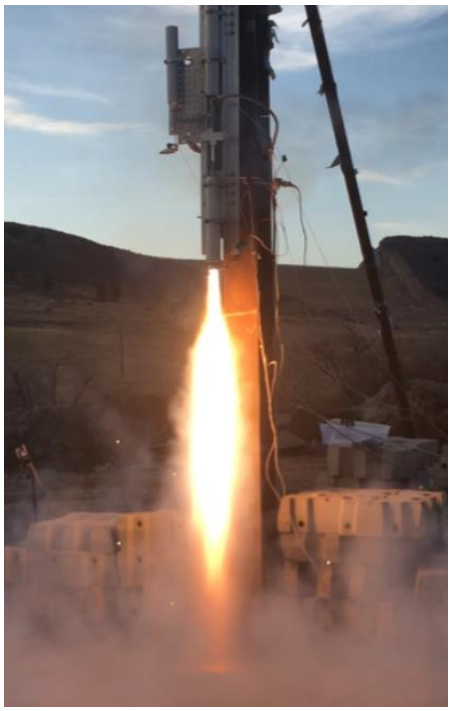

Figure 4-32. November 14th hot fire test: 50% nitrous oxide and 50% carbon dioxide.

Comparisons of Hybrid Motor Test Results

Although not as many hybrid tests were performed as desired, the results acquired proved to be interesting. The last two test fires were compared to the control data point-Test Fire 2. Below is a graph of the second firing, (Test Fire 2 - red) which had an oxidizer mixture of 100% nitrous oxide, the fourth firing, (Test Fire 4 - green) which had an oxidizer mixture of 50 % nitrous oxide and 50% carbon dioxide, and the fifth firing, (Test Fire 5 - blue) which also had an oxidizer mixture of 50 % nitrous oxide and 50% carbon dioxide (Figure 4-32). To quantitatively analyze these three firings, the total impulse (I_{tot}) of each was compared. Equation 3-5 was utilized to calculate the approximate total impulses from the combustion chamber pressure data.

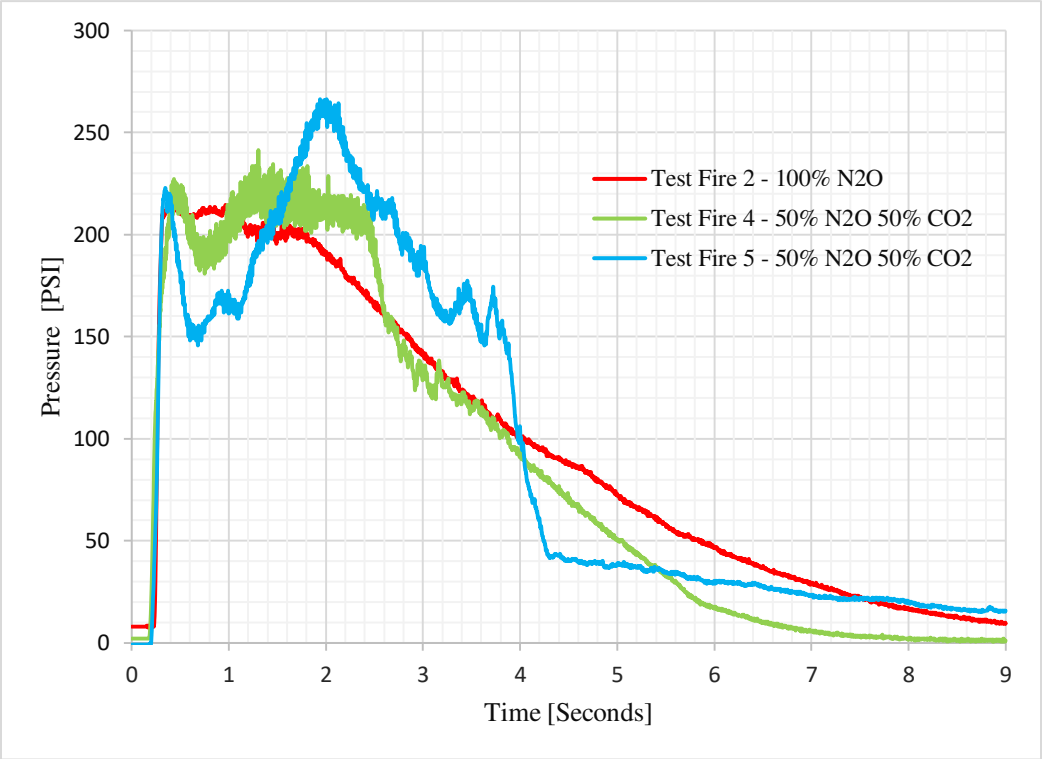

Figure 4-33. Overlapped combustion chamber pressure data from Test Fires 2, 4, and 5.

Test Fire 2 had a calculated total impulse of 228.7 lbf-seconds. Test Fire 4 was calculated at 230.7 lbf-seconds, and Test Fired 5 at 267.5 lbf-seconds. The average pressure of each firing was

also calculated to estimate an effective exhaust velocity (C*) using equation 4-4. Table 4-3 displays these exhaust velocities and their corresponding burned fuel mass.

Table 4-3. Calculated exhaust velocities (C*) and fuel mass burned ($m_{f\,B}$).

Test Number	C*	$m_{f\,B}$
Test Fire 2	1887.7 ft/sec	0.197 lbm
Test Fire 4	2035.7 ft/sec	0.291 lbm
Test Fire 5	2360.6 ft/sec	0.365 lbm

Below are two images of the fuel grain used in Test Fire 5. The left image was taken after casting (before the hot test fire), and the right was post-firing.

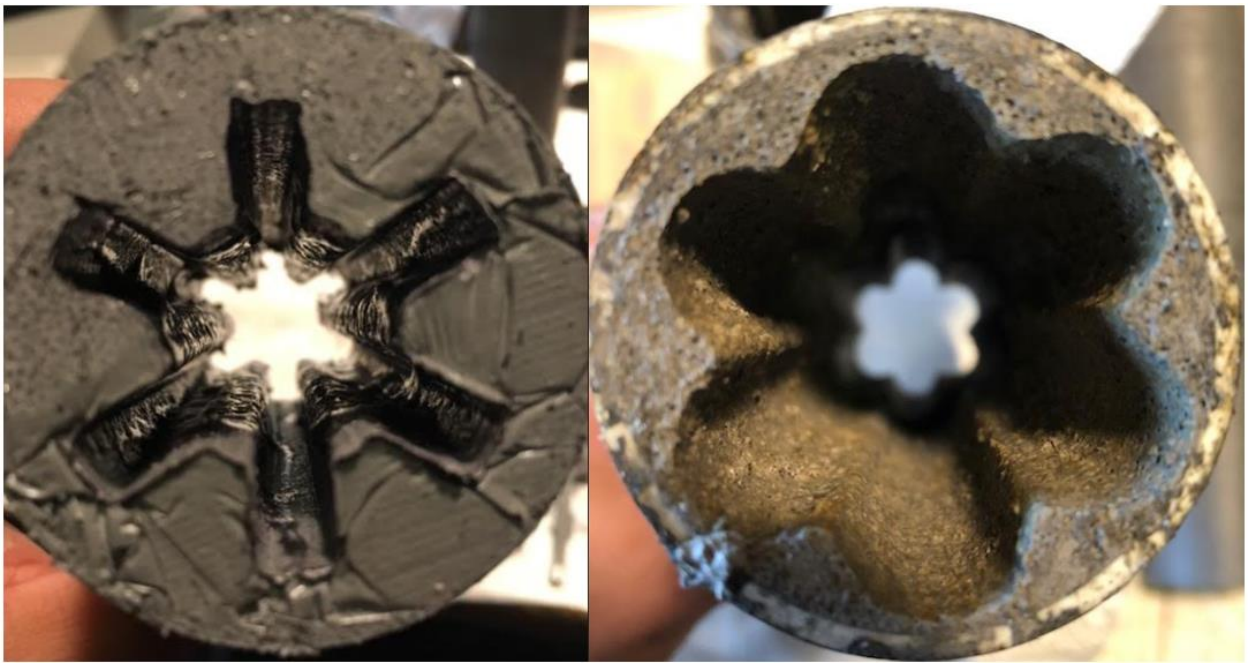

Figure 4-34. Test Fire 5 fuel grain before (left) and after (right) hot test firing.

Since the content of the metal in the fuel grain was approximately 50% of the total mass, it was unsure how the heat transfer would propagate. From the limited testing done on this project, estimates were made on the convective and radiative heat transfer. Using the convective heat

transfer coefficient equation 2-10 required a Stanton number. This was calculated using the following equation:

$$S_t = 0.023Re^{-0.2}Pr^{-0.67} \quad (4\text{-}12)$$

The heat transfer coefficient was then acquired, and an approximate convective heat transfer of 1191.9 W was calculated. Equation 2-11 was used to approximate a radiative heat transfer of 573.6 W. These values were instantaneous values calculated at the start of ignition. The ratio of radiative heat transfer to convective heat transfer was then calculated to be 0.481. As stated earlier in chapter two, Chiaverini specified if the radiative heat transfer is one half or less than the convective heat transfer, the net result is a small change in the regression rate (approximately equal to or less than 10%) [17]. In a fuel grain with higher metal content (greater than 50%), the total heat transfer would increase as the radiative heat transfer increased. Therefore, changes in the regression rate of the fuel will likely have to be taken in to account in hybrid motors with higher metal composition.

CHAPTER 5 – CONCLUSION AND FUTURE WORK

Conclusion

The ambition of this project was to observe and identify some of the key aspects of designing and operating a high metals rocket motor with a dual oxidizer comprised of carbon dioxide and nitrous oxide. Chapter one discussed the background of rocket propulsion and its impact on history. It then went into detail on how obtainable elements such as the atmosphere and metals within the regolith could be utilized in propulsion systems for traversing the planet or even returning back to the Earth. Chapter two described the different modes of combustion using metal powders and carbon dioxide and then put its focus on the powdered metal design and the traditional hybrid design. The chapter then defined different ways of calculating the regression of solid propellants and hybrid fuels in regards to convective and radiant heat transfer. It additionally showcased an experiment to observe the interactions between liquid carbon dioxide and liquid nitrous oxide within a clear mixing chamber. Lastly, chapter two compared the theoretical exhaust velocity and O/F ratio for different oxidizer mixture ratios with different metal fuel compositions. Chapter three then addressed the characterization of a preheater grain, which would deliver enough energy to aid in the initial startup and decomposition of the oxidizer mixture while retaining a similar theoretical regression rate to the calculated regression rate of the fuel grain. This was accomplished through hot fire tests of polychloroprene based composite propellants. After a series of unscheduled rapid disassemblies, a dual oxidizer propellant using ammonium nitrate and ammonium perchlorate with the common binder HTPB was tested successfully. The characterization process used different nozzle throat diameters for different tests to approximate a regression rate for the A206-B propellant. Chapter four finally discussed

the design and testing of the hybrid system. Using parameters such as theoretical exhaust velocity, regression rate, oxidizer, and fuel mass flow rate, and combustion chamber pressure estimated in chapters two and three, the design of the hybrid motor was established. The oxidizer tank, combustion chamber, nozzle, injector, and pyrotechnic valve were designed and hydrostatically tested to 1.5 times the maximum operating pressure. The system was then cold flow tested to observe the burn time of the preheater grain, and the flow time of the liquid oxidizer exiting the injector. This led to the hot test firings of the system. This chapter also addressed the various problems associated with this type of propulsion system such as oxidizer feed system induced instability and miscibility concerns with carbon dioxide and nitrous oxide oxidizer mixtures.

The results of this research concluded that though the carbon dioxide and nitrous oxide mixed into a homogenous fluid in the clear mixing chamber in Figure 2-11, the data in hybrid motor Tests 4 and 5 with a 50/50 oxidizer mixture suggest that one of the fluids may be coming out of solution during the burn when changes in headspace pressure are occurring. It was decided that at the scale of the motors and metal fuel content tested for this thesis, radiative heat transfer did not play a significant role in affecting the regression rate of the fuel grain. Larger scale hybrid motors with higher metal contents may have to combat new challenges with increased radiative heat transfer.

Future Work

There is much work to be done to understand the nature of carbon dioxide and metal rocket propulsion systems. The effort made in this project was an attempt to transmit the ideas of others into real hardware so work can be added to this topic's growing body of knowledge. There are many proposed ways of utilizing the resources of other planets and moons, but this thesis

focused on one particular method. At the time of this writing, companies such SpaceX and Blue Origin are developing propulsion systems that use liquid methane and liquid oxygen as propellants. This could be another very promising solution for in situ propellant resource utilization employing the Sabatier reaction on the surface of Mars. Nevertheless, there were things learned through this project that could be applied to future research for carbon dioxide and metal propulsion.

One aspect of the design that was assumed to hold true from bench testing to hot test fires was the homogeneity of the carbon dioxide and nitrous oxide oxidizers. Separated tanks for both oxidizers leading directly into the injector, although a heavier design when thinking of actual flight hardware, could be yield more favorable results in observing the combustion process.

Circulation zones within the combustion chamber could aid in better mixing between the oxidizer mixture and the fuel. These zones, called a precombustion chamber and a postcombustion chamber, are two spaces in between the injector and forward facing end of the fuel grain and the aft end of the fuel grain with the nozzle that support more efficient mixing to avoid fuel-rich exhaust exiting the nozzle.

This work involved bench-scale hardware where the motor size was kept to a maximum thrust of 50 pounds. Seeing certain tendencies like combustion instability and the effect of radiant heat transfer to the fuel grain was difficult. A large motor could be used to more thoroughly address the issues that will be faced by hardware intended for spaceflight. With that, a future recommendation would be to increase both the oxidizer mass flow rate and combustion chamber pressure on future test motors to record the range of performance achieved with these unique propellants.

Lastly, work that was completed towards the end of the project currently looks like an area of interest. Figure 2-1 shows the different modes of mixing and burning metal with carbon dioxide. Part (a) of that figure displays an image that looks similar to the traditional hybrid mode, except that the fuel grain is solid propellant with a high fuel (metal) content. This low oxidizer approach would entail that the motor would burn as a solid motor until the carbon dioxide was introduced. This type of system would not require a preheater grain and would be ignited in the same way a solid propellant grain would be with the addition of the pyrotechnic valve. A proof of concept propellant using only 20% oxidizer is shown below in Figure 5-1. Work on this technique will continue by the author in the coming months.

Figure 5-1. Low oxidizer fuel grain.

REFERENCES

[1] Von Braun, W., Ordway, F. I., Lange, H. H.-K., & Durant, F. C. (1966). *History of rocketry and space travel*. New York, NY: Crowell.

[2] Boiron, A. J., & Cantwell, B. (2013). Hybrid Rocket Propulsion and In-Situ Propellant Production for Future Mars Missions. 49th AIAA/ASME/SAE/ASEE Joint Propulsion Conference. doi:10.2514/6.2013-3899

[3] Zubrin, Robert, et al. "Mars Direct - A Simple, Robust, and Cost Effective Architecture for the Space Exploration Initiative." *29th Aerospace Sciences Meeting*, July 1991, doi:10.2514/6.1991-329.

[4] Sutton, G. P., & Biblarz, O. (2017). *Rocket propulsion elements*. Hoboken (N.Y.): Wiley.

[5] Goroshin, S., et al. "Powdered Magnesium-Carbon Dioxide Propulsion Concepts for Mars Missions." *35th Joint Propulsion Conference and Exhibit*, 1999, doi:10.2514/6.1999-2408.

[6] Shafirovich, E., Gükalp, I., & Baker, A. (2004). Metal-CO2 Propulsion System for Mars Missions. *Proceedings of the 2nd International Conference on Green Propellants for Space Propulsion*.

[7] Shafirovich, E., Shiryaev, A. and Goldshleger, U. (1993). Magnesium and Carbon Dioxide - A Rocket Propellant for Mars Missions. *Journal of Propulsion and Power*, 9(2), pp.197-203.

[8] Wickman Spacecraft &propulsion Co. http://www.wickmanspacecraft.com/marsjet.html

[9] Catalog Page For Pia22460 https://photojournal.jpl.nasa.gov/catalog/PIA22460

[10] Anderson, J. D. (2016). *Introduction to Flight*. New York: McGraw-Hill Education.

[11] Arg-http://www.military-today.com/aircraft/mq1_predator.htm

[12] Landis, G., Linne, D., & Taylor, D. (2000). A Mars rocket vehicle using in-situ propellants. *36th AIAA/ASME/SAE/ASEE Joint Propulsion Conference and Exhibit*. doi:10.2514/6.2000-3120

[13] Meyer, M. L. (1993). Powdered Aluminum and Oxygen Rocket Propellants: Subscale Combustion Experiments. *30th JANNAF Combustion Subcommittee Meeting sponsored by the Joint Army-Navy-NASA-Air Force Combustion Subcommittee* Monterey, California, November 15-19, 1993

[14] Foote, J.P., & Litchford, R.J. (2005). Powdered Magnesium - Carbon Dioxide Combustion for Mars Propulsion. *41st AIAA/ASME/SAE/ASEE Joint Propulsion Conference & Exhibit*. doi:10.2514/6.2005-4469

[15] Hinds, W. C. (1999). *"Aerosol technology: properties, behavior, and measurement of airborne particles"*.

[16] Wickman, J.H.: “In-Situ Martian Rocket and Airbreathing Jet Engines,” SBIR Phase II Final Report, NASA Contract NAS8–97048, 1998.

[17] Chiaverini, M. J., & Kuo, K. K. (2007). *Fundamentals of hybrid rocket combustion and propulsion*. American Institute of Aeronautics and Astronautics.

[18] Wickman, J. H. (2006). *How to make amateur rockets*. Casper, WY: CP Technologies.

[19] Nakka, R. (n.d.). Experiments with Ammonium Nitrate / Aluminum based Propellant Formulations. Retrieved from http://www.nakka-rocketry.net/anexp.html

[20] Nakka, R. (n.d.). Measuring Chamber Pressure and Determining C-Star and Thrust Coefficient. Retrieved from https://www.nakka-rocketry.net/pressure-measurement.html

[21] DeMar, J. S. (n.d.). A Practical Guide to Kn. Retrieved from http://www.thrustgear.com/topics/Kn_Notes.htm

[22] Yount, R. A., & Angelus, T. A. (1964). Chuffing and nonacoustic instability phenomena in solid propellant rockets. *AIAA Journal*, *2*(7), 1307–1313. doi: 10.2514/3.2537

[23] Mueller, T. (n.d.). Liquid Rocket Components: Pyrotechnic Valves. Retrieved from maxentropy.net/rocketry/pyrovalve/PyroValve.pdf

APPENDIX A

```
Code                                  WEIGHT     D-H  DENS     COMPOSITION
      0 AMMONIUM NITRATE                 40.500   -1090  0.06230   4 H    2 N    3 O
      0 SULFUR                            2.700       0  0.07470   1 S
      0 ALUMINUM (PURE CRYSTALINE)       15.700       0  0.09750   1 AL
      0 MAGNESIUM (PURE CRYSTALINE)      15.700       0  0.06280   1 MG
      0 CUPRIC OXIDE                      1.100    -473  0.22800   1 CU   1 O
      0 CHLOROPRENE                      24.300   -2000  0.05540   4 C    5 H    1 CL

THE PROPELLANT DENSITY IS  0.06491 LB/CU-IN OR   1.7966 GM/CC
THE TOTAL PROPELLANT WEIGHT IS  100.0000 GRAMS

NUMBER OF GRAM ATOMS OF EACH ELEMENT PRESENT IN INGREDIENTS

    3.396031 H
    1.097796 C
    1.011893 N
    1.531669 O
    0.645559 MG
    0.581913 AL
    0.084201 S
    0.274449 CL
    0.013830 CU

**************************CHAMBER RESULTS FOLLOW   ***************************
  T(K)  T(F)  P(ATM)   P(PSI) ENTHALPY  ENTROPY   CP/CV    GAS   RT/V
  2197  3496    13.60   200.00   -93.27   190.42  1.1621  3.117    4.510

SPECIFIC HEAT (MOLAR) OF GAS AND TOTAL =     8.604    11.333
NUMBER MOLS GAS AND CONDENSED =     3.012    0.955

 1.658868e+000 H2         5.596777e-001 C&         4.997452e-001 CO         4.690683e-001 N2
 2.578524e-001 MgAl2O4&   1.701420e-001 Mg         1.119757e-001 MgCl2      8.235873e-002 MgS&
```

```
 4.801712e-002 AlN&       2.556765e-002 CNH        1.684451e-002 AlCl       1.575310e-002 HCl
 1.349980e-002 MgCl       8.938317e-003 MgH        7.066680e-003 Cu*        5.174671e-003 Cu
 4.709573e-003 C2H2       3.356596e-003 H          2.810088e-003 CH4        1.492465e-003 CuCl
 1.108094e-003 H2S        9.285761e-004 AlCl2      3.819400e-004 MgS        2.276668e-004 H2O
 1.732802e-004 Mg2Cl4     1.425767e-004 CH3        1.403512e-004 CS         1.223963e-004 Al
 1.220937e-004 HS         1.004705e-004 NH3        8.287412e-005 AlCl3      7.889234e-005 C2H4
 5.841319e-005 AlH        4.870657e-005 Al2O       3.885018e-005 Cu2        3.162121e-005 MgHO
 2.337334e-005 Cl         1.524312e-005 AlHO       1.387876e-005 CO2        1.377748e-005 CSO
 1.274149e-005 C2H        9.910289e-006 MgN        4.301742e-006 S          3.922845e-006 C2N2
 3.593781e-006 AlOCl      3.205501e-006 CS2        2.624054e-006 AlS        2.480489e-006 CH2O
  2.47353E-06 CN          2.47353E-06 CN

THE MOLECULAR WEIGHT OF THE MIXTURE IS    25.208

*****************************EXHAUST RESULTS FOLLOW    *****************************
  T(K)  T(F)  P(ATM)    P(PSI) ENTHALPY  ENTROPY   CP/CV    GAS    RT/V
  1843  2857     1.00    14.70  -124.16   190.42  1.1463  2.835    0.353

SPECIFIC HEAT (MOLAR) OF GAS AND TOTAL =     8.403    11.147
NUMBER MOLS GAS AND CONDENSED =     2.835    1.126

 1.685273e+000 H2         7.288175e-001 C&         5.024772e-001 N2         3.604375e-001 CO
 2.895388e-001 MgAl2O4&   1.264004e-001 MgCl2      1.258634e-001 Mg         8.387965e-002 MgS&
 1.287126e-002 MgO&       1.206257e-002 HCl        1.052926e-002 Cu*        6.867503e-003 CNH
 5.408462e-003 MgCl       2.652523e-003 AlCl       2.487288e-003 Cu         1.360909e-003 MgH
 1.109941e-003 H          7.835975e-004 CuCl       6.187686e-004 CH4        4.729234e-004 C2H2
 1.969176e-004 H2S        1.215893e-004 AlCl2      9.073848e-005 Mg2Cl4     4.978285e-005 H2O
 3.007324e-005 MgS        1.539259e-005 AlCl3      1.493410e-005 NH3        1.324970e-005 HS
 1.293328e-005 CS         1.009812e-005 CH3        6.027795e-006 Cl         5.687462e-006 Cu2
 4.417745e-006 C2H4       3.303718e-006 Al         2.680807e-006 CO2        2.517445e-006 MgHO
  1.48268E-06 CSO         1.48268E-06 CSO

THE MOLECULAR WEIGHT OF THE MIXTURE IS    25.248

 **********PERFORMANCE:  FROZEN ON FIRST LINE, SHIFTING ON SECOND LINE**********
```

IMPULSE	IS EX	T*	P*	C*	ISP*	OPT-EX	D-ISP	A*M	EX-T
159.3	1.1807	2030	7.73	3848.0		2.84	286.3	0.59814	1525
164.0	1.0983	2119	8.19	3762.9	147.8	3.20	294.6	0.58490	1843

Figure A-1. PROPEP simulation output of A204 propellant.

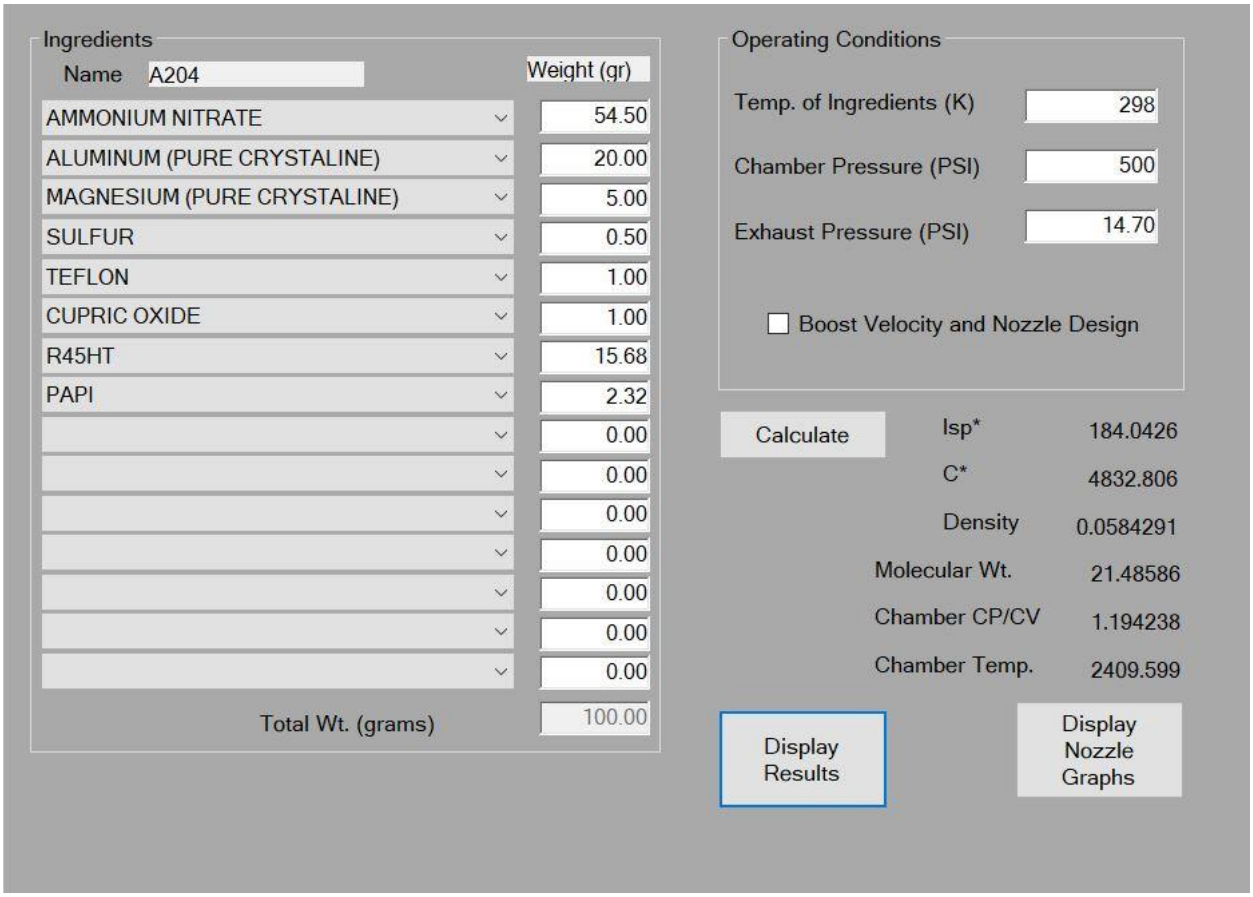

Figure A-2. PROPEP simulation of A204 propellant.

```
Code                                  WEIGHT     D-H  DENS     COMPOSITION
      0 AMMONIUM NITRATE                 54.500   -1090  0.06230   4 H    2 N    3 O
      0 ALUMINUM (PURE CRYSTALINE)       20.000       0  0.09750   1 AL
      0 MAGNESIUM (PURE CRYSTALINE)       5.000       0  0.06290   1 MG
      0 SULFUR                            0.500       0  0.07470   1 S
      0 TEFLON                            1.000   -1930  0.07940   1 C    2 F
      0 CUPRIC OXIDE                      1.000    -473  0.22800   1 CU   1 O
      0 R45HT                            15.680       0  0.03290 667 C  999 H    5 O
      0 PAPI                              2.320    -202  0.04480 224 C  155 H   27 O   27 N

THE PROPELLANT DENSITY IS  0.05843 LB/CU-IN OR   1.6173 GM/CC
THE TOTAL PROPELLANT WEIGHT IS  100.0000 GRAMS
```

```
NUMBER OF GRAM ATOMS OF EACH ELEMENT PRESENT IN INGREDIENTS

    4.543370 H
    1.311608 C
    1.378812 N
    2.080843 O
    0.039991 F
    0.205592 MG
    0.741290 AL
    0.015593 S
    0.012572 CU

**************************CHAMBER RESULTS FOLLOW   ****************************
  T(K)  T(F)  P(ATM)   P(PSI) ENTHALPY  ENTROPY   CP/CV    GAS   RT/V
  2410  3878    34.01   500.00   -62.28   238.69  1.1942  4.150    8.195

SPECIFIC HEAT (MOLAR) OF GAS AND TOTAL =     8.690    10.894
NUMBER MOLS GAS AND CONDENSED =     4.150    0.504

 2.222396e+000 H2         1.262124e+000 CO         5.284353e-001 N2         2.886782e-001 AlN&
 1.698566e-001 MgAl2O4*   4.531188e-002 Al2O3*     3.293581e-002 CNH        3.222422e-002 Mg
 1.218039e-002 Cu         1.175093e-002 AlF        1.118511e-002 H2S        8.684477e-003 H
 6.672794e-003 AlF4-      5.413245e-003 C2H2       3.284847e-003 CH4        2.644244e-003 MgH
 1.694661e-003 HS         1.288836e-003 H2O        1.279516e-003 CS         1.127253e-003 Al2O
 9.375042e-004 HF         7.429076e-004 Al         6.045477e-004 MgS        4.214206e-004 AlH
 3.077747e-004 CH3        2.462956e-004 CSO        2.333978e-004 NH3        2.000906e-004 MgF
 1.849083e-004 AlHO       1.545813e-004 Cu2        1.243918e-004 CO2        1.139189e-004 CS2
 9.268897e-005 AlS        9.061737e-005 C2H4       7.707536e-005 S          6.337954e-005 Cu*
 6.171667e-005 AlF2       5.508868e-005 S2         3.947983e-005 AlOF2      3.072291e-005 C2H
 2.806641e-005 MgHO       2.125584e-005 AlOF       1.434241e-005 CHO        1.385448e-005 CH2O
 8.455031e-006 CN         5.961351e-006 C2N2       5.052236e-006 MgN        4.745358e-006 MgF2
 3.365922e-006 CuF        3.223920e-006 S3         2.951964e-006 NH2        2.656711e-006 CNHO
   2.2509E-06 CH2          2.2509E-06 CH2          2.2509E-06 CH2

THE MOLECULAR WEIGHT OF THE MIXTURE IS    21.486

**************************EXHAUST RESULTS FOLLOW   ****************************
  T(K)  T(F)  P(ATM)   P(PSI) ENTHALPY  ENTROPY   CP/CV    GAS   RT/V
  1855  2880     1.00    14.70  -122.24   238.69  1.1842  3.880    0.259

SPECIFIC HEAT (MOLAR) OF GAS AND TOTAL =     8.344    10.627
NUMBER MOLS GAS AND CONDENSED =     3.880    0.783

 2.255466e+000 H2         9.471778e-001 CO         6.328545e-001 N2         3.517265e-001 C&
 1.924444e-001 MgAl2O4&   1.211585e-001 Al2O3&     1.035503e-001 AlN&       9.709841e-003
AlF4-
 9.469066e-003 CNH        8.636495e-003 Cu*        7.761848e-003 H2S        7.175529e-003 Mg
 5.808721e-003 MgS&       3.900006e-003 Cu         1.660821e-003 H          7.776448e-004 CH4
 7.641690e-004 AlF        6.976728e-004 C2H2       5.891314e-004 CS         5.632223e-004 HS
 2.431285e-004 CS2        1.955054e-004 HF         1.206335e-004 H2O        1.129297e-004 CSO
 7.697847e-005 MgH        5.389668e-005 S2         5.097482e-005 MgS        1.850255e-005 NH3
 1.677473e-005 S          1.417090e-005 CH3        1.260441e-005 CO2        1.060701e-005 Al
 9.626470e-006 S3         9.393910e-006 Cu2        8.450428e-006 MgF        5.874495e-006 C2H4
 3.192418e-006 AlH        2.490230e-006 Al2O       2.308685e-006 AlS        2.272648e-006 AlHO
  1.37874E-06 AlF2

THE MOLECULAR WEIGHT OF THE MIXTURE IS    21.445
```

```
**********PERFORMANCE:  FROZEN ON FIRST LINE, SHIFTING ON SECOND LINE**********

IMPULSE   IS EX      T*       P*      C*    ISP*  OPT-EX  D-ISP      A*M   EX-T
  214.8  1.2040    2187    19.17  4596.5            5.27  347.4  0.28579   1326
  228.4  1.1258    2346    19.63  4832.8   184.0    6.17  369.4  0.30048   1855
```

Figure A-3. PROPEP simulation output of A204 propellant.

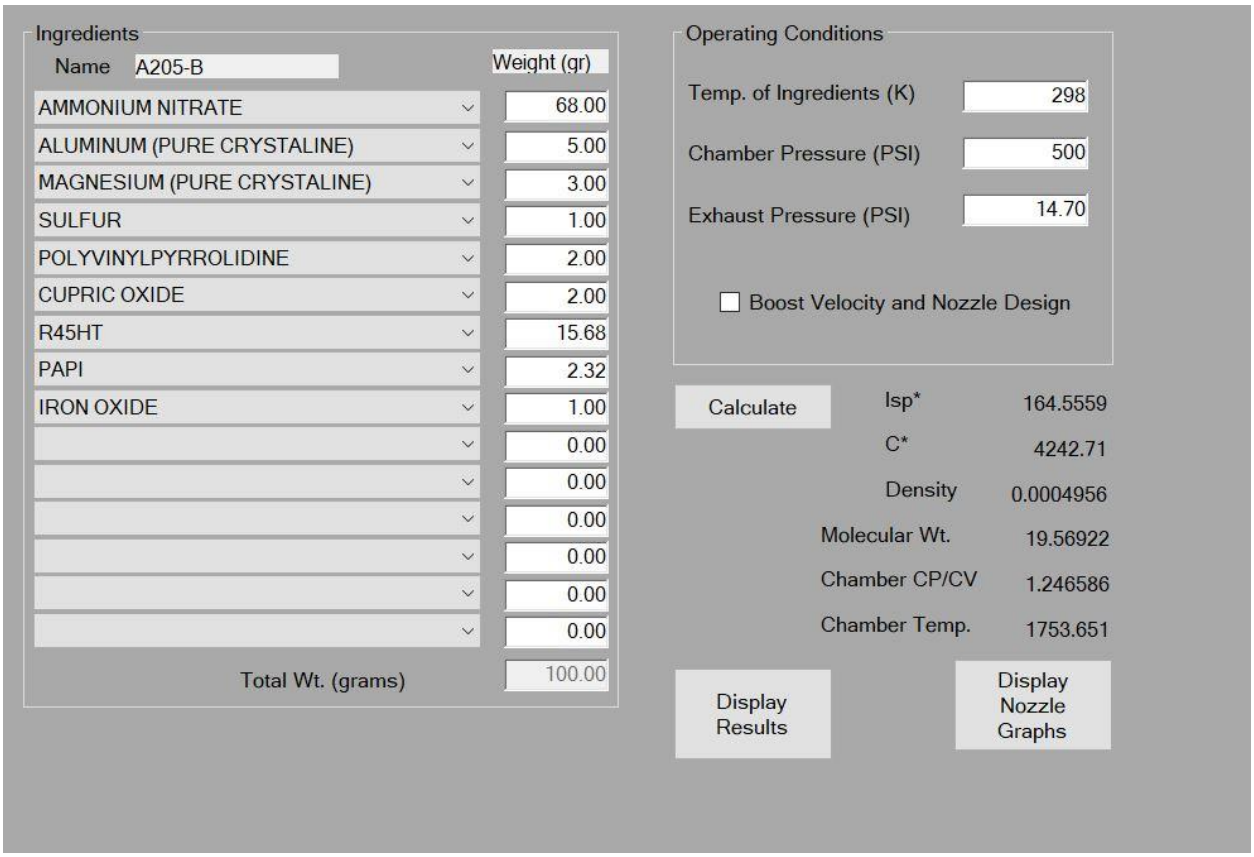

Figure A-4. PROPEP simulation of A205 propellant.

```
Code                                  WEIGHT     D-H  DENS     COMPOSITION
      0 AMMONIUM NITRATE                 68.000   -1090  0.06230   4 H    2 N    3 O
      0 ALUMINUM (PURE CRYSTALINE)        5.000       0  0.09750   1 AL
      0 MAGNESIUM (PURE CRYSTALINE)       3.000       0  0.06290   1 MG
      0 SULFUR                            1.000       0  0.07470   1 S
      0 POLYVINYLPYRROLIDINE              2.000    -331  0.00001 520 C  788 H  109 O   88 N
      0 CUPRIC OXIDE                      2.000    -473  0.22800   1 CU   1 O
      0 R45HT                            15.680       0  0.03290 667 C  999 H    5 O
      0 PAPI                              2.320    -202  0.04480 224 C  155 H   27 O   27 N
      0 IRON OXIDE                        1.000   -1230  0.18400   3 O    2 FE

THE PROPELLANT DENSITY IS  0.00050 LB/CU-IN OR   0.0137 GM/CC
THE TOTAL PROPELLANT WEIGHT IS  100.0000 GRAMS

NUMBER OF GRAM ATOMS OF EACH ELEMENT PRESENT IN INGREDIENTS
```

```
    5.375302 H
    1.395438 C
    1.733680 N
    2.639910 O
    0.123355 MG
    0.185323 AL
    0.031186 S
    0.012523 FE
    0.025145 CU

***************************CHAMBER RESULTS FOLLOW   ***************************
  T(K)  T(F)  P(ATM)   P(PSI) ENTHALPY  ENTROPY   CP/CV    GAS   RT/V
  1754  2697    34.01   500.00   -77.43   258.42  1.2466  4.949    6.872

SPECIFIC HEAT (MOLAR) OF GAS AND TOTAL =     8.964     9.729
NUMBER MOLS GAS AND CONDENSED =     4.949    0.161

 1.941426e+000 H2         1.265828e+000 CO         8.665043e-001 N2         7.146036e-001 H2O
 1.286092e-001 CO2        9.264272e-002 MgAl2O4&   3.068559e-002 MgO&       3.007260e-002 H2S
 2.508502e-002 Cu*        1.243097e-002 Fe&        6.796719e-004 CSO        5.673295e-004 NH3
 2.478442e-004 HS         1.858373e-004 CH4        1.278419e-004 H          6.432230e-005
FeH2O2
 5.355606e-005 CNH        4.556015e-005 Cu         2.446437e-005 S3         2.108894e-005 S2
 1.216583e-005 CH2O       2.937854e-006 MgH2O2     2.849574e-006 HO         2.608657e-006 SO2
  2.37895E-06 SO          2.37895E-06 SO          2.37895E-06 SO

THE MOLECULAR WEIGHT OF THE MIXTURE IS    19.569

***************************EXHAUST RESULTS FOLLOW   ***************************
  T(K)  T(F)  P(ATM)   P(PSI) ENTHALPY  ENTROPY   CP/CV    GAS   RT/V
   958  1265     1.00    14.70  -121.69   258.42  1.2715  4.796    0.209

SPECIFIC HEAT (MOLAR) OF GAS AND TOTAL =     8.338     9.003
NUMBER MOLS GAS AND CONDENSED =     4.796    0.161

 2.000721e+000 H2         9.127297e-001 CO         8.666007e-001 N2         5.143215e-001 H2O
 4.055806e-001 CO2        9.264272e-002 MgAl2O4&   7.679141e-002 CH4        3.068753e-002 MgO&
 2.512958e-002 Cu&        1.835016e-002 H2S        1.249548e-002 FeS&       4.274137e-004 NH3
  0.000265601 CSO         0.000265601 CSO         0.000265601 CSO

THE MOLECULAR WEIGHT OF THE MIXTURE IS    20.174

 **********PERFORMANCE:  FROZEN ON FIRST LINE, SHIFTING ON SECOND LINE**********

 IMPULSE   IS EX      T*      P*      C*    ISP*  OPT-EX  D-ISP      A*M   EX-T
   193.9  1.2700    1545   18.75  4192.8            4.77    2.7  0.26069    829
   196.3  1.2448    1563   18.91  4242.7   164.6    5.22    2.7  0.26379    958
```

Figure A-5. PROPEP simulation output of A205 propellant.

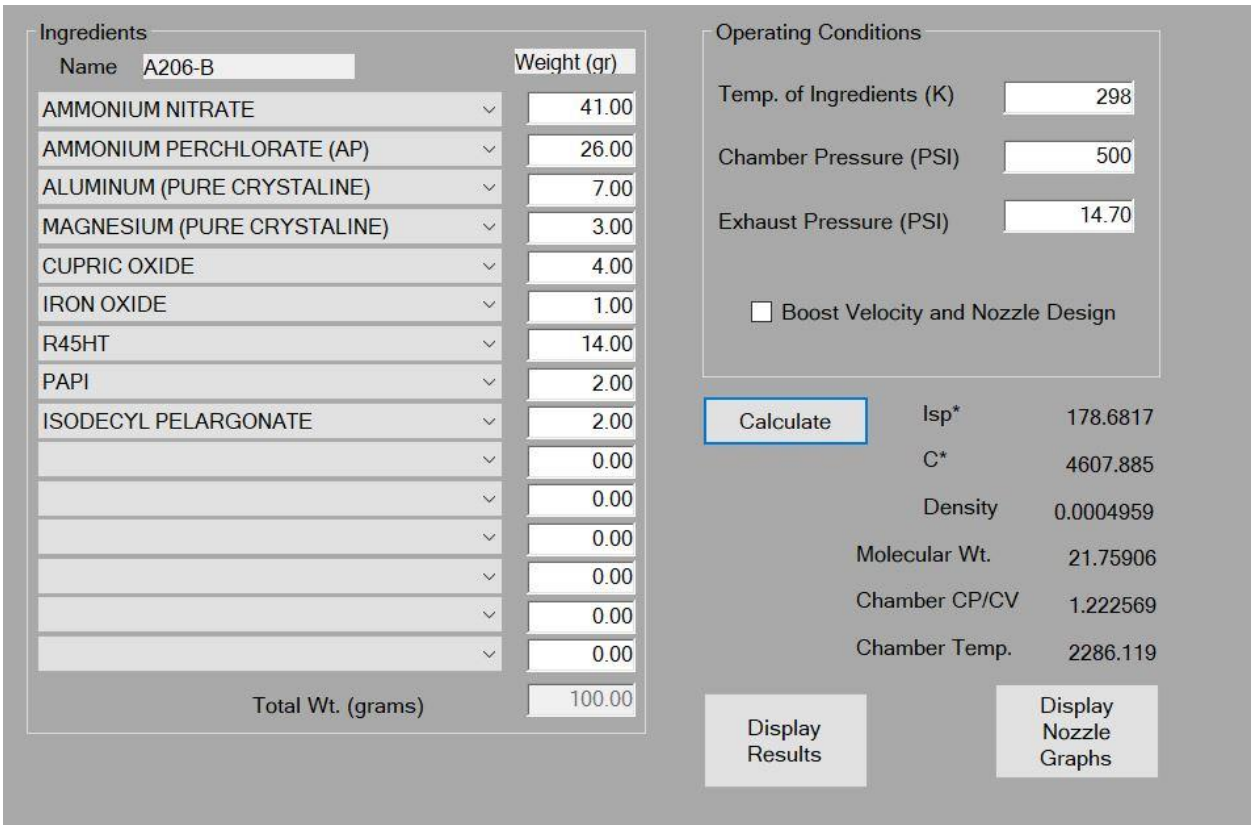

Figure A-6. PROPEP simulation of A206-B propellant.

```
Code                                  WEIGHT     D-H  DENS     COMPOSITION
      0 AMMONIUM NITRATE                 41.000   -1090  0.06230   4 H    2 N    3 O
      0 AMMONIUM PERCHLORATE (AP)        26.000    -602  0.07040   1 CL   4 H    1 N    4 O
      0 ALUMINUM (PURE CRYSTALINE)        7.000       0  0.09750   1 AL
      0 MAGNESIUM (PURE CRYSTALINE)       3.000       0  0.06290   1 MG
      0 CUPRIC OXIDE                      4.000    -473  0.22800   1 CU   1 O
      0 IRON OXIDE                        1.000   -1230  0.18400   3 O    2 FE
      0 R45HT                            14.000       0  0.03290 667 C  999 H    5 O
      0 PAPI                              2.000    -202  0.04480 224 C  155 H   27 O   27 N
      0 ISODECYL PELARGONATE              2.000    -714  0.00001  19 C   38 H    2 O

THE PROPELLANT DENSITY IS  0.00050 LB/CU-IN OR   0.0137 GM/CC
THE TOTAL PROPELLANT WEIGHT IS  100.0000 GRAMS

NUMBER OF GRAM ATOMS OF EACH ELEMENT PRESENT IN INGREDIENTS

    4.810471 H
    1.276147 C
    1.260434 N
    2.526641 O
    0.123355 MG
    0.259451 AL
    0.221282 CL
    0.012523 FE
    0.050289 CU
```

```
**************************CHAMBER RESULTS FOLLOW   ****************************
  T(K)  T(F)  P(ATM)   P(PSI) ENTHALPY  ENTROPY   CP/CV    GAS   RT/V
  2295  3672    68.02  1000.00   -65.30   243.40  1.2219  4.433   15.344

SPECIFIC HEAT (MOLAR) OF GAS AND TOTAL =     9.318    10.552
NUMBER MOLS GAS AND CONDENSED =     4.433    0.164

 1.658123e+000 H2         1.191274e+000 CO         6.534647e-001 H2O        6.299686e-001 N2
 1.820415e-001 HCl        1.224986e-001 MgAl2O4&   8.465954e-002 CO2        3.394235e-002 Cu*
 1.317653e-002 CuCl       1.199278e-002 FeCl2      7.196286e-003 Al2O3&     3.107765e-003 H
 3.042050e-003 Cu         8.005038e-004 MgCl2      3.513191e-004 NH3        2.932094e-004
FeH2O2
 2.447859e-004 Cl         2.000871e-004 HO         1.834684e-004 Fe         8.077266e-005 CNH
 2.953793e-005 Cu2        2.094415e-005 FeCl       1.905454e-005 Cu3Cl3     1.862019e-005 CH2O
 1.549791e-005 CH4        1.346110e-005 MgH2O2     1.093698e-005 CHO        7.907403e-006 MgCl
 7.304391e-006 AlCl       6.513335e-006 Mg         6.506301e-006 NO         6.172385e-006
AlCl2
 6.035017e-006 AlCl3      5.272190e-006 MgHO       4.274430e-006 CNHO       3.575557e-006
FeCl3
 3.355228e-006 AlOCl      2.686556e-006 FeO        2.356756e-006 AlHO2      2.081062e-006 NH2
  1.90942E-06 Fe2Cl4      1.90942E-06 Fe2Cl4      1.90942E-06 Fe2Cl4

THE MOLECULAR WEIGHT OF THE MIXTURE IS    21.753

**************************EXHAUST RESULTS FOLLOW   ****************************
  T(K)  T(F)  P(ATM)   P(PSI) ENTHALPY  ENTROPY   CP/CV    GAS   RT/V
  1059  1447     1.00    14.70  -124.81   243.40  1.2616  4.411    0.227

SPECIFIC HEAT (MOLAR) OF GAS AND TOTAL =     8.225     9.193
NUMBER MOLS GAS AND CONDENSED =     4.411    0.188

 1.832246e+000 H2         9.897875e-001 CO         6.300987e-001 N2         4.553475e-001 H2O
 2.805540e-001 CO2        2.117907e-001 HCl        1.233272e-001 MgAl2O4&   5.025307e-002 Cu&
 7.812337e-003 FeO&       6.377964e-003 Al2O3&     5.717097e-003 CH4        4.641406e-003
FeCl2
 1.797015e-004 NH3        2.137024e-005 Fe2Cl4     5.509669e-006 Cu3Cl3     4.576720e-006 CuCl
  1.93138E-06 CNH

THE MOLECULAR WEIGHT OF THE MIXTURE IS    21.747

 **********PERFORMANCE:  FROZEN ON FIRST LINE, SHIFTING ON SECOND LINE**********

 IMPULSE   IS EX      T*      P*      C*    ISP*  OPT-EX  D-ISP      A*M   EX-T
   226.0  1.2441    2046   37.82  4568.5           8.15    3.1  0.14202   1003
   227.6  1.2257    2064   38.06  4608.9   178.8   8.43    3.1  0.14328   1059

   Code                                  WEIGHT     D-H  DENS     COMPOSITION
      0 AMMONIUM NITRATE                 41.000   -1090  0.06230   4 H    2 N    3 O
      0 AMMONIUM PERCHLORATE (AP)        26.000    -602  0.07040   1 CL   4 H    1 N    4 O
      0 ALUMINUM (PURE CRYSTALINE)        7.000       0  0.09750   1 AL
      0 MAGNESIUM (PURE CRYSTALINE)       3.000       0  0.06290   1 MG
      0 CUPRIC OXIDE                      4.000    -473  0.22800   1 CU   1 O
      0 IRON OXIDE                        1.000   -1230  0.18400   3 O    2 FE
      0 R45HT                            14.000       0  0.03290 667 C  999 H    5 O
      0 PAPI                              2.000    -202  0.04480 224 C  155 H   27 O   27 N
      0 ISODECYL PELARGONATE              2.000    -714  0.00001  19 C   38 H    2 O
```

```
THE PROPELLANT DENSITY IS  0.00050 LB/CU-IN OR   0.0137 GM/CC
THE TOTAL PROPELLANT WEIGHT IS  100.0000 GRAMS

NUMBER OF GRAM ATOMS OF EACH ELEMENT PRESENT IN INGREDIENTS

    4.810471 H
    1.276147 C
    1.260434 N
    2.526641 O
    0.123355 MG
    0.259451 AL
    0.221282 CL
    0.012523 FE
    0.050289 CU

****************************CHAMBER RESULTS FOLLOW   ****************************
  T(K)  T(F)  P(ATM)   P(PSI) ENTHALPY  ENTROPY   CP/CV    GAS   RT/V
  2286  3656    34.01   500.00   -65.30   249.51  1.2226  4.439    7.662

SPECIFIC HEAT (MOLAR) OF GAS AND TOTAL =     9.308    10.543
NUMBER MOLS GAS AND CONDENSED =     4.439    0.157

 1.660319e+000 H2         1.191088e+000 CO         6.530403e-001 H2O        6.300757e-001 N2
 1.779754e-001 HCl        1.225457e-001 MgAl2O4&   8.491249e-002 CO2        2.677049e-002 Cu*
 1.764768e-002 CuCl       1.181777e-002 FeCl2      7.148674e-003 Al2O3&     5.712558e-003 Cu
 4.194917e-003 H          7.450123e-004 MgCl2      3.516596e-004 Fe         3.230318e-004 Cl
 2.934143e-004 FeH2O2     2.661283e-004 HO         1.777854e-004 NH3        5.421408e-005 Cu2
 4.043360e-005 CNH        2.815415e-005 FeCl       1.271978e-005 MgH2O2     1.266669e-005
Cu3Cl3
 1.183664e-005 Mg         1.013211e-005 MgCl       9.323606e-006 CH2O       9.181666e-006 AlCl
 8.550765e-006 NO         7.487685e-006 CHO        6.845460e-006 MgHO       5.503530e-006
AlCl2
 5.050926e-006 FeO        4.239520e-006 AlOCl      4.067429e-006 CH4        3.872889e-006
AlCl3
 3.018051e-006 AlHO2      2.441979e-006 FeCl3      2.130740e-006 CNHO       1.852660e-006 AlHO
  1.41669E-06 NH2

THE MOLECULAR WEIGHT OF THE MIXTURE IS    21.759

****************************EXHAUST RESULTS FOLLOW   ****************************
  T(K)  T(F)  P(ATM)   P(PSI) ENTHALPY  ENTROPY   CP/CV    GAS   RT/V
  1201  1702     1.00    14.70  -117.92   249.51  1.2555  4.422    0.226

SPECIFIC HEAT (MOLAR) OF GAS AND TOTAL =     8.376     9.373
NUMBER MOLS GAS AND CONDENSED =     4.422    0.184

 1.788972e+000 H2         1.055133e+000 CO         6.301472e-001 N2         5.135182e-001 H2O
 2.206845e-001 CO2        2.041884e-001 HCl        1.233273e-001 MgAl2O4&   5.020511e-002 Cu&
 8.440249e-003 FeCl2      6.377962e-003 Al2O3&     4.035075e-003 FeO&       2.417367e-004 CH4
 8.232492e-005 NH3        4.878739e-005 CuCl       1.058194e-005 Fe2Cl4     6.754619e-006
Cu3Cl3
  1.69092E-06 CNH

THE MOLECULAR WEIGHT OF THE MIXTURE IS    21.713

 **********PERFORMANCE:  FROZEN ON FIRST LINE, SHIFTING ON SECOND LINE**********
```

```
 IMPULSE   IS EX      T*      P*      C*    ISP*  OPT-EX  D-ISP      A*M   EX-T
   212.5  1.2408    2040   18.93  4574.8           4.98    2.9  0.28444   1153
   214.0  1.2223    2060   19.05  4607.9   178.7    5.09    2.9  0.28650   1201

   Code                                  WEIGHT     D-H  DENS     COMPOSITION
      0 AMMONIUM NITRATE                 41.000   -1090  0.06230   4 H    2 N    3 O
      0 AMMONIUM PERCHLORATE (AP)        26.000    -602  0.07040   1 CL   4 H    1 N    4 O
      0 ALUMINUM (PURE CRYSTALINE)        7.000       0  0.09750   1 AL
      0 MAGNESIUM (PURE CRYSTALINE)       3.000       0  0.06290   1 MG
      0 CUPRIC OXIDE                      4.000    -473  0.22800   1 CU   1 O
      0 IRON OXIDE                        1.000   -1230  0.18400   3 O    2 FE
      0 R45HT                            14.000       0  0.03290 667 C  999 H    5 O
      0 PAPI                              2.000    -202  0.04480 224 C  155 H   27 O   27 N
      0 ISODECYL PELARGONATE              2.000    -714  0.00001  19 C   38 H    2 O

THE PROPELLANT DENSITY IS  0.00050 LB/CU-IN OR   0.0137 GM/CC
THE TOTAL PROPELLANT WEIGHT IS  100.0000 GRAMS

NUMBER OF GRAM ATOMS OF EACH ELEMENT PRESENT IN INGREDIENTS

    4.810471 H
    1.276147 C
    1.260434 N
    2.526641 O
    0.123355 MG
    0.259451 AL
    0.221282 CL
    0.012523 FE
    0.050289 CU

**************************CHAMBER RESULTS FOLLOW   ****************************
  T(K)  T(F)  P(ATM)   P(PSI) ENTHALPY  ENTROPY   CP/CV    GAS   RT/V
  2286  3656    34.01   500.00   -65.30   249.51  1.2226  4.439    7.662

SPECIFIC HEAT (MOLAR) OF GAS AND TOTAL =     9.308    10.543
NUMBER MOLS GAS AND CONDENSED =     4.439    0.157

 1.660319e+000 H2         1.191088e+000 CO         6.530403e-001 H2O        6.300757e-001 N2
 1.779754e-001 HCl        1.225457e-001 MgAl2O4&   8.491249e-002 CO2        2.677049e-002 Cu*
 1.764768e-002 CuCl       1.181777e-002 FeCl2      7.148674e-003 Al2O3&     5.712558e-003 Cu
 4.194917e-003 H          7.450123e-004 MgCl2      3.516596e-004 Fe         3.230318e-004 Cl
 2.934143e-004 FeH2O2     2.661283e-004 HO         1.777854e-004 NH3        5.421408e-005 Cu2
 4.043360e-005 CNH        2.815415e-005 FeCl       1.271978e-005 MgH2O2     1.266669e-005
Cu3Cl3
 1.183664e-005 Mg         1.013211e-005 MgCl       9.323606e-006 CH2O       9.181666e-006 AlCl
 8.550765e-006 NO         7.487685e-006 CHO        6.845460e-006 MgHO       5.503530e-006
AlCl2
 5.050926e-006 FeO        4.239520e-006 AlOCl      4.067429e-006 CH4        3.872889e-006
AlCl3
 3.018051e-006 AlHO2      2.441979e-006 FeCl3      2.130740e-006 CNHO       1.852660e-006 AlHO
  1.41669E-06 NH2

THE MOLECULAR WEIGHT OF THE MIXTURE IS    21.759

**************************EXHAUST RESULTS FOLLOW   ****************************
  T(K)  T(F)  P(ATM)   P(PSI) ENTHALPY  ENTROPY   CP/CV    GAS   RT/V
  1201  1702     1.00    14.70  -117.92   249.51  1.2555  4.422    0.226
```

```
SPECIFIC HEAT (MOLAR) OF GAS AND TOTAL =     8.376     9.373
NUMBER MOLS GAS AND CONDENSED =     4.422     0.184

 1.788972e+000 H2         1.055133e+000 CO         6.301472e-001 N2         5.135182e-001 H2O
 2.206845e-001 CO2        2.041884e-001 HCl        1.233273e-001 MgAl2O4&   5.020511e-002 Cu&
 8.440249e-003 FeCl2      6.377962e-003 Al2O3&     4.035075e-003 FeO&       2.417367e-004 CH4
 8.232492e-005 NH3        4.878739e-005 CuCl       1.058194e-005 Fe2Cl4     6.754619e-006
Cu3Cl3
  1.69092E-06 CNH

THE MOLECULAR WEIGHT OF THE MIXTURE IS    21.713

 **********PERFORMANCE:  FROZEN ON FIRST LINE, SHIFTING ON SECOND LINE**********

 IMPULSE   IS EX      T*       P*       C*     ISP*  OPT-EX  D-ISP      A*M    EX-T
   212.5  1.2408    2040    18.93  4574.8             4.98    2.9  0.28444    1153
          214.0  1.2223    2060    19.05  4607.9    178.7    5.09    2.9  0.28650    1201
```

Figure A-7. PROPEP simulation output of A206-B propellant.

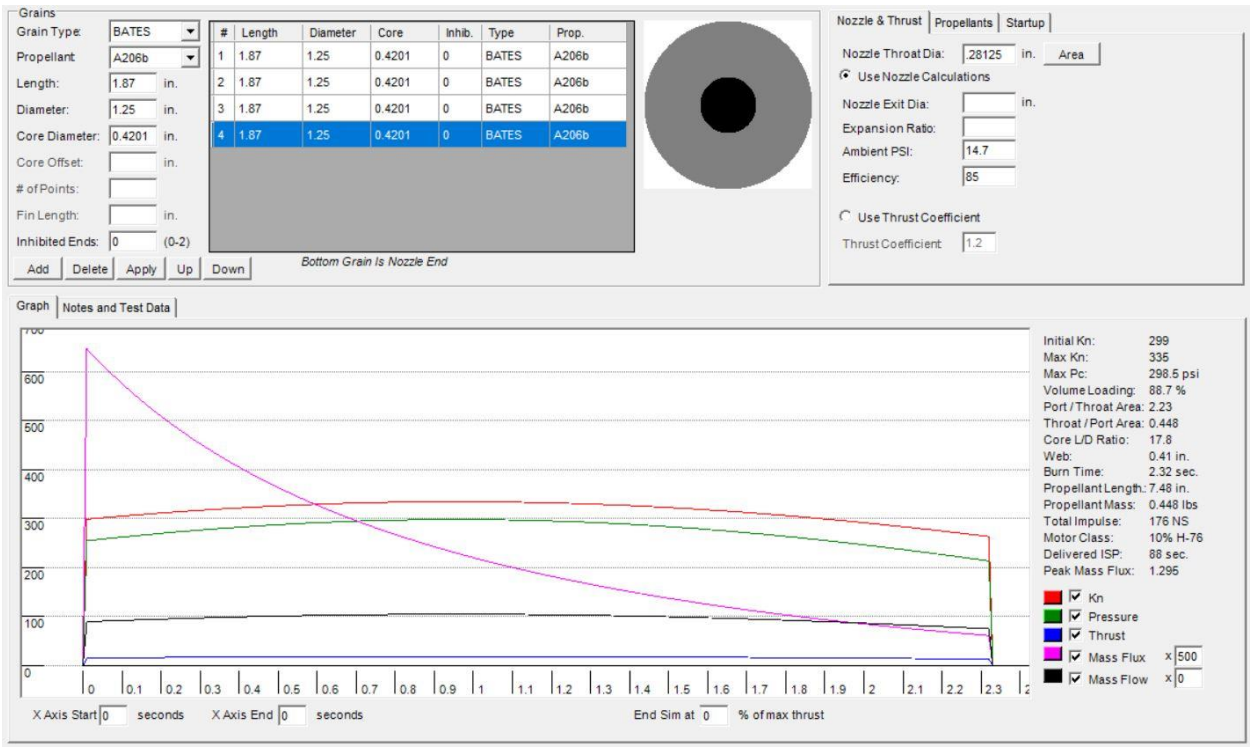

Figure A-8. BurnSim output of A206-B propellant.

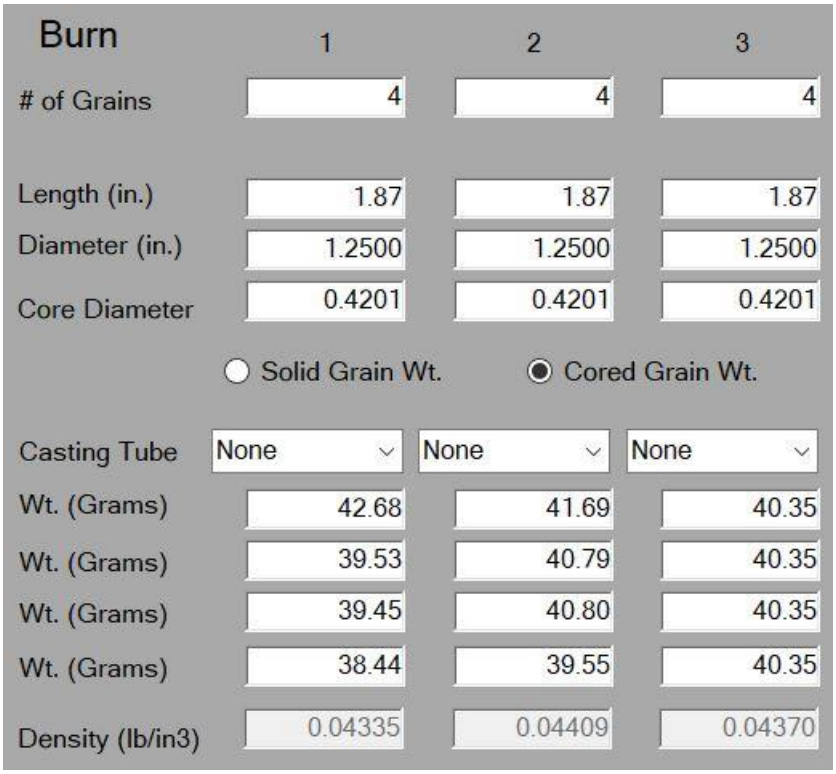

Figure A-9. ProPEP regression rate input for hypothetical third test fire-1.

Figure A-10. ProPEP regression rate input for hypothetical third test fire-2.

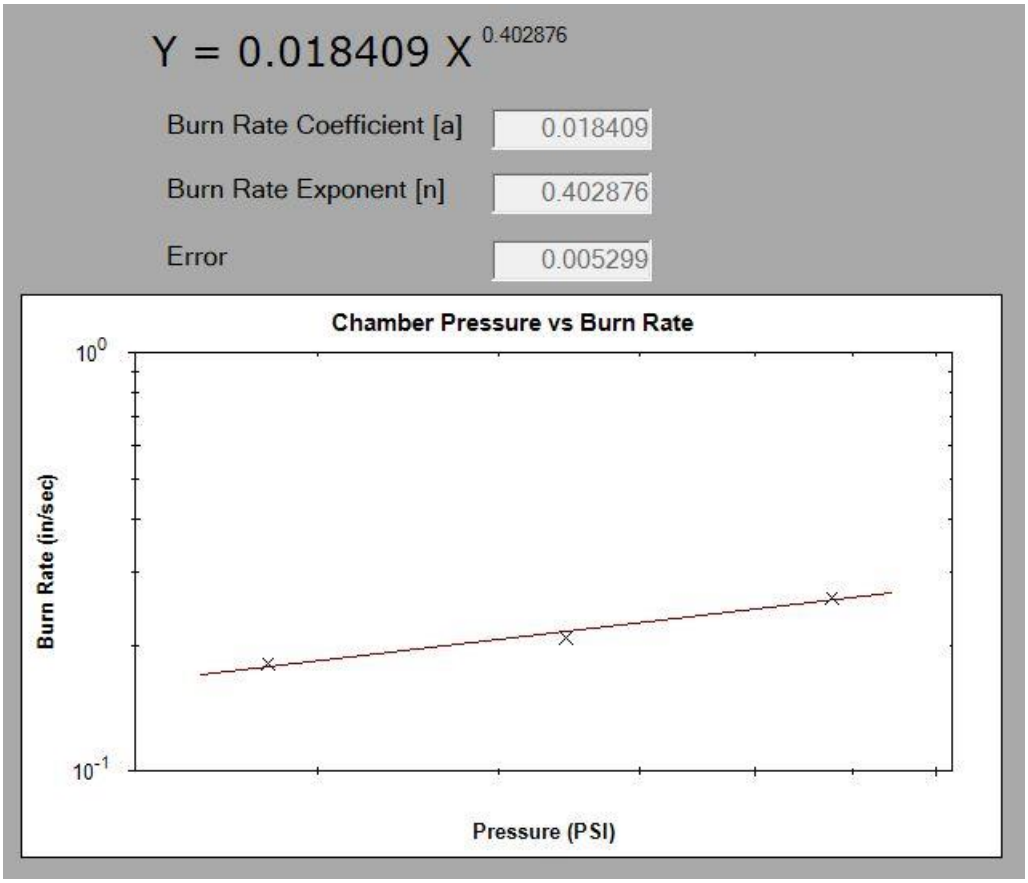

Figure A-11. ProPEP regression rate input for hypothetical third test fire-3.

Inputs	Outputs					
Injector				**Nitrous Oxide**		
Diameter of orifice (single injector)	0.1094	in		Tank Pressure	733	PSI
Area of orifice	0.0094	in^2		Liquid Density	48	lbs/ft^3
Discharge Coefficient	0.175			Liquid Density	0.027778	lbs/in^3
Number of orifices	3			Molecular Weight	44	g/mol
Diameter of singlet orifice	0.063162	in		Oxidizer Mass	1.094851	lbs
Tank				**Fuel Grain Geometry**		
Inner Diameter	2.045	in		Port Area for non Cylinder		in^2
Total length of tank	12	in		Fuel Grain Diameter	2	in
Volume of Tank	39.41462	in^3		Cylinder Port diameter	0.625	in
				Cylinder Port area	0.306796	in^2
Chamber				Cylinder Port circumference	1.963494	in
Initial Chamber Pressure	200	PSI		Grain length	9	in
O/F	3.840291	Pc/Pe		Grain End Burning Area	2.834794	in^2
Pe/Pc	0.055	18.181818		Total Grain Burning Area	23.34103	in^2
Chamber length	9	in				
Chamber Diameter	2	in				
Chamber Volume	28.27431	in^3		**Nitrous Oxide Mass Flow Rate**		
Characteristic Length (Liquids)	83.71135	in		0.372101506	lbs/s	
Nozzle				**Fuel Mass Flow Rate**		
Area Ratio (At/Ae)	Ae/At			0.096894099	lbm/s	
0.365332675	2.737231					
Area of Throat, At				**Total Mass Flow Rate m_dot tot**		
0.337759582	in^2			0.468995605	lb/s	
Diameter of Throat						
0.655781381	in			**Total Burn Time**		
Area of Exit, Ae				2.942345574	s	
0.924526068	in^2					
Diameter of Exit						
1.084962739	in					

Figure B-1. Hybrid design motor parameters Excel sheet-1.

Oxidizer Mass Flux (G_o)				**Ideal Initial Thrust**		k Correlations	
1.212863367	lb/s*in^2			91.856033	lbs	2k^2/k-1	9.8
						2/(k+1)	0.833333
Initial Chamber Temperature						k+1/k-1	6
2677	K	4818.6	°R	**Thrust Coefficient, Cf**		(Pe/Pc)^(k-1/k)	0.43662
				1.3597843		(Pe-Pa)*Ae If different Pa and Pe	
Fuel Regression Rate						k	1.4
a	0.104	in/s / (lbm/s/in2)^.681					
n	0.681						
Density (Rho)	0.035	lb/in^3					
r_dot	0.118606702	in/s					
Ratio of Specific Heats, k							
1.4							
Ambient Pressure							
11	PSI						
Gas Constant, R	65	ft-lb/lb °R					
Gravity, Gc	32.2	ft/s^2					
Throat Temperature							
4015.5	°R						
Throat Pressure							
105.6563575	PSI						
	Initial C*						
4637.936227	ft/s	1413.642962	m/s				
Initial ISP							
195.8569167	s						

Figure B-2. Hybrid design motor parameters Excel sheet-2.

a	n	a	n	a	n	a	n
0.104	0.1	0.104	0.2	0.104	0.3	0.104	0.4
r_dot	m dot ox	r_dot	m dot ox	r_dot	m dot ox	r_dot	m dot ox
0.0867452	0.05	0.072353148	0.05	0.060349	0.05	0.050336	0.05
0.0929712	0.1	0.083111942	0.1	0.074298	0.1	0.066419	0.1
0.0968183	0.15	0.090132555	0.15	0.083908	0.15	0.078114	0.15
0.0996441	0.2	0.095470551	0.2	0.091472	0.2	0.087641	0.2
0.1018925	0.25	0.099827784	0.25	0.097805	0.25	0.095823	0.25
0.1037673	0.3	0.103535117	0.3	0.103303	0.3	0.103072	0.3
0.1053793	0.35	0.106776834	0.35	0.108193	0.35	0.109628	0.35
0.1067959	0.4	0.109666865	0.4	0.112615	0.4	0.115643	0.4
0.1080612	0.45	0.112280912	0.45	0.116665	0.45	0.121221	0.45
0.1092057	0.5	0.114672011	0.5	0.120412	0.5	0.126439	0.5

Figure B-3. Hybrid design motor parameters- regression rate calculations-1.

a	n	a	n	a	n	a	n
0.104	0.5	0.104	0.6	0.104	0.681	0.104	0.7
r_dot	m dot ox	r_dot	m dot ox	r_dot	m dot ox	r_dot	m dot ox
0.041985	0.05	0.035019	0.05	0.030233	0.05	0.029209	0.05
0.059376	0.1	0.053079	0.1	0.048472	0.1	0.04745	0.1
0.07272	0.15	0.067698	0.15	0.063886	0.15	0.063024	0.15
0.08397	0.2	0.080453	0.2	0.077712	0.2	0.077083	0.2
0.093881	0.25	0.091979	0.25	0.090466	0.25	0.090115	0.25
0.102842	0.3	0.102612	0.3	0.102426	0.3	0.102382	0.3
0.111082	0.35	0.112555	0.35	0.113763	0.35	0.114048	0.35
0.118751	0.4	0.121944	0.4	0.124592	0.4	0.125222	0.4
0.125955	0.45	0.130873	0.45	0.134998	0.45	0.135984	0.45
0.132768	0.5	0.139414	0.5	0.14504	0.5	0.146392	0.5

Figure B-4. Hybrid design motor parameters- regression rate calculations-2.

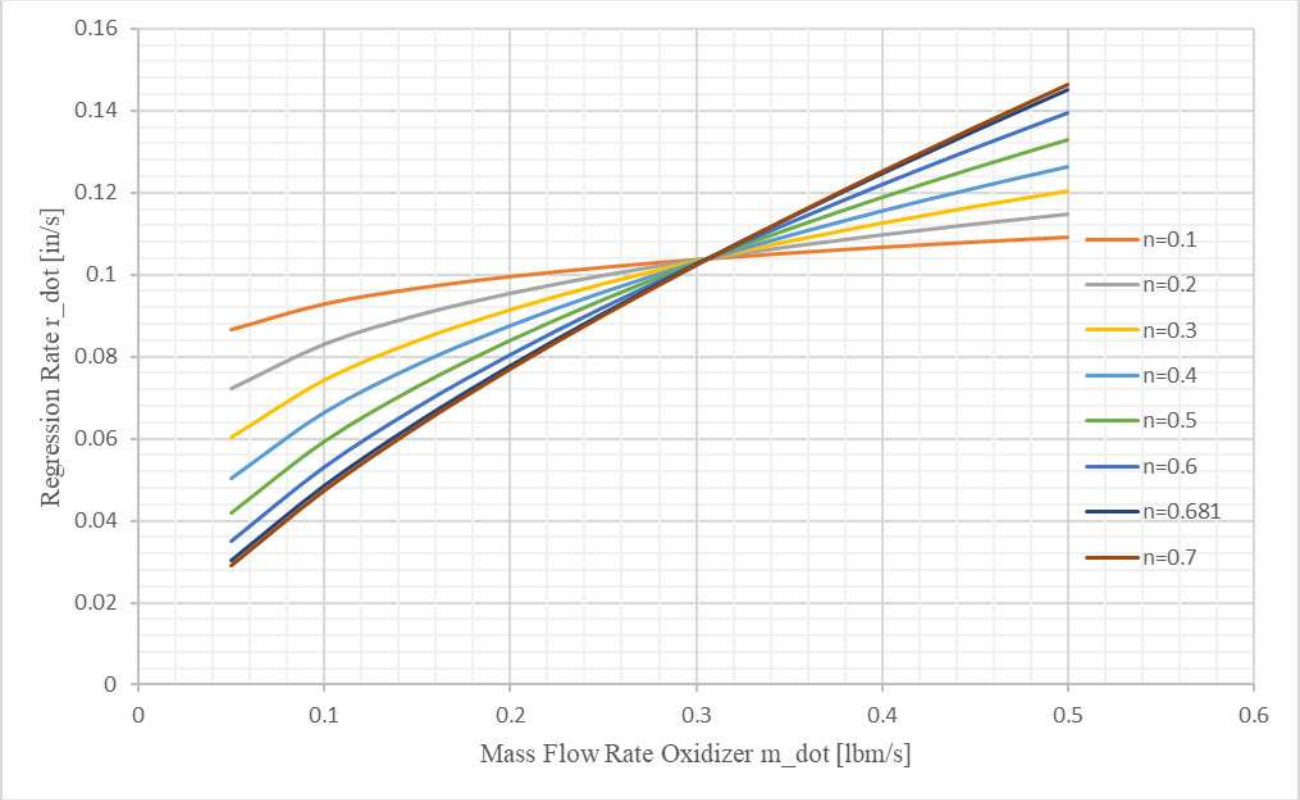

Figure B-5. Regression rate versus oxidizer mass flow rate.

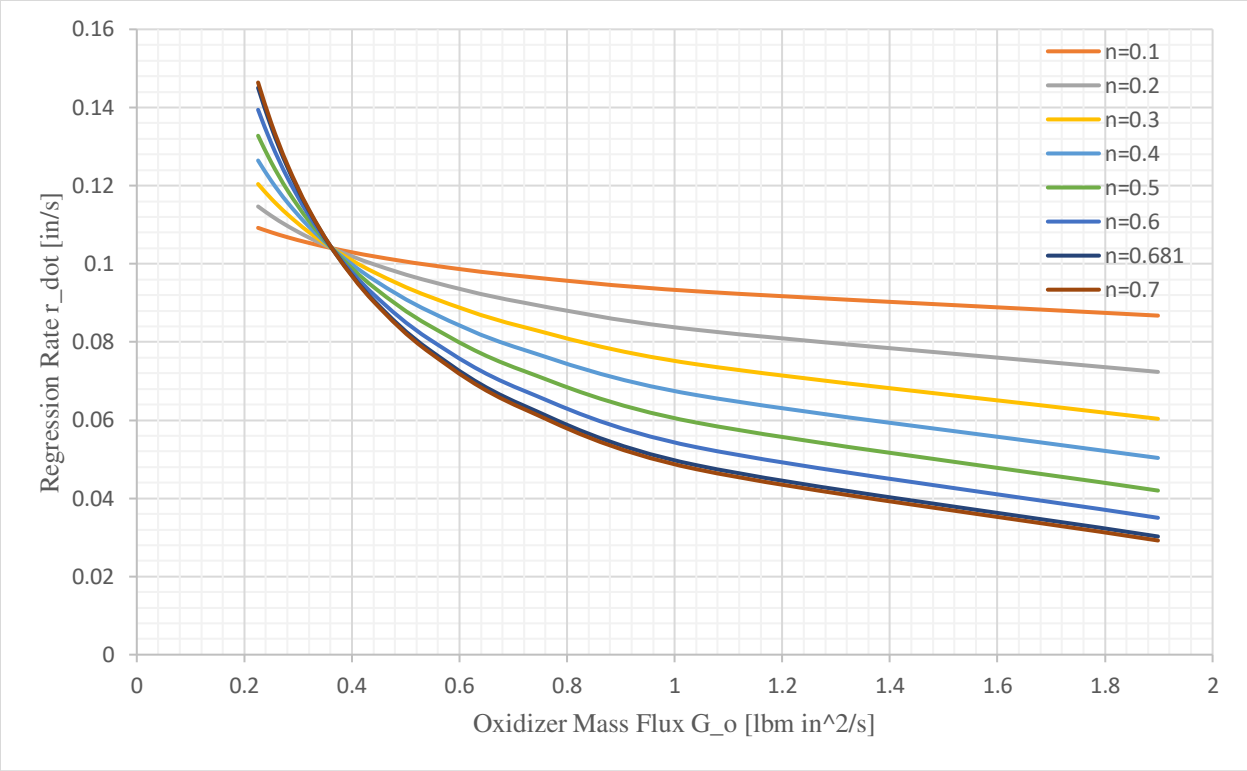

Figure B-6. Regression rate versus oxidizer mass flux.

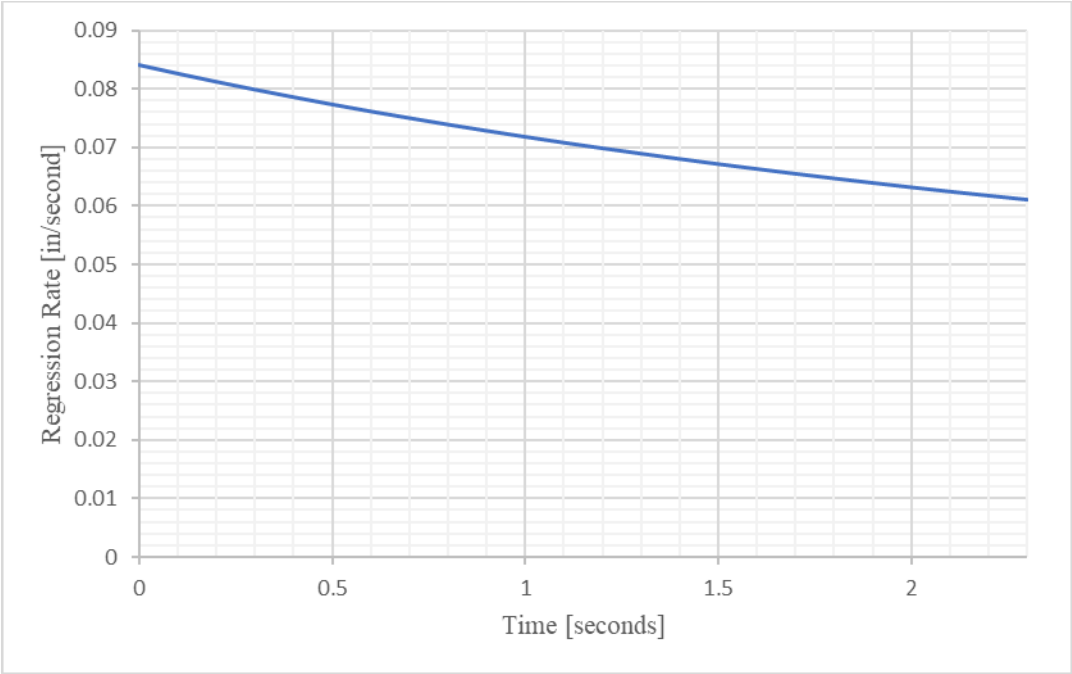

Figure B-7. Regression rate versus time for hybrid motor.

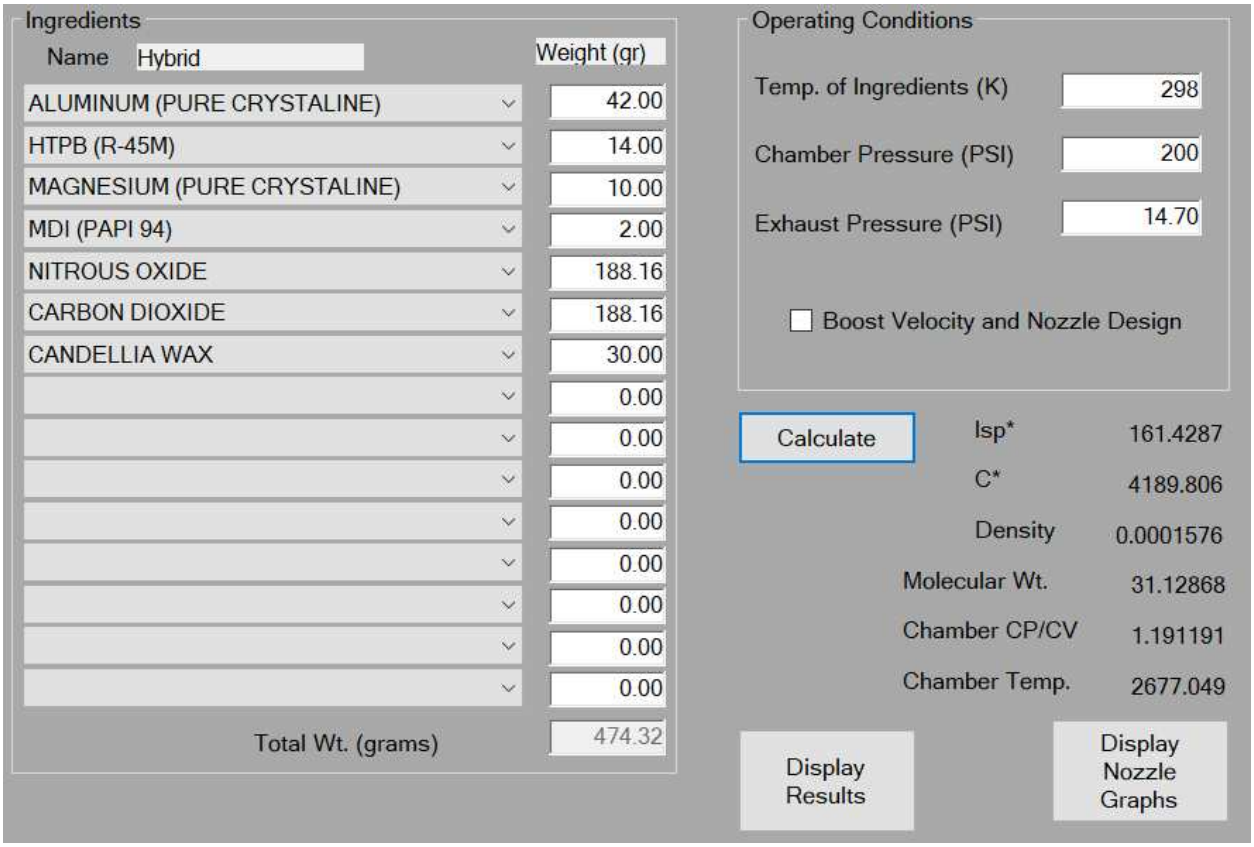

Figure B-8. PROPEP simulation of hybrid motor.

```
Code                                WEIGHT     D-H  DENS     COMPOSITION
      0 ALUMINUM (PURE CRYSTALINE)     42.000       0  0.09750   1 AL
      0 HTPB (R-45M)                   14.000    -367  0.03250 200 C  302 H    2 O
      0 MAGNESIUM (PURE CRYSTALINE)    10.000       0  0.06290   1 MG
      0 MDI (PAPI 94)                   2.000    -202  0.04460 224 C  155 H   27 O   27 N
      0 NITROUS OXIDE                 188.160     443  0.07140   2 N    1 O
      0 CARBON DIOXIDE                188.160   -2137  0.03980   1 C    2 O
      0 CANDELLIA WAX                  30.000    -142  0.00001  69 C  122 H    3 O

THE PROPELLANT DENSITY IS  0.00016 LB/CU-IN OR   0.0044 GM/CC
THE TOTAL PROPELLANT WEIGHT IS  474.3200 GRAMS

NUMBER OF GRAM ATOMS OF EACH ELEMENT PRESENT IN INGREDIENTS

    5.289587 H
    7.490766 C
    8.564385 N
   12.940410 O
    0.411184 MG
    1.556709 AL

*****************************CHAMBER RESULTS FOLLOW    *****************************
  T(K)  T(F)  P(ATM)   P(PSI) ENTHALPY  ENTROPY   CP/CV    GAS    RT/V
  2692  4386    68.02  1000.00  -328.55   929.25  1.1908 14.437    4.712

SPECIFIC HEAT (MOLAR) OF GAS AND TOTAL =     9.737    11.768
NUMBER MOLS GAS AND CONDENSED =    14.437    0.778
```

```
 6.273701e+000 CO         4.281273e+000 N2         1.476287e+000 H2O        1.216590e+000 CO2
 1.149593e+000 H2         4.105543e-001 MgAl2O4*   3.676328e-001 Al2O3*     2.722816e-002 H
 9.070792e-003 HO         1.403917e-003 NO         1.942911e-004 Mg         1.890234e-004
MgH2O2
 1.582458e-004 AlHO2      1.506881e-004 MgHO       1.348846e-004 O          1.079823e-004 NH3
 8.741456e-005 CNH        8.662519e-005 CHO        7.053144e-005 O2         3.490664e-005 AlHO
 1.975549e-005 CH2O       1.682842e-005 CNHO       9.682570e-006 MgH        8.640460e-006 NH2
  5.60763E-06 MgO

THE MOLECULAR WEIGHT OF THE MIXTURE IS    31.175

**************************EXHAUST RESULTS FOLLOW   ***************************
  T(K)  T(F)  P(ATM)   P(PSI) ENTHALPY  ENTROPY   CP/CV    GAS   RT/V
  1441  2135     1.00    14.70  -576.43   929.25  1.2148 14.418    0.069

SPECIFIC HEAT (MOLAR) OF GAS AND TOTAL =     9.099    10.663
NUMBER MOLS GAS AND CONDENSED =    14.418    0.778

 5.839312e+000 CO         4.282065e+000 N2         1.651172e+000 CO2        1.592194e+000 H2
 1.052401e+000 H2O        4.110807e-001 MgAl2O4&   3.671985e-001 Al2O3&     4.051431e-005 H
  2.16841E-05 NH3

THE MOLECULAR WEIGHT OF THE MIXTURE IS    31.214

 **********PERFORMANCE:  FROZEN ON FIRST LINE, SHIFTING ON SECOND LINE**********

 IMPULSE   IS EX      T*      P*      C*    ISP*  OPT-EX  D-ISP      A*M   EX-T
   207.9  1.1990    2448   38.41  4166.2            8.89    0.9  0.12952   1336
   213.3  1.1280    2531   39.38  4302.3   163.4    9.04    0.9  0.13375   1441

   Code                                  WEIGHT     D-H  DENS     COMPOSITION
      0 ALUMINUM (PURE CRYSTALINE)        42.000       0  0.09750   1 AL
      0 HTPB (R-45M)                      14.000    -367  0.03250 200 C  302 H    2 O
      0 MAGNESIUM (PURE CRYSTALINE)       10.000       0  0.06290   1 MG
      0 MDI (PAPI 94)                      2.000    -202  0.04460 224 C  155 H   27 O   27 N
      0 NITROUS OXIDE                    188.160     443  0.07140   2 N    1 O
      0 CARBON DIOXIDE                   188.160   -2137  0.03980   1 C    2 O
      0 CANDELLIA WAX                     30.000    -142  0.00001  69 C  122 H    3 O

THE PROPELLANT DENSITY IS  0.00016 LB/CU-IN OR   0.0044 GM/CC
THE TOTAL PROPELLANT WEIGHT IS  474.3200 GRAMS

NUMBER OF GRAM ATOMS OF EACH ELEMENT PRESENT IN INGREDIENTS

    5.289587 H
    7.490766 C
    8.564385 N
   12.940410 O
    0.411184 MG
    1.556709 AL

**************************CHAMBER RESULTS FOLLOW   ***************************
  T(K)  T(F)  P(ATM)   P(PSI) ENTHALPY  ENTROPY   CP/CV    GAS   RT/V
  2677  4359    13.60   200.00  -328.55   975.45  1.1912 14.459    0.941

SPECIFIC HEAT (MOLAR) OF GAS AND TOTAL =     9.719    11.748
NUMBER MOLS GAS AND CONDENSED =    14.459    0.778

 6.271924e+000 CO         4.280623e+000 N2         1.462807e+000 H2O        1.218513e+000 CO2
 1.143138e+000 H2         4.096834e-001 MgAl2O4*   3.684027e-001 Al2O3*     5.745606e-002 H
 1.879828e-002 HO         2.879292e-003 NO         8.872195e-004 Mg         5.945503e-004 O
```

```
 3.197032e-004 AlHO2      3.103395e-004 O2         3.101451e-004 MgHO       1.787887e-004
MgH2O2
 7.043558e-005 AlHO       3.718529e-005 CHO        2.440923e-005 MgO        2.164593e-005 NH3
  1.96234E-05 MgH         1.96234E-05 MgH         1.96234E-05 MgH

THE MOLECULAR WEIGHT OF THE MIXTURE IS    31.129

**************************EXHAUST RESULTS FOLLOW   ***************************
  T(K)  T(F)  P(ATM)   P(PSI) ENTHALPY  ENTROPY   CP/CV    GAS   RT/V
  1893  2947     1.00    14.70  -499.84   975.45  1.2047 14.419    0.069

SPECIFIC HEAT (MOLAR) OF GAS AND TOTAL =     9.418    11.098
NUMBER MOLS GAS AND CONDENSED =    14.419    0.778

 6.083424e+000 CO         4.282071e+000 N2         1.407058e+000 CO2        1.346610e+000 H2
 1.296250e+000 H2O        4.110806e-001 MgAl2O4&   3.671986e-001 Al2O3&     3.302896e-003 H
  0.000262593 HO          0.000262593 HO          0.000262593 HO

THE MOLECULAR WEIGHT OF THE MIXTURE IS    31.210

 **********PERFORMANCE:  FROZEN ON FIRST LINE, SHIFTING ON SECOND LINE**********

 IMPULSE   IS EX      T*      P*      C*    ISP*  OPT-EX  D-ISP      A*M   EX-T
   173.3  1.1951    2439    7.69  4170.7            2.79    0.8  0.64829   1748
   177.3  1.1815    2458    7.73  4189.8   161.4    2.93    0.8  0.65126   1893
```

Figure B-9. PROPEP simulation output of hybrid propellants.

APPENDIX C

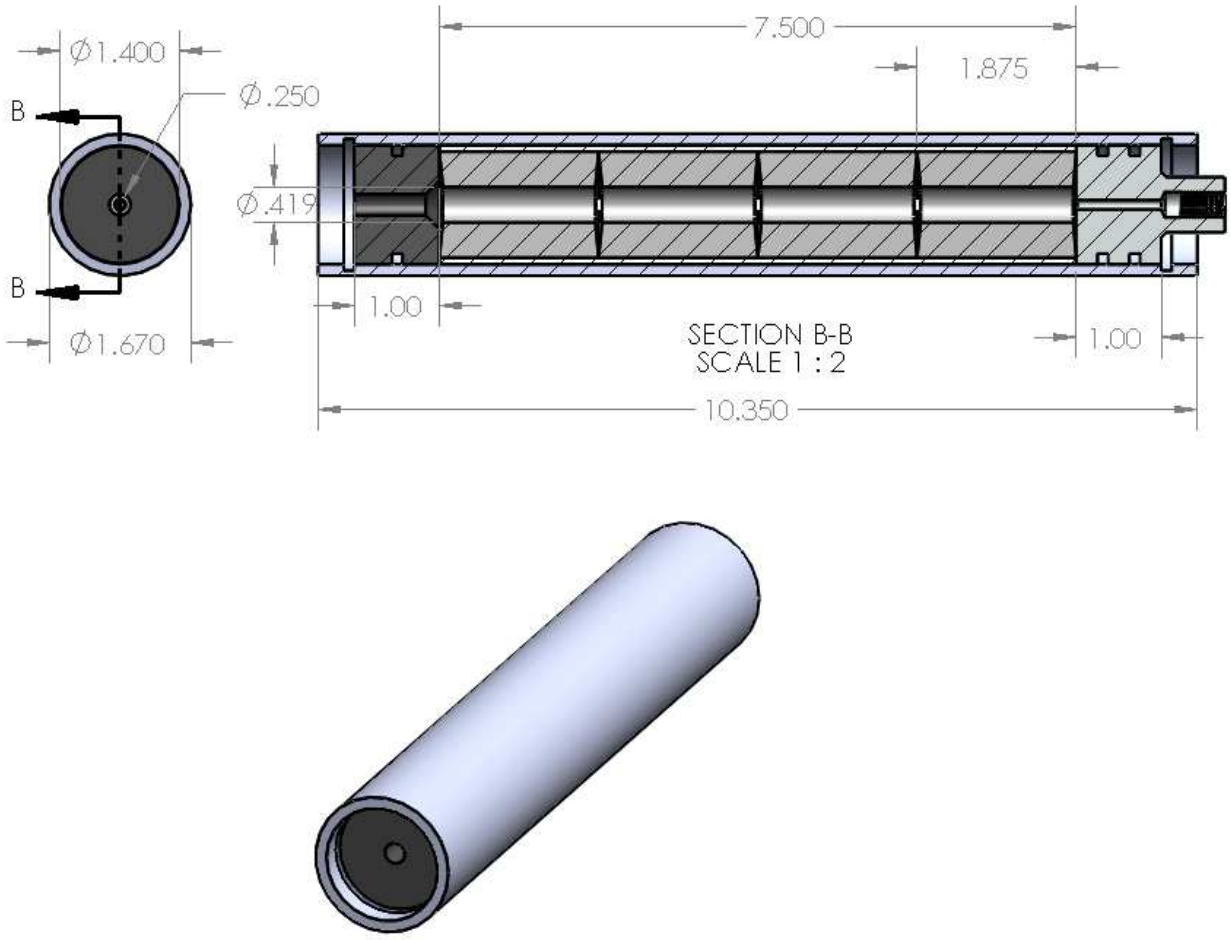

Figure C-1. Solidworks drawing of A206-B propellant rocket motor.

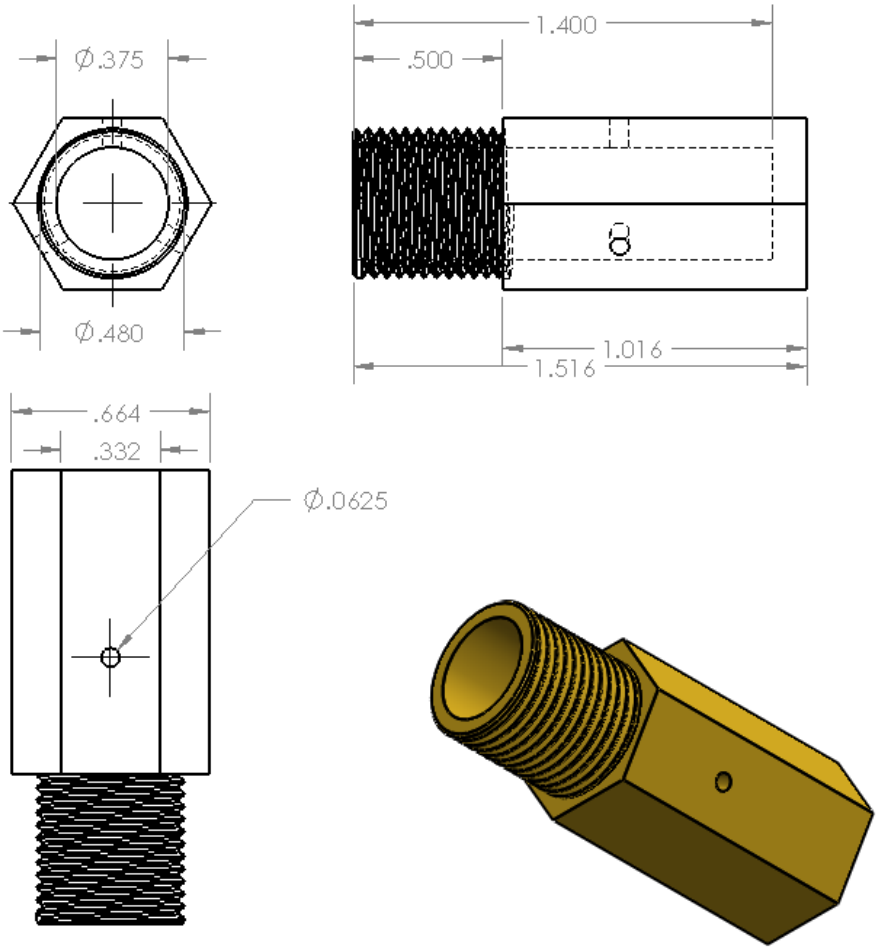

Figure C-2. Solidworks drawing of pintle.

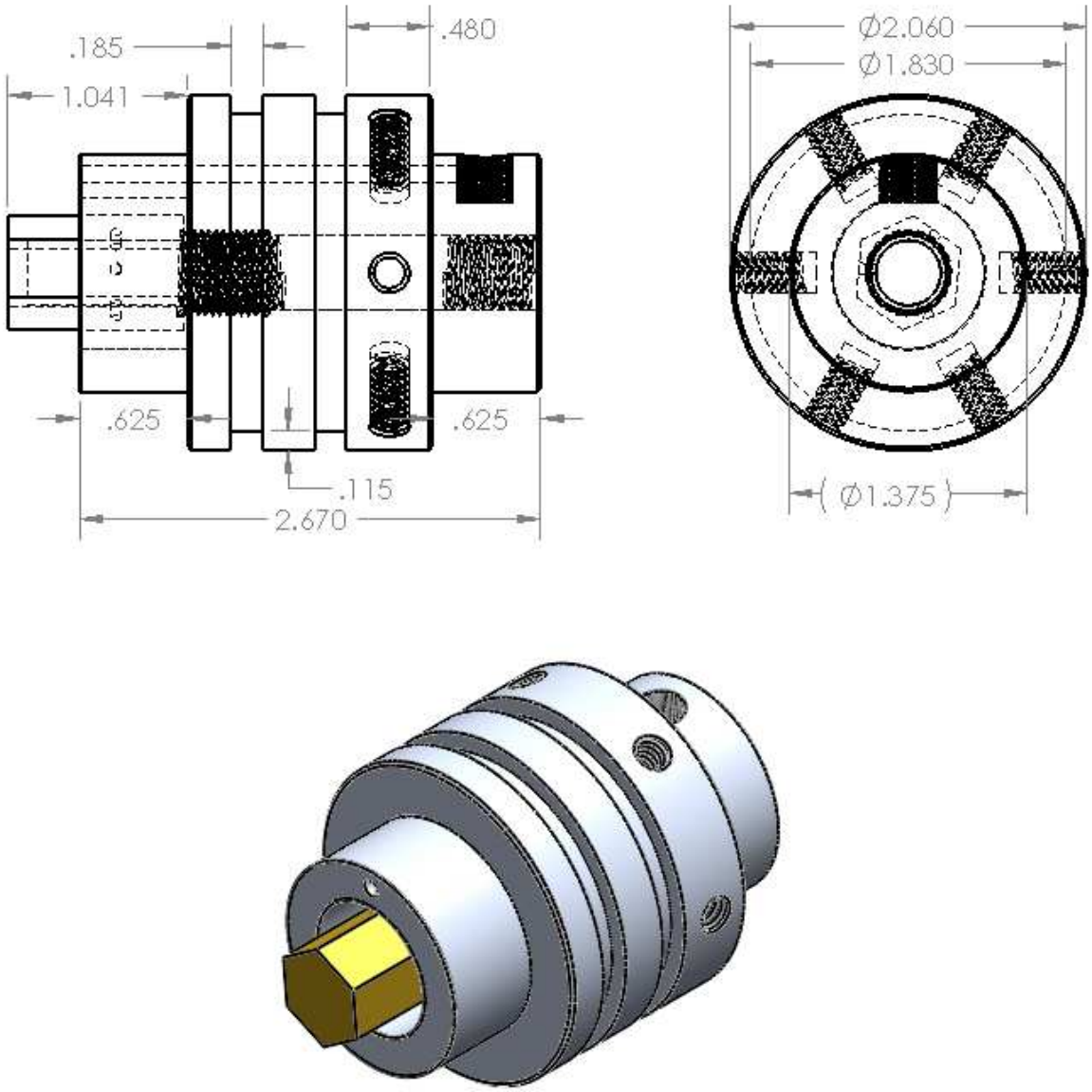

Figure C-3. Solidworks drawing of injector assembly.

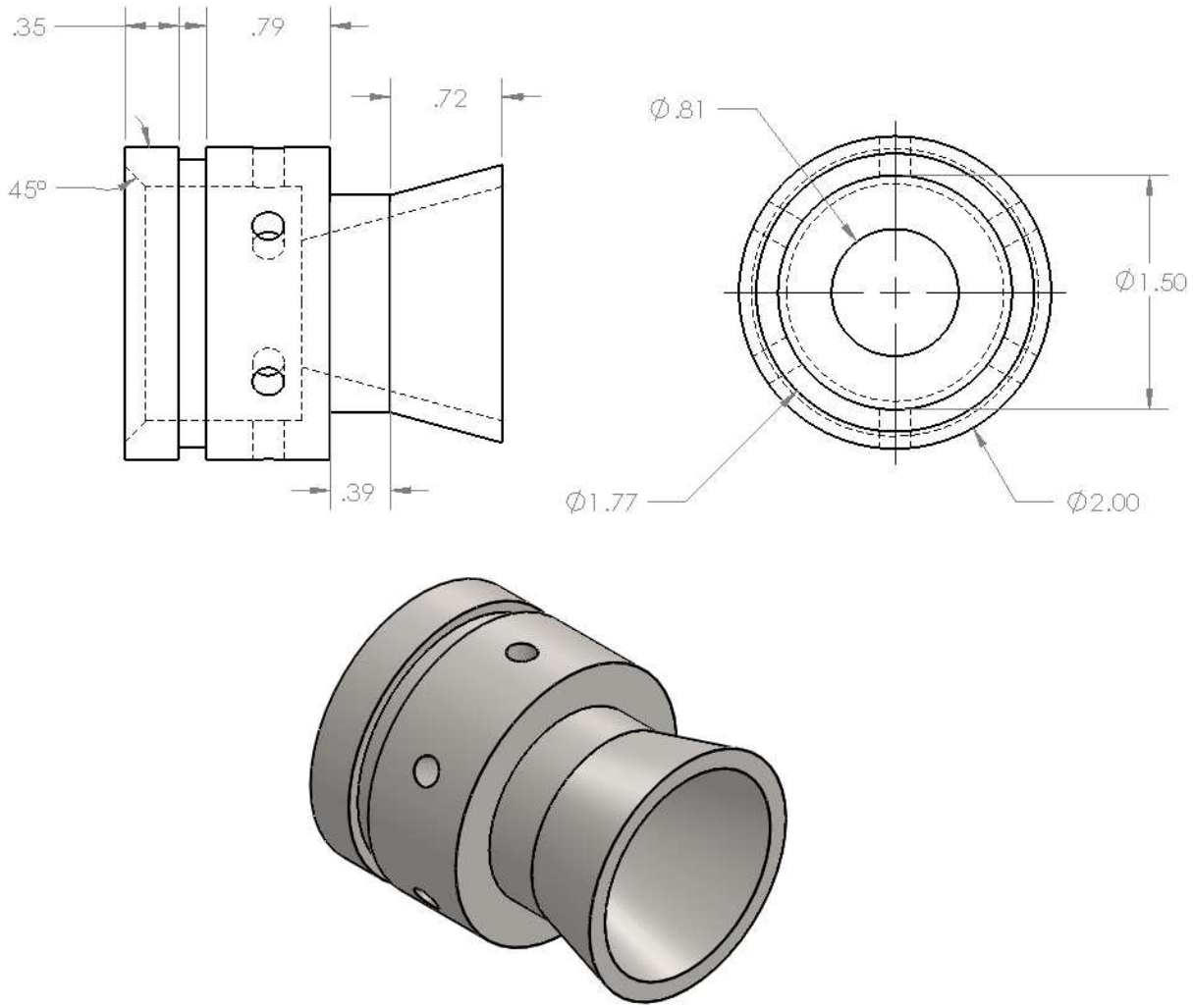

Figure C-4. Solidworks drawing of nozzle carrier.

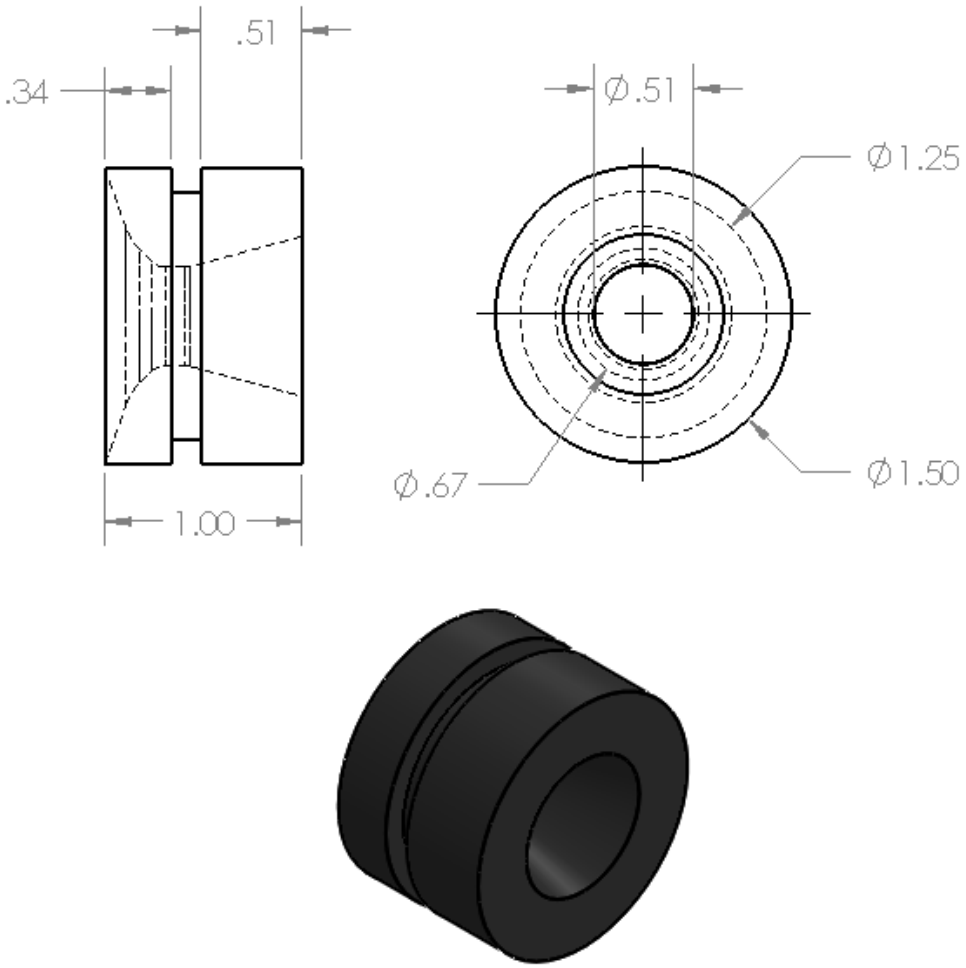

Figure C-5. Solidworks drawing of nozzle insert.

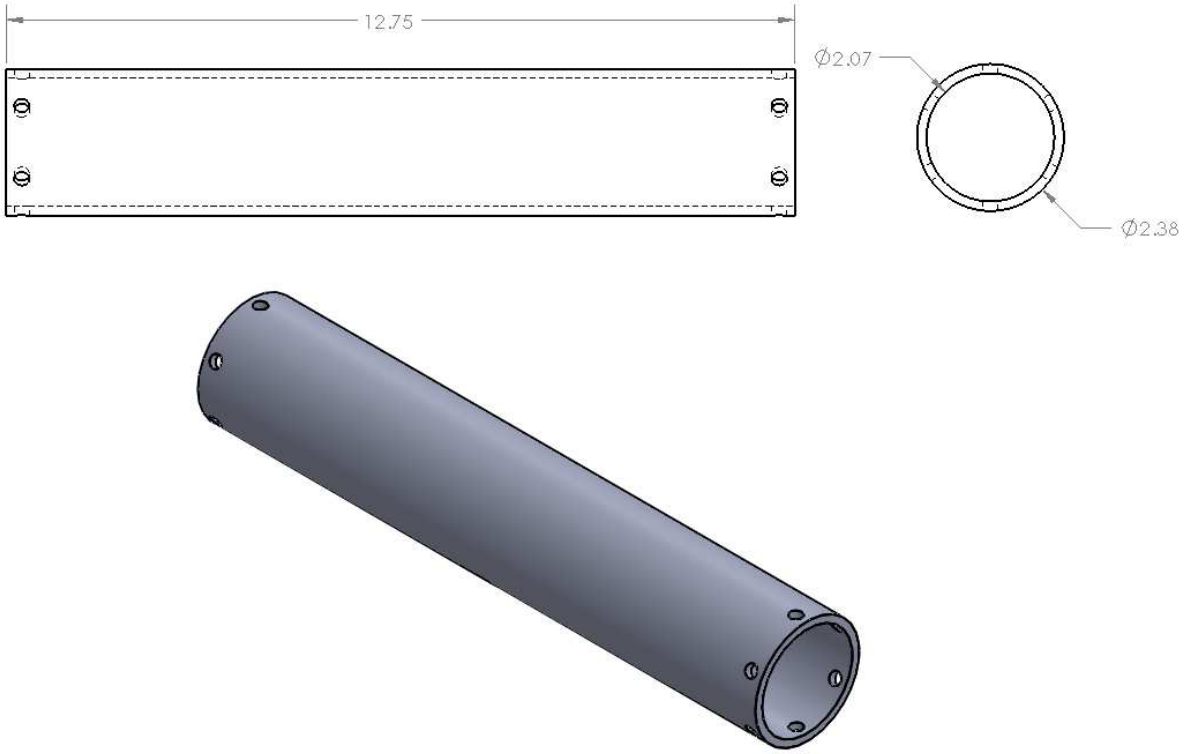

Figure C-6. Solidworks drawing of combustion chamber.

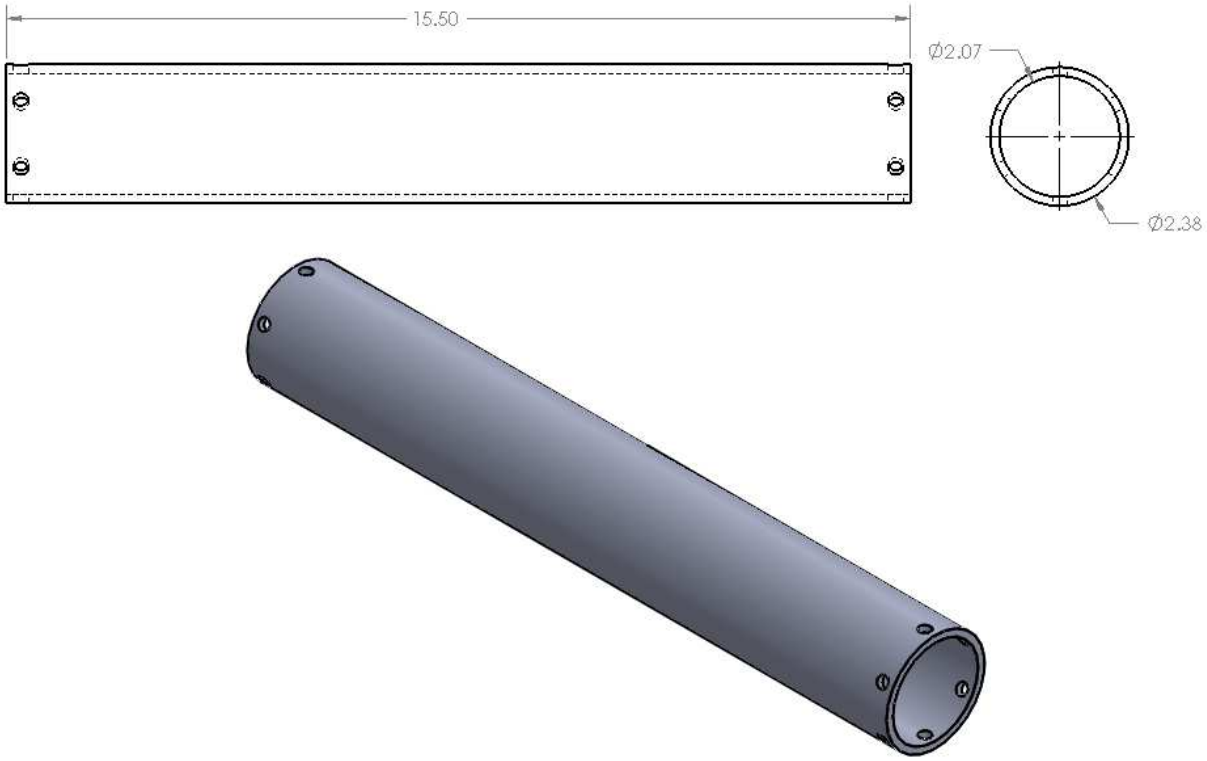

Figure C-7. Solidworks drawing of oxidizer tank.

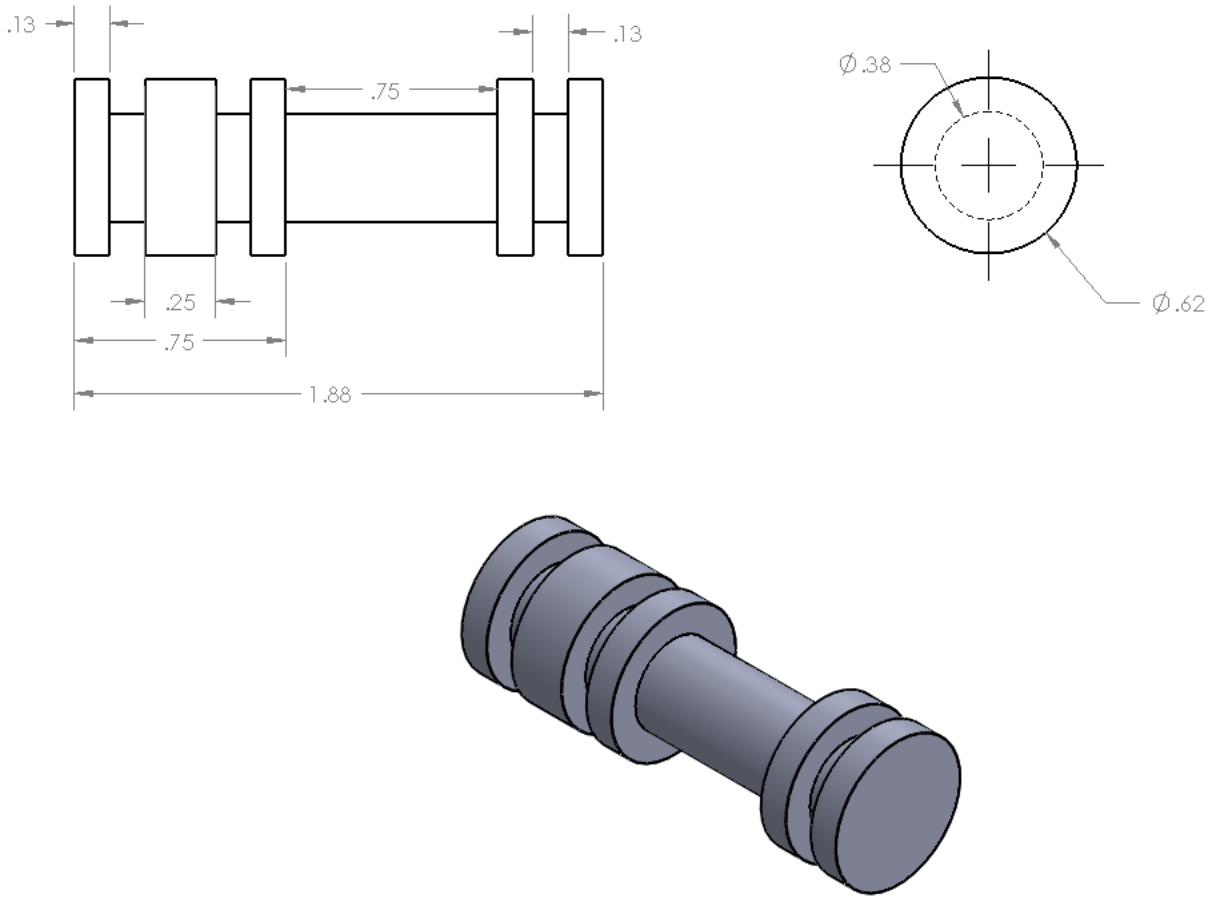

Figure C-8. Solidworks drawing of pyrotechnic valve piston.

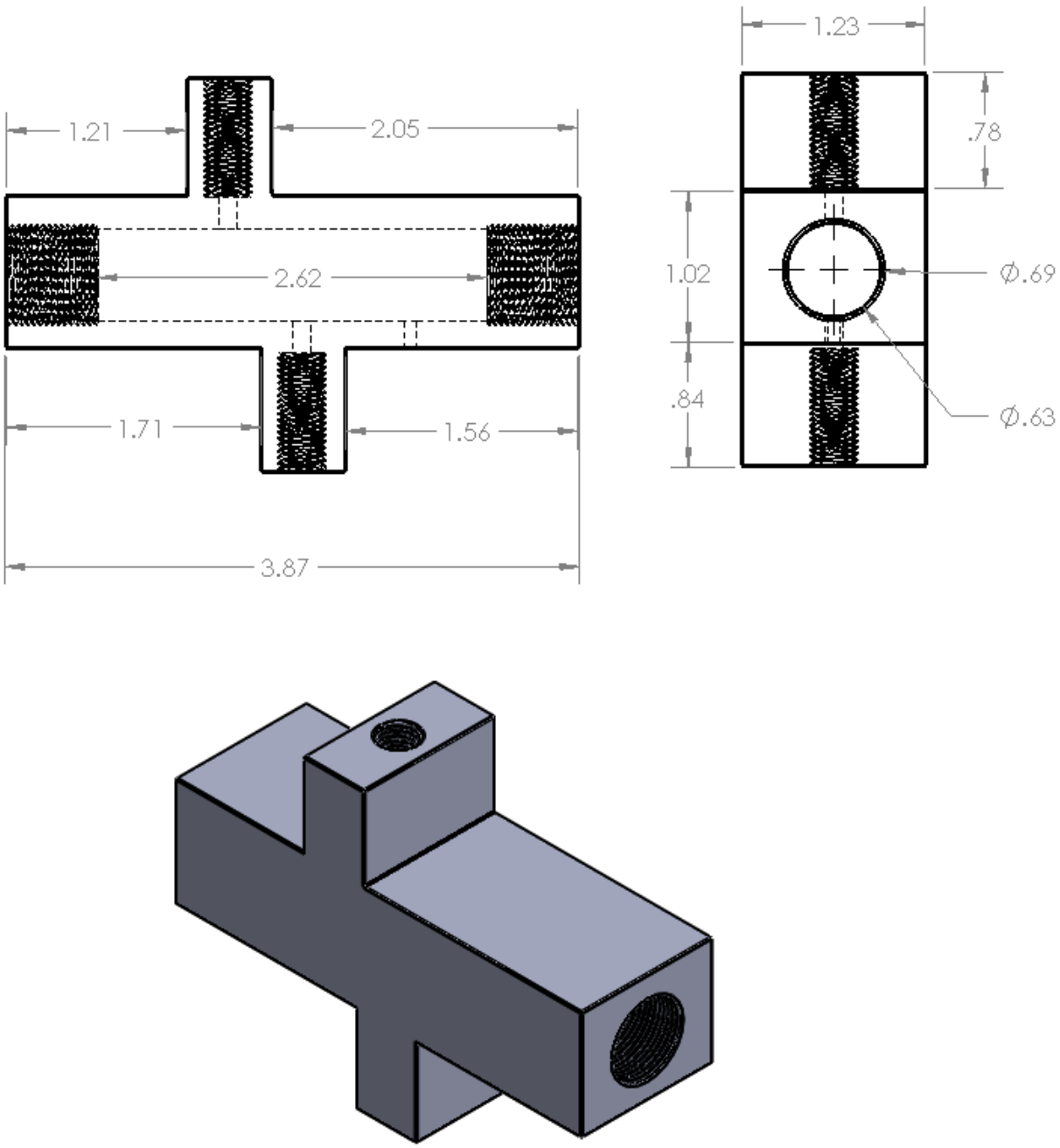

Figure C-9. Solidworks drawing of pyrotechnic valve housing.

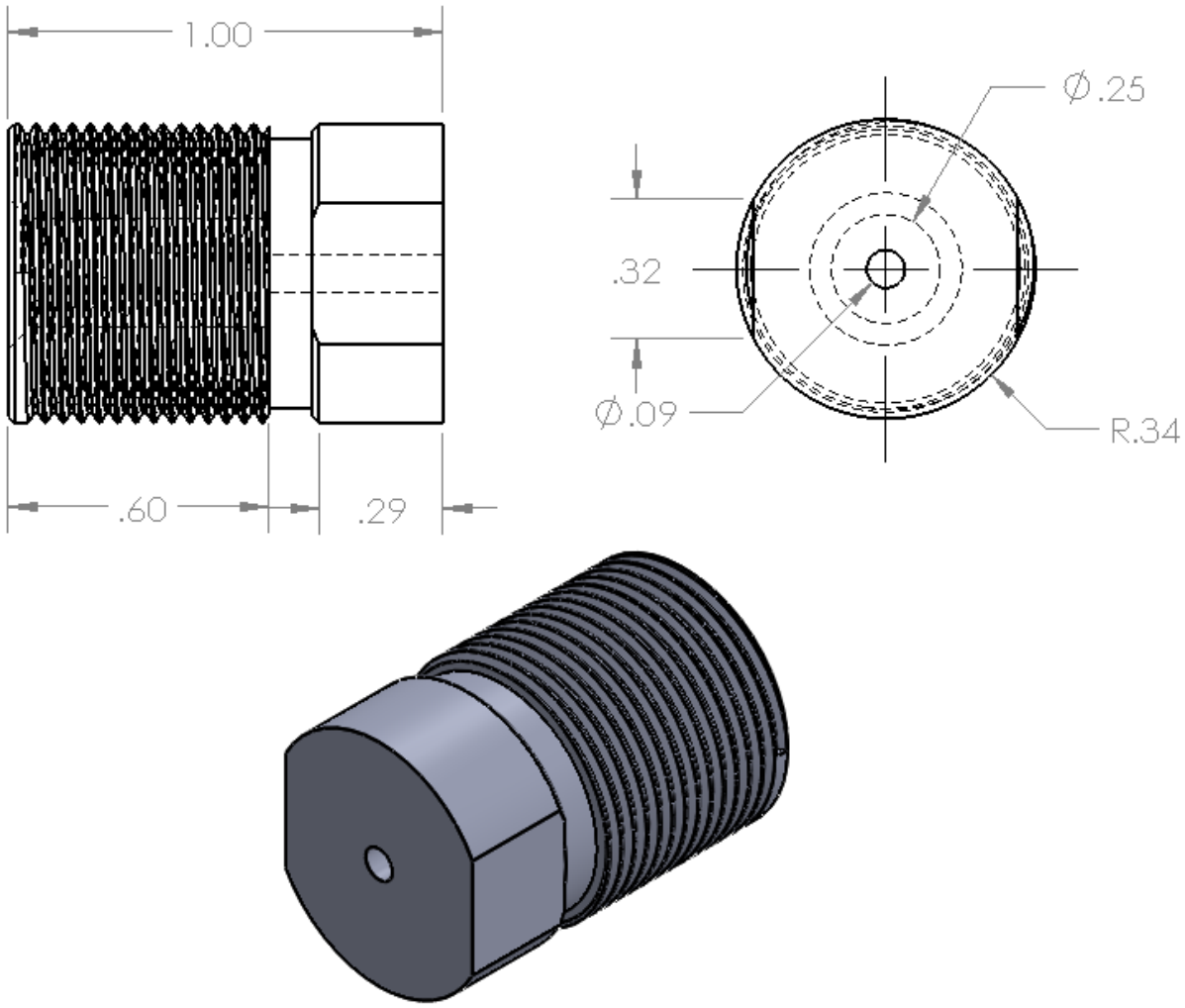

Figure C-10. Solidworks drawing of pyrotechnic valve squib cap.

Figure C-11. Solidworks drawing of hybrid motor assembly.